

Landsat 7
Image Assessment System (IAS)
Geometric Algorithm Theoretical Basis
Document

TABLE OF CONTENTS

1. INTRODUCTION	1
1.1 Purpose	1
1.2 Applicable Documents	2
2. OVERVIEW AND BACKGROUND INFORMATION	6
2.1 Experimental Objective	6
2.2 Historical Perspective	6
2.3 Instrument Characteristics	7
2.4 Ancillary Input Data	7
3. ALGORITHM DESCRIPTION	8
3.1 Theoretical Description	8
3.1.1 Landsat 7 ETM+ Viewing Geometry Overview	8
3.1.2 Coordinate Systems	10
3.1.3 Coordinate Transformations	16
3.1.4 Time Systems	19
3.1.5 Mathematical Description of Algorithms	22
3.1.5.1 ETM+ Instrument Model	22
3.1.5.1.1 Detector/Focal Plane Geometry	22
3.1.5.1.2 Scan Mirror Model	23
3.1.5.1.3 Scan Line Corrector Mirror Model	24
3.1.5.2 Landsat 7 Platform Model	24
3.1.5.2.1 Sensor Pointing (Attitude and Jitter) Model	24
3.1.5.2.2 Platform Position and Velocity	25
3.1.5.3 Level 1 Processing Algorithms	26
3.1.5.3.1 PCD Processing	28
3.1.5.3.2 MSCD Processing	32
3.1.5.3.3 Platform/Sensor Model Creation	34
3.1.5.3.3.1 Smoothing Low Frequency Attitude Information	48
3.1.5.3.3.2 Combining Low and High frequency Attitude Information	56
3.1.5.3.4 Line of Sight Generation and Projection	65
3.1.5.3.5 Correction Grid Generation	73
3.1.5.3.6 Resampling	78
3.1.5.3.6.1 Detector Delays	91
3.1.5.3.7 Precision Correction	94
3.1.5.3.7.1 Precision Correction Outlier Detection	105
3.1.5.3.7.2 Inverse Mapping	109
3.1.5.3.7.3 Precision Ephemeris Update	110
3.1.5.3.8 Terrain Correction	112
3.1.5.4 Geometric Calibration Algorithms	116
3.1.5.4.1 Sensor Alignment Calibration	116
3.1.5.4.2 Focal Plane Calibration	123
3.1.5.4.3 Scan Mirror Calibration	127
3.1.5.5 Geometric Characterization Algorithms	135

IAS Geometric ATBD Version 3

3.1.5.5.1 Band to Band Registration	135
3.1.5.5.2 Image to Image Registration	143
3.1.5.5.3 Geodetic Accuracy	150
3.1.5.5.4 Geometric Accuracy	151
3.1.6 Variance or Uncertainty Estimates	154
3.1.6.1 Level 1 Processing Accuracy	154
3.1.6.2 Geometric Calibration Accuracy	158
3.1.6.2.1 Sensor Alignment Calibration Accuracy	158
3.1.6.2.2 Scan Mirror Calibration Accuracy	160
3.1.6.2.3 Band Placement Calibration Accuracy	163
3.1.6.3 Geometric Characterization Accuracy	165
3.1.6.3.1 Band-to-Band Registration Accuracy	165
3.1.6.3.2 Image-to-Image Registration Accuracy	167
4. CONSTRAINTS, LIMITATIONS, ASSUMPTIONS	170

TABLE OF FIGURES

FIGURE 3.1.1-1 ETM+ GEOMETRY OVERVIEW	9
FIGURE 3.1.1-2 ETM+ DETECTOR ARRAY GROUND PROJECTION	10
FIGURE 3.1.2-1 ETM+ FOCAL PLANE COORDINATE SYSTEM	11
FIGURE 3.1.2-2 ETM+ SENSOR COORDINATE SYSTEM	12
FIGURE 3.1.2-3 ORBITAL COORDINATE SYSTEM	13
FIGURE 3.1.2-4 EARTH CENTERED INERTIAL (ECI) COORDINATE SYSTEM	14
FIGURE 3.1.2-5 EARTH CENTERED ROTATING (ECR) COORDINATE SYSTEM	15
FIGURE 3.1.2-6 GEODETIC COORDINATE SYSTEM	16
FIGURE 3.1.5- 1 MODEL INITIALIZATION	26
FIGURE 3.1.5- 2 RECTIFICATION AND RESAMPLING	27
FIGURE 3.1.5- 3 PRECISION CORRECTION SOLUTION	27
FIGURE 3.1.5- 4 PRECISION/TERRAIN CORRECTION	28
FIGURE 3.1.5- 5 SCAN MIRROR PROFILE DEVIATIONS	44
FIGURE 3.1.5- 6 EFFECT OF ROLL JITTER ON LINE OF SIGHT DIRECTION	47
FIGURE 3.1.5- 7 MAGNITUDE RESPONSE OF GYRO AND ADS	57
FIGURE 3.1.5- 8 MAGNITUDE RESPONSE OF GYRO PLUS ADS	58
FIGURE 3.1.5- 9 MAGNITUDE RESPONSE OF GYRO + MAGNITUDE RESPONSE OF ADS	58
FIGURE 3.1.5- 10 ATTITUDE PROCESSING NETWORK	59
FIGURE 3.1.5- 11 INPUT IMAGE GRIDDING PATTERN	77
FIGURE 3.1.5- 12 EXTENDED PIXELS AND SCAN ALIGNMENT	86
FIGURE 3.1.5- 13 CALCULATION OF SCAN GAP	87
FIGURE 3.1.5- 14 SCAN MISALIGNMENT AND GAP	88
FIGURE 3.1.5- 15 EXTENDED SCAN LINES	88
FIGURE 3.1.5- 16 CUBIC SPLINE WEIGHTS	89
FIGURE 3.1.5- 17 INVERSE MAPPING WITH "ROUGH" POLYNOMIAL	89
FIGURE 3.1.5- 18 "ROUGH" POLYNOMIAL – FIRST ITERATION	90
FIGURE 3.1.5- 19 RESULTS MAPPED BACK TO INPUT SPACE	90
FIGURE 3.1.5- 20 NEAREST NEIGHBOR RESAMPLING	90
FIGURE 3.1.5- 21 DETECTOR DELAY DEFINITION	92
FIGURE 3.1.5- 22 RESAMPLING WEIGHT DETERMINATION	94
FIGURE 3.1.5- 23 DEFINITION OF ORBIT REFERENCE SYSTEM	95
FIGURE 3.1.5- 24 LOOK VECTOR GEOMETRY	99
FIGURE 3.1.5- 25 TERRAIN CORRECTION GEOMETRY	115
FIGURE 3.1.5- 26 DOQ QUARTER-QUAD IMAGES COVERING ABOUT 20 TM SCANS	133
FIGURE 3.1.5- 27 LEGENDRE DIFFERENCES	134
FIGURE 3.1.5- 28 DIFFERENCE BETWEEN ACTUAL MIRROR PROFILES	135
FIGURE 3.1.5- 29 CORRELATION ERRORS	146
FIGURE 3.1.5- 30 CORRELATION STANDARD DEVIATIONS	147
FIGURE 3.1.5- 31 ROAD CROSS SECTION EXAMPLE	148
FIGURE 3.1.5- 32 CORRELATION ERRORS	149
FIGURE 3.1.6.2.1- 1 ALIGNMENT ESTIMATION ACCURACY VS. NUMBER OF SCENES	162
FIGURE 3.1.6.2.3- 1 BAND-TO-BAND TEST POINT NUMBER VS. ACCURACY	165

1. Introduction

1.1 Purpose

This document describes the geometric algorithms used by the Landsat 7 Image Assessment System (IAS). These algorithms are implemented as part of the IAS Level 1 processing, geometric characterization, and geometric calibration software components. The overall purpose of the IAS geometric algorithms is to use Earth ellipsoid and terrain surface information in conjunction with spacecraft ephemeris and attitude data, and knowledge of the Enhanced Thematic Mapper Plus (ETM+) instrument and Landsat 7 satellite geometry to relate locations in ETM+ image space (band, scan, detector, sample) to geodetic object space (latitude, longitude, and height). These algorithms are used for purposes of creating accurate Level 1 output products, characterizing the ETM+ absolute and relative geometric accuracy, and deriving improved estimates of geometric calibration parameters such as the sensor to spacecraft alignment. This document presents background material describing the relevant coordinate systems, time systems, ETM+ sensor geometry, and Landsat 7 spacecraft geometry as well as descriptions of the IAS processing algorithms.

The Level 1 processing algorithms include:

1. Payload Correction Data (PCD) processing;
2. Mirror Scan Correction Data (MSCD) processing;
3. ETM+/Landsat 7 sensor/platform geometric model creation;
4. sensor line of sight generation and projection;
5. output space/input space correction grid generation;
6. image resampling;
7. geometric model precision correction using ground control;
8. terrain correction.

These algorithms are discussed in detail in section 3.1.5.3.

The geometric calibration algorithms, discussed in section 3.1.5.4, include:

1. ETM+ sensor alignment calibration;
2. focal plane calibration (focal plane band-to-band alignment);
3. scan mirror calibration.

The geometric characterization algorithms, discussed in section 3.1.5.5, include:

1. band to band registration;
2. image to image registration;
3. geodetic accuracy assessment (absolute external accuracy);
4. geometric accuracy assessment (relative internal accuracy).

1.2 Applicable Documents

Reference 1

Landsat 7 System Data Format Control Book (DFCB) Volume IV - Wideband Data, Revision H, prepared by Martin Marietta Astro Space, document number 23007702-IVH, dated 26 February 1998.

Reference 2

Landsat 7 System Program Coordinates System Standard, Revision B, prepared by Martin Marietta Astro Space, document number PS23007610B, dated 2 December 1994.

Reference 3

Landsat 7 System Image Assessment System (IAS) Element Specification (Revision 1), NASA Goddard Space Flight Center, document number 430-15-01-001-1, dated February 1998.

Reference 4

Theoretical Basis of the Science Data Processing Toolkit Geolocation Package for the ECS Project, prepared by the EOSDIS Core System Project, document number 445-TP-002-002, dated May 1995.

Reference 5

Landsat 7 System Specification, Revision H, Goddard Space Flight Center, document number 430-L-0002-H, dated June 1996.

Reference 6

Press, Teukolsky, Vetterling, and Flannery, Numerical Recipes in C, 2nd edition, Cambridge University Press, 1992.

Reference 7

DMA TR 8350.2-A, DMA Technical Report, Supplement to Department of Defense World Geodetic System 1984 Technical Report, prepared by the Defense Mapping Agency WGS84 Development Committee, dated December 1, 1987.

Reference 8

Snyder, John P., Map Projections - A Working Manual, United States Geological Survey Professional Paper 1395, U. S. Government Printing Office, Washington, 1987.

Reference 9

Landsat 7 Space Segment Technical Description Document - Enhanced Thematic Mapper Plus, prepared by Hughes Santa Barbara Research Center, May 1994, updated by NASA Goddard Space Flight Center, September 1995.

Reference 10

Sehn, G. J. and S. F. Miller, "LANDSAT Thematic Mapper Attitude Data Processing", presented at the AIAA/AAS Astrodynamics Conference, Seattle, Washington, August 20-22, 1984.

Reference 11

Landsat to Ground Station Interface Description, Revision 9, Goddard Space Flight Center, Greenbelt, Maryland, January 1986.

Reference 12

Park, S.K., R.A. Schowengerdt, Image Reconstruction by Parametric Cubic Convolution, Computer Vision, Graphics and Image Processing, v.23, no.3, September 1983.

Reference 13

Rosborough, G.W., D.G. Baldwin and W.J. Emery, "Precise AVHRR Image Navigation", IEEE Transaction on Geoscience and Remote Sensing, Vol. 32, No. 3., May 1994.

Reference 14

Rao, C.R., "Linear Statistical Inference and Its Applications", John Wiley and Sons, Inc., 1973.

Reference 15

Sahin, M., P.A. Cross, and P.C. Sellers, "Variance Component Estimation Applied to Satellite Laser Ranging", Bulletin Geodesique, 66: 284-295, 1992.

Reference 16

Yuan, Dah-ning, "Optimum Determination of the Earth's Gravitational Field from Satellite Tracking and Surface Measurements", Dissertation, The University of Texas at Austin, 1991.

Reference 17

Snyder, John P., Space Oblique Mercator Projection Mathematical Development, United States Geological Survey Bulletin 1518, U. S. Government Printing Office, Washington, 1981.

Reference 18

LAS 6.0 Geometric Manipulation Package Overview Document, USGS EROS Data Center.

Reference 19

LAS 6.0 Programmer's Document, USGS EROS Data Center

Reference 20

Escobal, Pedro R., Methods of Orbit Determination, 2nd edition, John Wiley & Sons, Inc., New York, 1976.

Reference 21

Dvornychenko, V.N., Bounds on (Deterministic) Correlation Functions with Application to Registration, IEEE Transactions on Pattern Analysis and Machine Intelligence, v.5, n.2, Mar 1983

Reference 22

Steinwand, D. and Wivell, C., Landsat Thematic Mapper Terrain Corrections in LAS, HSTX Inter-Office Memo OAB8-21, USGS EROS Data Center, August 12, 1993.

Reference 23

Brown, R.G., Introduction to Random Signal Analysis and Kalman Filtering, John Wiley and Sons, New York, 1983.

Reference 24

Landsat 7 System Calibration Parameter File Definition, Revision 1, 430-15-01-002-0
NASA Goddard Space Flight Center, Greenbelt, Maryland, January 1998.

Reference 25

Burt P. and Adelson E., The Laplacian Pyramid as a Compact Image Code, IEEE
Transactions on Communications, vol. Com-31, no. 4, April 1983.

Reference 26

Prakash, A. and Beyer, E.P., Landsat D Thematic Mapper Image Resampling for Scan
Geometry Correction.

Reference 27

Beyer, E.P., An Overview of the Thematic Mapper Geometric Correction System

Reference 28

Wolberg, G., Digital Image Warping, IEEE Computer Science Press, 1990.

Reference 29

Gonzalez, R.C. and Wintz, P., Digital Image Processing, 2nd Edition, Addison-Wesley
Publishing Company, 1987.

Reference 30

Fischel, D., "Validation of the Thematic Mapper Radiometric and Geometric Correction
Algorithms" IEEE Transactions on Geoscience and Remote Sensing, Vol. GE-22 No. 3
May 1984.

Reference 31

Golub, G.H. and Van Loan, C.F., Matrix Computations (2nd ed.), John Hopkins University
Press, Baltimore, 1989.

Reference 32

Landsat 7 ETM+ Geometric Calibration Plan, EROS Data Center, December 2, 1996

Reference 33

Goodman, D.J. and Carey, M.J., Nine Digital Filters for decimation and Interpolation,
IEEE Transactions on Acoustics, Speech, and Signal Processing, vol. 25, April 1977

Reference 34

Haykin, Simon, "Adaptive Filtering Theory", Prentice Hall, 1991.

Reference 35

Landsat 7 Celestial Sensor Assembly, Including Star Transit Processing Electronics and
Celestial Sensor Sun Shield, Martin Marietta Astro Space, PS23007911A, 9 September
1994.

Reference 36

Cook, R. Dennis, "Detection of Influential Observations in Linear Regression", Technometrics, Volume 19, Number 1, February, 1977.

Reference 37

IAS Radiometry Algorithm 6.6a, "Outliers in a Regression", Goddard Space Flight Center, 1996.

Reference 38

EOSAT Ground Segment Interface Control Document Volume 2D, G/S-ICD-2040
Revision D, Nov, 1, 1996.

Reference 39

Gore, Robert, "Landsat 4/5 Attitude Jitter Processing Analysis", Lockheed/Martin Marietta, interoffice memo.

Reference 40

Gore, Robert, "Landsat 7 System ETM+ Process Algorithms (Attitude Jitter Processing)", contract No. NAS5-32633.

2. Overview and Background Information

The Landsat 7 Enhanced Thematic Mapper Plus (ETM+) continues the Landsat program of multispectral space-borne Earth remote sensing satellites that began with the launch of Landsat 1 in 1972. Landsat 7 will provide data consistent with the Landsat historical record in the time period between the decommissioning of the still-functioning Landsat 5 and the introduction of successor instruments based on newer technology in the next century. The basic sensor technology used in the ETM+ is similar to the Thematic Mapper instruments flown in Landsats 4 and 5, and the Enhanced Thematic Mapper built for Landsat 6, which suffered a launch failure. The geometric processing, characterization, and calibration algorithms described in this document take into account the new 15 meter panchromatic band (also present in Landsat 6) and the higher resolution thermal band in adapting the processing techniques applied to Landsat 4/5 Thematic Mapper data to the Landsat 7 ETM+.

The inclusion of an Image Assessment System as an integral part of the Landsat 7 ground system illustrates the more systematic approach to instrument calibration and in-orbit monitoring and characterization necessitated by the more stringent calibration requirements of the Landsat 7 ETM+ as compared to earlier Landsat missions. This is especially true of the radiometric calibration requirements which include using partial- and full-aperture solar calibrations to monitor the stability and performance of the ETM+ detectors and on-board calibration lamps. The IAS also provides the platform for systematic geometric performance monitoring, characterization and calibration as described in the remainder of this document.

2.1 Experimental Objective

The objective of the Landsat 7 ETM+ mission is to provide high resolution (15 m panchromatic, 30 meter multispectral, 60 meter thermal) imagery of Earth's land areas from near polar, sun-synchronous orbit. These data will continue and extend the continuous data record collected by Landsats 1-5, provide higher spatial resolution in the new panchromatic band, provide greater calibration accuracy to support new and improved analysis applications, and provide a high resolution reference for the EOS-AM1 MODIS, MISR, and ASTER instruments. The geometric algorithms described in this document will be used by the Landsat 7 Image Assessment System and by the Level-1 Product Generation System (LPGS) to ensure that the complex ETM+ internal geometry is sufficiently modeled and characterized to permit the generation of Level 1 products which meet the Landsat 7 system geometric accuracy specifications.

2.2 Historical Perspective

The Landsat 7 ETM+ mission continues the evolutionary improvement of the Landsat family of satellites which began with Landsats 1, 2, and 3 carrying the Multi-Spectral

Scanner (MSS), and builds on the Landsat 4 and 5 Thematic Mapper (TM) heritage. The ETM+ adds a 15 meter GSD panchromatic band, similar to that used in the Enhanced Thematic Mapper (ETM) instrument built for Landsat 6, improves the thermal band spatial resolution from 120 meters (TM/ETM) to 60 meters (ETM+), and improves the radiometric calibration accuracy from 10% (TM/ETM) to 5% (ETM+). The Landsat 7 system is also taking a more systematic approach to monitoring and measuring system geometric performance in flight than was applied to Landsats 4 and 5, which were turned over to commercial operations in October, 1985.

2.3 Instrument Characteristics

The fundamental ETM+ instrument geometric characteristics include:

- Nadir viewing +/- 7.5 degree instrument FOV;
- Bi-directional cross track scanning mirror;
- Along track scan line corrector mirrors;
- 8 bands, 3 resolutions, 2 focal planes;
- Even/odd detectors staggered on focal planes;
- Pre-launch ground calibrated non-linear mirror profile;
- Scan angle monitor measures actual mid-scan and scan end times (as deviations from nominal);
- High frequency (2-125 Hz) angular displacement sensors to measure instrument jitter.

2.4 Ancillary Input Data

The Landsat 7 ETM+ geometric characterization, calibration, and correction algorithms are applied to the wideband (image plus supporting PCD and MSCD) data contained in level 0R (raw) or 1R (radiometrically corrected) products. Some of these algorithms also require additional ancillary input data sets. These include:

1. Precise ephemeris from the Flight Dynamics Facility - used to minimize ephemeris error when performing sensor to spacecraft alignment calibration.
2. Ground control/reference images for geometric test sites - used in precision correction, geodetic accuracy assessment, and geometric calibration algorithms.
3. Digital elevation data for geometric test sites - used in terrain correction and geometric calibration.
4. Pre-launch ground calibration results including band/detector placement and timing, scan mirror profiles, and attitude sensor data transfer functions (gyro and ADS), to be used in the generation of the initial Calibration Parameter File.
5. Earth parameters including: static Earth model parameters (*e.g.*, ellipsoid axes, gravity constants) and dynamic Earth model parameters (*e.g.*, polar wander offsets, UT1-UTC time corrections) - used in systematic model creation and incorporated into the Calibration Parameter File.

3. Algorithm Descriptions

This section presents the underlying theory and mathematical development of the IAS geometric algorithms.

3.1 Theoretical Description

The supporting theoretical concepts and mathematics of the IAS geometric algorithms are presented in the following subsections. Section 3.1.1 presents a review of the Landsat 7 ETM+ viewing geometry to put the subsequent discussion in context. Sections 3.1.2 and 3.1.3 address the coordinate systems used by the algorithms and the relationships between them, citing references where appropriate. Section 3.1.4 briefly defines and discusses the various time systems used by the IAS algorithms. Section 3.1.5 presents the mathematical development of, and solution procedures for the Level 1 processing, geometric calibration, and geometric characterization algorithms. Section 3.1.6 discusses estimates of uncertainty (error analysis) associated with each of the algorithms.

3.1.1 Landsat 7 ETM+ Viewing Geometry Overview

The ETM+ instrument detectors are aligned in parallel rows on two separate focal planes: the primary focal plane, containing bands 1-4 and 8 (panchromatic), and the cold focal plane containing bands 5, 6, and 7. The primary focal plane is illuminated by the ETM+ scanning mirror, primary mirror, secondary mirror, and scan line corrector mirror. In addition to these optical elements, the cold focal plane optical train includes the relay folding mirror and the spherical relay mirror. This is depicted in Figure 1. The ETM+ scan mirror provides a nearly linear cross track scan motion which covers a 185 km wide swath on the ground. The scan line corrector compensates for the forward motion of the spacecraft and allows the scan mirror to produce usable data in both scan directions.

Within each focal plane, the rows of detectors from each band are separated in the along-scan (cross-track) direction. The odd and even detectors from each band are also separated slightly. The detector layout geometry is shown in Figure 3.1.1-2.. Samples from the ETM+ detectors are packaged into minor frames as they are collected (in time order) for downlink in the wideband data stream. Within each minor frame, the output from the odd detectors from bands 1-5, and 7 and all band 8 detectors are held at the beginning of the minor frame. The even detectors from bands 1-5, and 7 and all band 8 detectors are held at the midpoint of the minor frame. The even and odd detectors from band 6 are held at the beginning of alternate minor frames. The bands are nominally aligned during level 0R ground processing by delaying the even and odd detector samples from each band to account for the along-scan motion needed to view the same target point. These delays are implemented as two sets of fixed integer offsets for the even and odd detectors of each band--one set for forward scans and one set for reverse

scans. Two sets of offset delays are necessary since the band/detector sampling sequence with respect to a ground target is inverted for reverse scans. Level 0R ground processing also reverses the sample time sequence for reverse scans to provide nominal spatial alignment between forward and reverse scans.

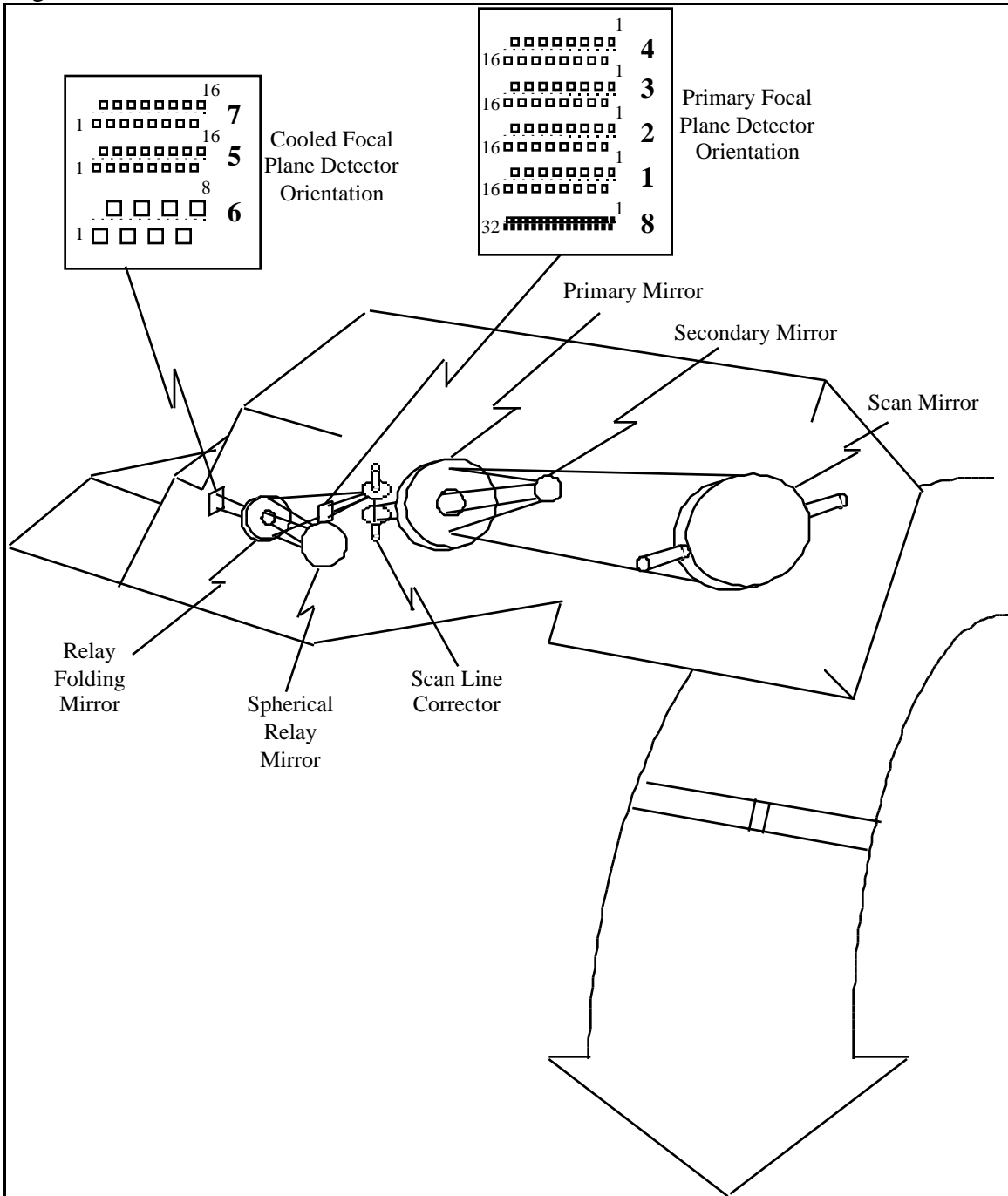


Figure 1 ETM+ Geometry Overview

The instrument's 15-degree field of view is swept over the ETM+ focal planes by the scan mirror. Each scan cycle, consisting of a forward and reverse scan, has a period of

142.245 milliseconds. The scan mirror period for a single forward or reverse scan is nominally 71.462 milliseconds. Of this time, approximately 60.743 milliseconds is devoted to the Earth viewing portion of the scan with 10.719 milliseconds devoted to the collection of calibration data and mirror turnaround. Within each scan, detector samples (minor frames) are collected every 9.611 microseconds (with two samples per minor frame for the 15 meter resolution panchromatic band). More detailed information on the ETM+ instrument's construction, operation, and pre-flight testing is provided in Reference 5.

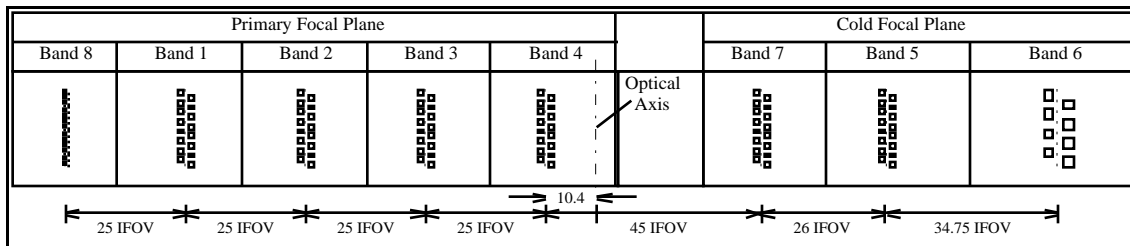


Figure 2 ETM+ Detector Array Ground Projection

The 15-degree instrument field of view sweeps out a ground swath approximately 185 kilometers wide. This swath is sampled 6,320 (nominally) times by the ETM+ 30-meter resolution bands. Since sixteen detectors from each 30-meter band are sampled in each data frame, the nominal scan width is 480 meters. The scan line corrector compensates for spacecraft motion during the scan to prevent excessive (more than 1 pixel) overlap or underlap at the scan edges. Despite this, the varying effects of Earth rotation and spacecraft altitude (both of which are functions of position in orbit) will lead to variations in the scan-to-scan gap observed.

3.1.2 Coordinate Systems

The coordinate systems used by the Landsat 7 system are described in detail in Reference 2. There are ten coordinate systems of interest for the Landsat 7 Image Assessment System geometric algorithms. These coordinate systems are referred to frequently in the remainder of this document and are briefly defined here to provide a context for the subsequent discussion. They are presented in the logical order in which they would be used to transform a detector and sample time into a ground position.

1. ETM+ Array Reference (Focal Plane) Coordinate System

The focal plane coordinate system is used to define the band and detector offsets from the instrument optical axis which are ultimately used to generate the image space viewing vectors for individual detector samples. It is defined so that the Z axis is along the optical axis and is positive toward the scan mirror. The origin is where the optical axis intersects the focal planes (see Figure 3). The X axis is parallel to the scan mirror's axis of rotation

and is in the along-track direction after a reflection off the scan mirror with the positive direction toward detector 1. The Y axis is in the focal plane's along-scan direction with the positive direction toward band 8. This definition deviates from the description in the Landsat 7 Program Coordinate System Standard document in that the origin is placed at the focal plane/optical axis intersection rather than at an arbitrary reference detector location.

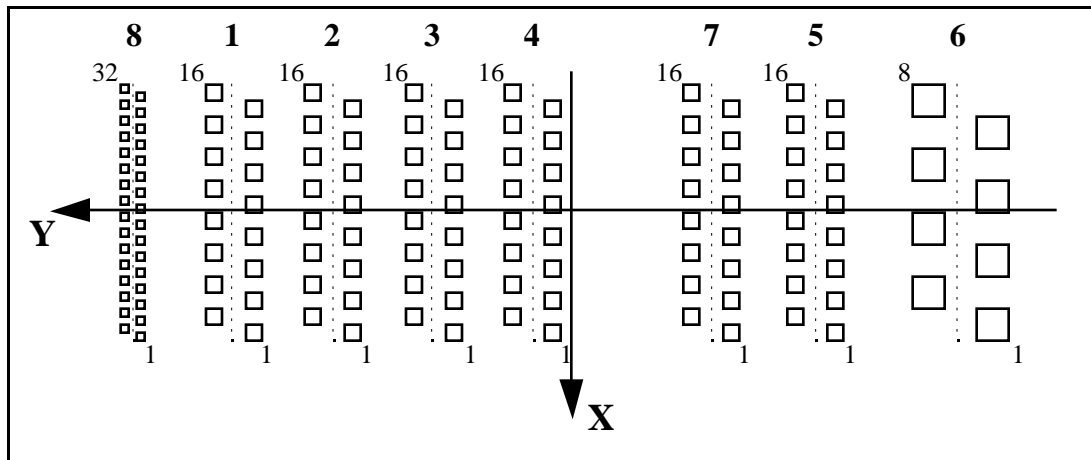


Figure 3 ETM+ Focal Plane Coordinate System

2. ETM+ Sensor Coordinate System

The scan mirror and scan line corrector models are defined in the sensor coordinate system. This is the coordinate system in which an image space vector, representing the line of sight from the center of a detector, and scan mirror and scan line corrector angles are converted to an object space viewing vector. The Z axis corresponds to the Z axis of the focal plane coordinate system (optical axis) after reflection off the scan mirror and is positive outward (toward the Earth). The X axis is parallel to the scan mirror axis of rotation and is positive in the along-track direction. The Y axis completes a right handed coordinate system. Scan mirror angles are rotations about the sensor X axis and are measured in the sensor Y-Z plane with the Z axis corresponding to a zero scan angle and positive angles toward the Y axis (west in descending mode). Scan line corrector angles are rotations about the sensor Y axis and are measured in the sensor X-Z plane with the Z axis corresponding to a zero scan line corrector angle and positive angles toward the X axis (the direction of flight). The sensor coordinate system is depicted in Figure 4. In this coordinate system, the scan line corrector performs a negative rotation (from a positive angle to a negative angle) on every scan while the scan mirror performs a positive to negative rotation for forward scans and a negative to positive rotation for reverse scans.

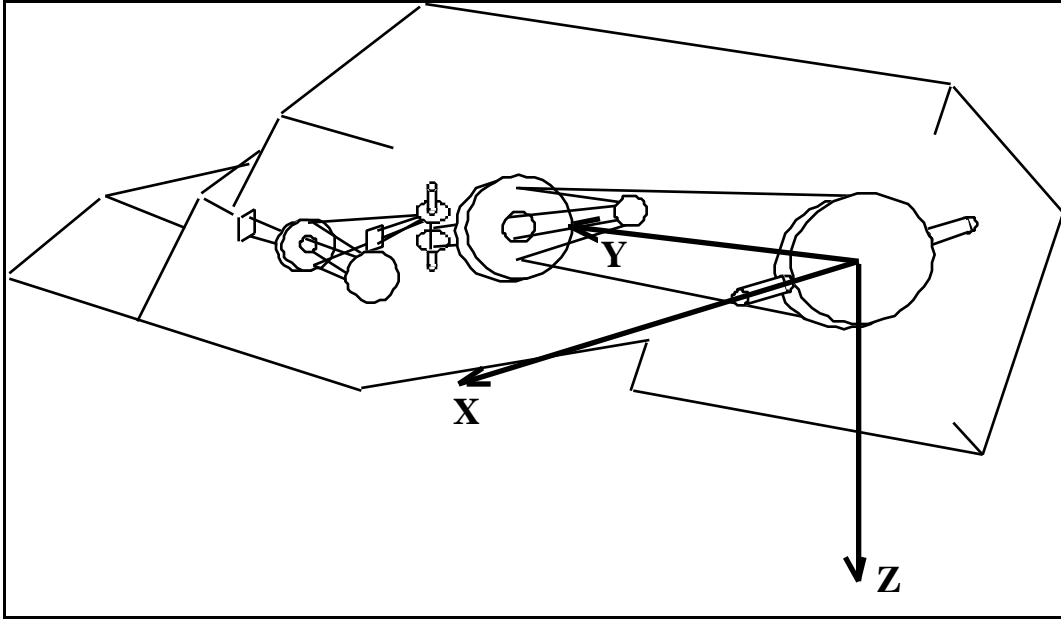


Figure 4 ETM+ Sensor Coordinate System

3. Navigation Reference Coordinate System

The navigation reference frame is the body-fixed coordinate system used for spacecraft attitude determination and control. The coordinate axes are defined by the spacecraft attitude control system (ACS) which attempts to keep the navigation reference frame aligned with the orbital coordinate system so that the ETM+ optical axis is always pointing toward the center of the Earth. It is the orientation of this coordinate system relative to the inertial coordinate system that is captured in the spacecraft attitude data.

4. Inertial Measurement Unit (IMU) Coordinate System

The spacecraft orientation data provided by the gyros in the inertial measurement unit are referenced to the IMU coordinate system. This coordinate system is nominally aligned with the navigation reference coordinate system. The actual alignment of the IMU with respect to the navigation reference will be measured pre-flight as part of the attitude control system calibration. This alignment transformation is used by the IAS to convert the gyro data contained in the Landsat 7 Payload Correction Data (PCD) to the navigation reference coordinate system for blending with the ACS quaternions and the Angular Displacement Assembly (ADA) jitter measurements.

5. Angular Displacement Assembly (ADA) Coordinate System

The high frequency angular displacements of the sensor line of sight (jitter) measured by the ADA are referenced to the ADA coordinate system. This reference frame is at a nominal 20-degree angle with respect to the sensor coordinate system, corresponding to a 20-degree rotation about the ADA X axis, which is nominally coincident with the sensor

X axis. The ADA output recorded in the Landsat 7 PCD is converted from the ADA coordinate system to the sensor coordinate system, using the ADA alignment matrix, and then to the navigation reference coordinate system (using the sensor alignment matrix) so that the high frequency jitter data can be combined with the low frequency gyro data to determine the actual ETM+ sensor line-of-sight pointing as a function of time.

6. Orbital Coordinate System

The orbital coordinate system is centered on the satellite, and its orientation is based on the spacecraft position in inertial space (see Figure 5). The origin is the spacecraft center of mass, with the Z axis pointing from the spacecraft center of mass to the Earth center of mass. The Y axis is the normalized cross product of the Z axis and the instantaneous (inertial) velocity vector, and corresponds to the negative of the instantaneous angular momentum vector direction. The X axis is the cross product of the Y and Z axes.

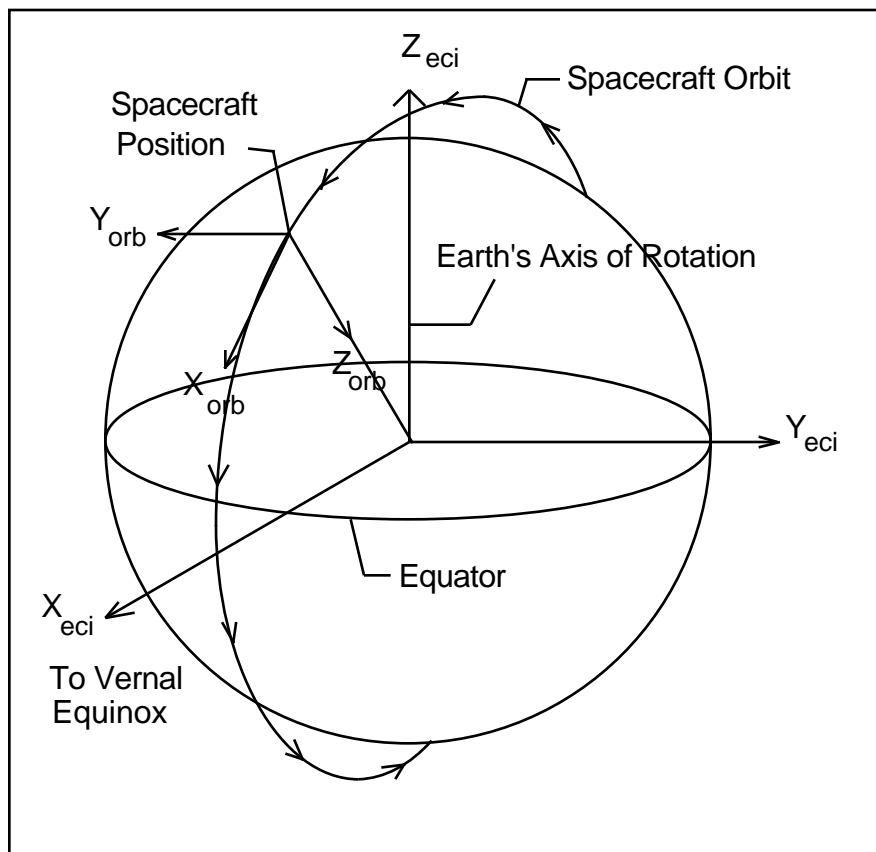


Figure 5 Orbital Coordinate System

7. Earth Centered Inertial (ECI) Coordinate System

The ECI coordinate system is space-fixed with its origin at the Earth's center of mass (see Figure 6). The Z axis corresponds to the mean north celestial pole of epoch J2000.0. The X axis is based on the mean vernal equinox of epoch J2000.0. The Y axis is the cross product of the Z and X axes. This coordinate system is described in detail in Reference 7 and in Reference 2. Data in the ECI coordinate system will be present in the Landsat 7 ETM+ Level 0R product in the form of ephemeris and attitude data contained in the spacecraft PCD.

Although the IAS uses J2000, there is some ambiguity in the existing Landsat 7 system documents which discuss the inertial coordinate system. Reference 2 states that the ephemeris and attitude data provided to and computed by the spacecraft on-board computer are referenced to the ECI True of Date (ECITOD) coordinate system (which is based on the celestial pole and vernal equinox of date rather than at epoch J2000.0). This appears to contradict Reference 1 which states that the ephemeris and attitude data contained in the Landsat 7 PCD (*i.e.*, from the spacecraft on-board computer) is referenced to J2000.0. The relationship between these two inertial coordinate systems consists of the slow variation in orientation due to nutation and precession. This is described in Reference 2 and 7.

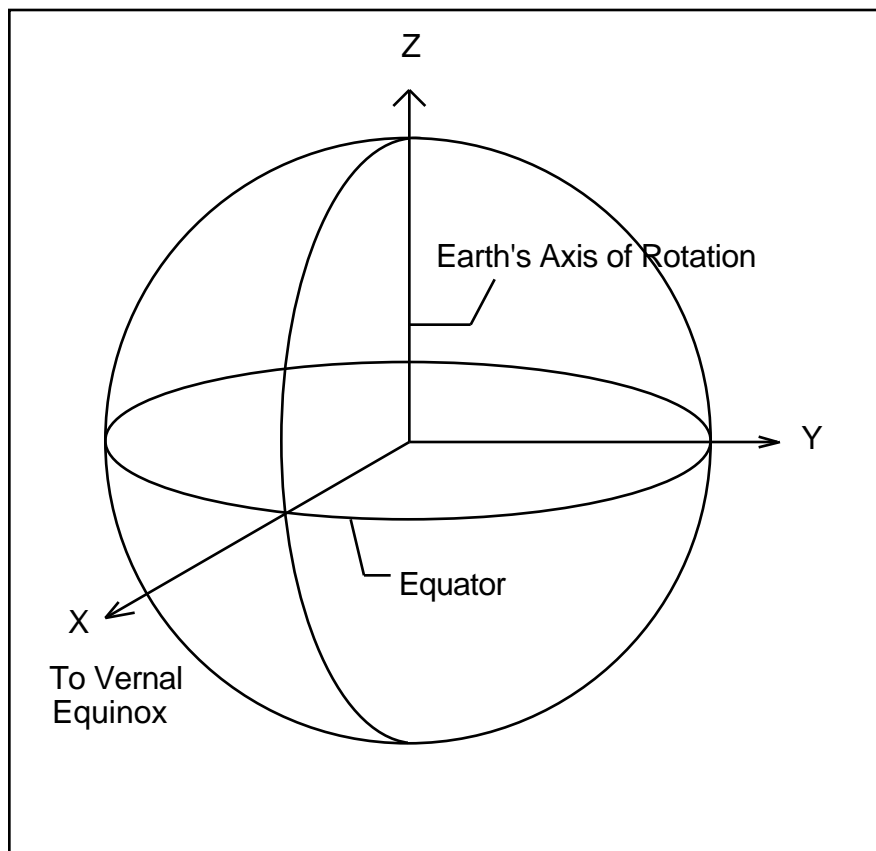
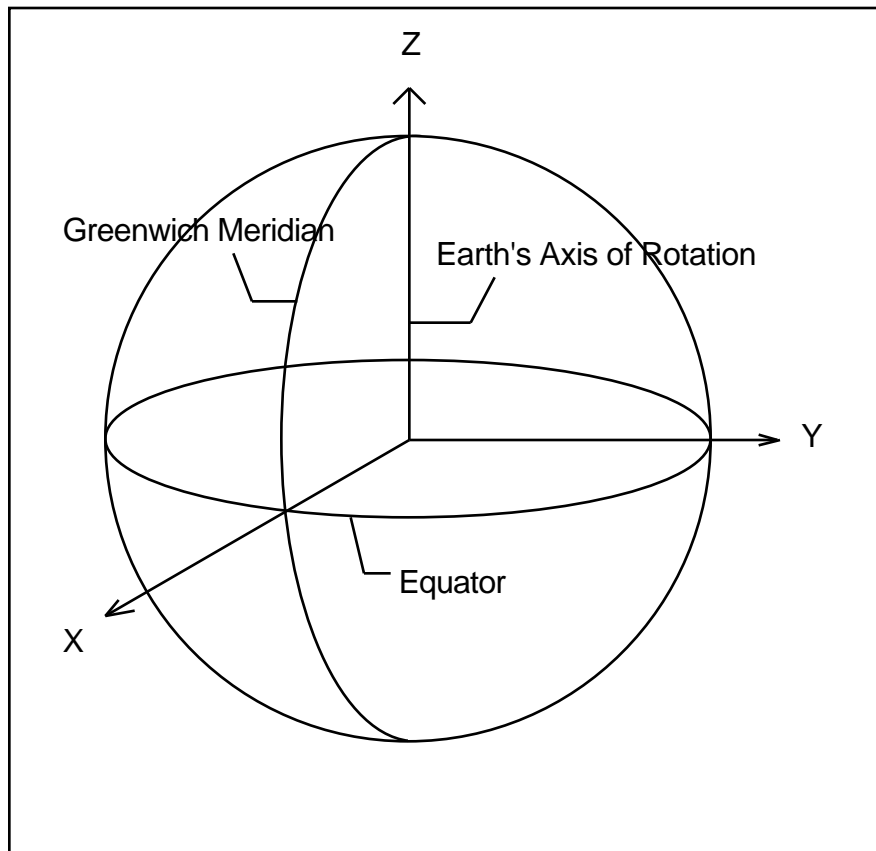


Figure 6 Earth Centered Inertial (ECI) Coordinate System

8. Earth Centered Rotating (ECR) Coordinate System

The ECR coordinate system is Earth-fixed with its origin at the center of mass of the Earth (see Figure 7). It corresponds to the Conventional Terrestrial System defined by the Bureau International de l'Heure (BIH) which is the same as the U. S. Department of Defense World Geodetic System 1984 (WGS84) geocentric reference system. This coordinate system is described in Reference 7.

**Figure 7 Earth Centered Rotating (ECR) Coordinate System**

9. Geodetic Coordinate System

The geodetic coordinate system is based on the WGS84 reference frame with coordinates expressed in latitude, longitude, and height above the reference Earth ellipsoid (see Figure 8). No ellipsoid is required by the definition of the ECR coordinate system, but the geodetic coordinate system depends on the selection of an Earth ellipsoid. Latitude and longitude are defined as the angle between the ellipsoid normal and its projection onto the equator, and the angle between the local meridian and the Greenwich meridian,

respectively. The scene center and scene corner coordinates in the Level 0R product metadata are expressed in the geodetic coordinate system.

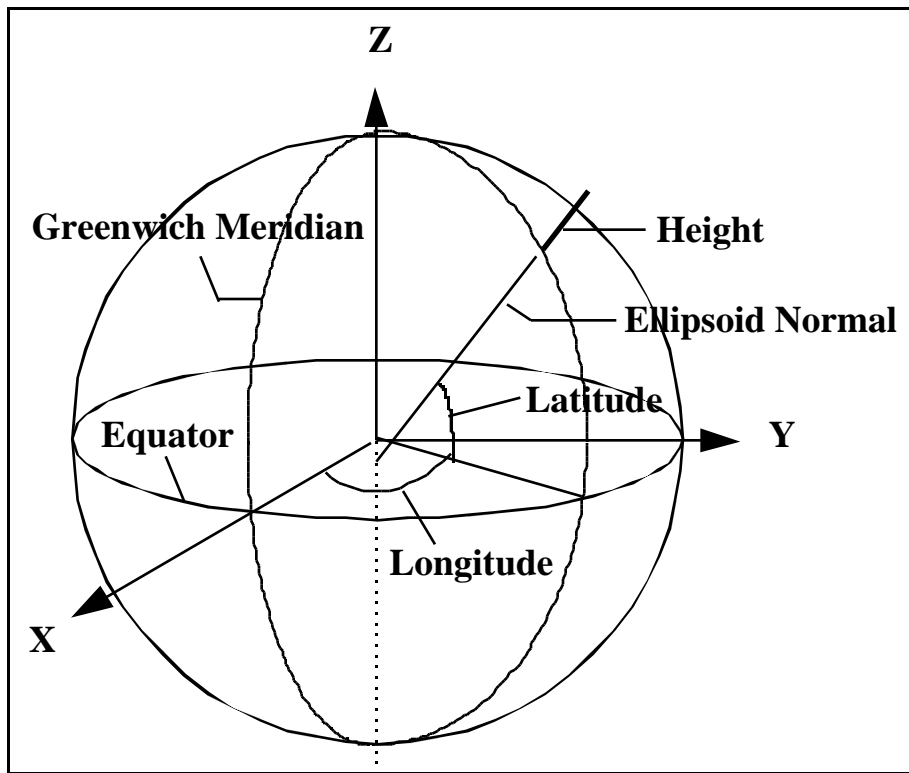


Figure 8 Geodetic Coordinate System

10. Map Projection Coordinate System

Level 1 products are generated with respect to a map projection coordinate system, such as Universal Transverse Mercator, which provides a mapping from latitude and longitude to a plane coordinate system which is an approximation to a Cartesian coordinate system for a portion of the Earth's surface. It is used for convenience as a method of providing the digital image data in an Earth-referenced grid that is compatible with other ground referenced data sets. Although the map projection coordinate system is only an approximation to a true local Cartesian coordinate system at the Earth's surface, the mathematical relationship between the map projection and geodetic coordinate systems is precisely and unambiguously defined; the map projections the IAS uses are described in Reference 8.

3.1.3 Coordinate Transformations

There are nine transformations between the ten coordinate systems used by the IAS geometric algorithms. These transformations are referred to frequently in the remainder of this document and are defined here. They are presented in the logical order in which a detector and sample number would be transformed into a ground position.

1. Focal Plane to Sensor

The relationship between the focal plane and sensor coordinate systems is a rapidly varying function of time, incorporating the scan mirror and scan line corrector models. The focal plane location of each detector from each band can be specified by a set of field angles in the focal plane coordinate system, as described in section 3.1.5.1.1. These are transformed to sensor coordinates based on the sampling time (sample/minor frame number from scan start) which is used to compute mirror and scan line corrector angles based on the models described in sections 3.1.5.1.2 and 3.1.5.1.3.

2. Sensor to Navigation Reference

The relationship between the sensor and navigation reference coordinate systems is described by the ETM+ instrument alignment matrix. The transformation from sensor coordinates to navigation reference coordinates is described in section 4.21 of Reference 2. It includes a three-dimensional rotation, implemented as a matrix multiplication, and an offset to account for the distance between the ACS reference and the instrument scan mirror. The transformation matrix will initially be defined to be fixed (non-time varying) with improved estimates being provided post-launch. Subsequent analysis may detect repeatable variations with time that can be effectively modeled, making this a (slowly) time-varying transformation. The nominal rotation matrix is the identity matrix.

3. IMU to Navigation Reference

The IMU coordinate system is related to the navigation reference coordinate system by the IMU alignment matrix which captures the orientation of the IMU axes with respect to the navigation base. This transformation is applied to gyro data prior to its integration with the ADA data and the ACS quaternions. The IMU alignment will be measured pre-flight and is nominally the identity matrix. This transformation is defined in section 4.22 of Reference 2.

4. ADA to Sensor

The angular displacement assembly (ADA) is nominally aligned with the sensor coordinate system with a 20-degree rotation about the X axis. The actual alignment will be measured pre-launch and will be used to rotate the ADA jitter observations into the sensor coordinate system, from which they can be further rotated into the navigation reference system using the sensor to navigation reference alignment matrix.

5. Navigation Reference to Orbital

The relationship between the navigation reference and orbital coordinate systems is defined by the spacecraft attitude. This transformation is a three-dimensional rotation matrix with the components of the rotation matrix being functions of the spacecraft roll,

pitch, and yaw attitude angles. The nature of the functions of roll, pitch, and yaw depends on the exact definition of these angles (*i.e.*, how they are generated by the attitude control system). In the initial model, it is assumed that the rotations are performed in the order roll-pitch-yaw as shown in section 4.17 of Reference 2. Since the spacecraft attitude is constantly changing, this transformation is time varying. The nominal rotation matrix is the identity matrix since the ACS strives to maintain the ETM+ instrument pointing toward the center of the Earth.

6. Orbital to ECI

The relationship between the orbital and ECI coordinate systems is based on the spacecraft's instantaneous ECI position and velocity vectors. The rotation matrix to convert from orbital to ECI can be constructed by forming the orbital coordinate system axes in ECI coordinates:

$$\begin{aligned}
 \mathbf{p} & \quad - && \text{spacecraft position vector in ECI} \\
 \mathbf{y} & \quad - && \text{spacecraft velocity vector in ECI} \\
 \mathbf{T}_{\text{eci/orb}} & \quad - && \text{rotation matrix from orbital to ECI} \\
 \\
 \mathbf{b}_3 & = -\mathbf{p} / |\mathbf{p}| && \text{(nadir vector direction)} \\
 \mathbf{b}_2 & = (\mathbf{b}_3 \times \mathbf{y}) / |\mathbf{b}_3 \times \mathbf{y}| && \text{(negative of angular momentum vector direction)} \\
 \mathbf{b}_1 & = \mathbf{b}_2 \times \mathbf{b}_3 && \text{(circular velocity vector direction)} \\
 \\
 \mathbf{T}_{\text{eci/orb}} & = [\mathbf{b}_1 \quad \mathbf{b}_2 \quad \mathbf{b}_3]
 \end{aligned}$$

7. ECI to ECR

The transformation from ECI to ECR coordinates is a time-varying rotation due primarily to Earth rotation, but also containing more slowly varying terms for precession, astronomic nutation, and polar wander. The ECI to ECR rotation matrix can be expressed as a composite of these transformations:

$$\mathbf{T}_{\text{ecr/eci}} = \mathbf{A} \mathbf{B} \mathbf{C} \mathbf{D}$$

A = Polar Motion

B = Sidereal Time

C = Astronomic Nutation

D = Precession

Each of these transformation terms is defined in Reference 2 and is described in detail in Reference 7.

8. ECR to Geodetic

The relationship between ECR and geodetic coordinates can be expressed simply in its direct form:

$$\begin{aligned}
 e^2 &= 1 - b^2 / a^2 \\
 N &= a / (1 - e^2 \sin^2(lat))^{1/2} \\
 X &= (N + h) \cos(lat) \cos(lon) \\
 Y &= (N + h) \cos(lat) \sin(lon) \\
 Z &= (N (1 - e^2) + h) \sin(lat)
 \end{aligned}$$

where:

X, Y, Z	-	ECR coordinates
lat, lon, h	-	Geodetic coordinates
N	-	Ellipsoid radius of curvature in the prime vertical
e^2	-	Ellipsoid eccentricity squared
a, b	-	Ellipsoid semi-major and semi-minor axes

The closed-form solution for the general inverse problem (which is the problem of interest here) involves the solution of a quadratic equation and is not typically used in practice. Instead, an iterative solution is used for latitude and height for points that do not lie on the ellipsoid surface. A procedure for performing this iterative calculation is described in section 6.4.3.3 of Reference 4.

9. Geodetic to Map Projection

The transformation from geodetic coordinates to the output map projection depends on the type of projection selected. The mathematics for the forward and inverse transformations for the Universal Transverse Mercator (UTM), Lambert Conformal Conic, Transverse Mercator, Oblique Mercator, Polyconic, Polar Stereo Graphic, and the Space Oblique Mercator (SOM) are given in Reference 8. Further details of the SOM mathematical development are presented in Reference 17.

3.1.4 Time Systems

Four time systems are of primary interest for the IAS geometric algorithms. These include: International Atomic Time (Temps Atomique International or TAI), Universal Time - Coordinated (UTC), Universal Time corrected for polar motion (UT1), and Spacecraft Time (the readout of the spacecraft clock, nominally coincident with UTC). Spacecraft Time is the time system applicable to the spacecraft time codes found in the Level 0R PCD and MSCD. UTC (which the spacecraft clock aspires to) is the standard reference for civil timekeeping. UTC is adjusted periodically by whole leap seconds to keep it within 0.9 seconds of UT1. UT1 is based on the actual rotation of the Earth and is needed to provide the transformation from stellar-referenced inertial coordinates (ECI)

to terrestrial-referenced Earth-fixed coordinates (ECR). TAI provides a uniform, continuous time stream which is not interrupted by leap seconds or other periodic adjustments. It provides a consistent reference for resolving ambiguities arising from the insertion of leap seconds into UTC (which can lead to consecutive seconds with the same UTC time). These and a variety of other time systems and their relationships are described in Reference 4. The significance of each of these four time systems with respect to the IAS geometric algorithms is described below.

1. Spacecraft Time

The Landsat 7 Mission Operations Center will attempt to maintain the on-board spacecraft clock time to within 145 milliseconds of UTC (Reference 5, section 3.7.1.3.16) by making clock updates nominally once per day during periods of ETM+ inactivity. Additionally, the spacecraft PCD includes a quadratic clock correction model which can be used to correct the spacecraft clock readout to within 15 milliseconds of UTC, according to Reference 1. The clock correction algorithm is:

$$\begin{aligned} dt &= t_{s/c} - t_{\text{update}} \\ t_{\text{UTC}} &= t_{s/c} + C_0 + C_1 dt + 0.5 C_2 dt^2 \end{aligned}$$

where:

dt	= spacecraft clock time since last update
t _{UTC}	= corrected spacecraft time (UTC +/- 15 milliseconds)
t _{s/c}	= spacecraft clock time
t _{update}	= spacecraft clock time of last ground commanded clock update
C ₀	= clock correction bias term
C ₁	= clock drift rate
C ₂	= clock drift acceleration

The Landsat 7 on-board computer is using corrected spacecraft clock data to interpolate the ephemeris data (which is inserted into the PCD) from the uplinked ephemeris (which is referenced to UTC). The residual clock error of 15 milliseconds (3 sigma) leads to an additional ephemeris position uncertainty of approximately 114 meters (3 sigma) which is included in the overall geodetic accuracy error budget. Since the time code readouts in both the PCD and MSCD are uncompensated, the clock correction algorithm must be applied on the ground to get the Level 0R time reference to within 15 milliseconds of UTC.

Note that if the on-board computer were not using the clock drift correction model for ephemeris interpolation the ground processing problem would become more complicated. Since the spacecraft time is used as a UTC index to interpolate the ephemeris points, the times associated with these ephemeris points are true UTC - they just do not correspond to the actual (corrected) UTC spacecraft time. In this case, the PCD time code errors of

up to 145 milliseconds would cause a temporal misregistration of the interpolated ephemeris and the associated orbital orientation reference coordinate system, relative to the spacecraft clock. In making the spacecraft clock corrections, the times associated with the ephemeris points would not be changed in recognition of the fact that they are interpolation indices against a UTC time reference.

2. UTC

As mentioned above, UTC is maintained within 0.9 seconds of UT1 by the occasional insertion of leap seconds. It is assumed that the insertion of leap seconds into the spacecraft clock will be performed on the appropriate dates as part of the daily clock update, and that this clock update will be coordinated with the ephemeris updates provided by the FDF, so that the spacecraft clock UTC epoch is the same as the FDF provided ephemeris UTC epoch. Although for any given scene or sub-interval UTC provides a uniform time reference, it will be beneficial for the IAS to have access to a table of leap seconds relating UTC to TAI to support time-related problem tracking and resolution. This information will be obtained from the National Earth Orientation Service (NEOS) web site at <http://maia.usno.navy.mil>.

3. UT1

UT1 represents time with respect to the actual rotation of the Earth, and is used by the IAS algorithms which transform inertial ECI coordinates or lines of sight to Earth-fixed ECR coordinates. Failure to account for the difference between UT1 and UTC in these algorithms can lead to ground position errors as large as 400 meters at the equator (assuming the maximum 0.9 second UT1 - UTC difference). The UT1 - UTC correction typically varies at the rate of approximately 2 milliseconds per day, corresponding to an Earth rotation error of about 1 meter. Thus, UT1 - UTC corrections should be interpolated or predicted to the actual image acquisition time to avoid introducing errors of this magnitude. This information will be obtained from the National Earth Orientation Service (NEOS) web site at <http://maia.usno.navy.mil>.

4. TAI

Although none of the IAS algorithms are being designed to use TAI in normal operations it is included here for completeness. As mentioned above, there is the potential for system anomalies to be introduced as a result of timing errors, particularly in the vicinity of UTC leap seconds. The ability to use TAI as a standard reference which can be related to UTC and spacecraft time using a leap second file, will assist IAS operations staff in anomaly resolution. For this reason, although there are no IAS software requirements for a leap second reference it is strongly recommended that access be provided to the ECS SDP Toolkit leap second file.

3.1.5 Mathematical Description of Algorithms

3.1.5.1 ETM+ Instrument Model

3.1.5.1.1 Detector/Focal Plane Geometry

The location of each detector for each band is described in the ETM+ array reference coordinate system by using a pair of angles, one in the along-scan, or coordinate Y, direction and one in the across-scan, or coordinate X, direction. In implementing the IAS level 1 processing algorithm, each of these angles is separated into two parts: the ideal band/detector locations used to model the relationship between the sensor image space and ground object space, and the sub-pixel offsets unique to each detector which are applied during the image resampling process. This approach makes it possible to construct a single analytical model for each band from which nominal detector projections can be interpolated and then refined during resampling, rather than performing the image to ground projection computation for each detector. The capability to rigorously project each detector, including all sub-pixel detector placement and timing offsets, has been developed to support geometric characterization and calibration.

Along-scan angles are modeled as the sum of the band odd detector angle from the optical axis, common to all detectors for one band, and the sub-pixel offset and time delay unique to each detector within the band. Note that the IAS algorithms assume that the angular displacement between even and odd detectors in each band is exactly compensated for by the time delay used to nominally align the even and odd detectors. Band center location angles, relative to the sensor optical axis, are stored in the Calibration Parameter File. The odd detector offset from band center (1.25 IFOVs for the 30 meter bands) is subtracted from the band center angle to yield the nominal detector locations. The along-scan angle is computed as:

$$\text{along_angle} = \text{bandoff_along}[\text{BAND}] - \text{odd_det_off}[\text{BAND}]$$

where:

- along_angle = nominal along-scan location of detector
- bandoff_along = along-scan band center offset (indexed by band)
- BAND = band number (1..8)
- odd_det_off = odd detector offset from band center (indexed by band)

The individual detector offsets from their ideal locations are stored in the Calibration Parameter File in the form of detector delays which incorporate both sample timing offsets and detector along-scan positioning errors. These sub-pixel corrections are applied during the image resampling process.

Similarly, the across-scan angles are separated into the nominal detector location component, used for line of sight construction and projection, and the sub-pixel detector placement corrections unique to each detector, applied during resampling. The nominal detector location is computed as:

$$\text{cross_angle} = \text{bandoff_cross}[\text{BAND}] + ((\text{ndets}[\text{BAND}] + 1) / 2 - N) * \text{IFOV}[\text{BAND}]$$

where:

cross_angle	= nominal across-scan location of detector N
bandoff_cross	= across-scan band center offset (indexed by band)
BAND	= band number (1..8)
ndets	= number of detectors in band (indexed by band)
N	= detector number (1..ndets)
IFOV	= detector angular field of view (indexed by band)

Using these nominal detector locations in the line of sight projection computations makes it possible to rigorously project the first and last detectors in each band and to interpolate the image space to ground space transformation for the interior detectors. This reduces the computational load in level 1 processing where the unique sub-pixel detector placement corrections are applied by the resampling algorithm. To precisely project an individual detector to ground space, the sub-pixel along-scan and across-scan corrections are added to the nominal detector location.

3.1.5.1.2 Scan Mirror Model

The ETM+ scan mirror rotates about the sensor X axis providing nearly linear motion in the along-scan direction in both the forward and reverse directions. The scan mirror's departure from linear motion is characterized pre-launch using a set of fifth-order polynomials which model the repeatable acceleration and deceleration deviations from linearity for forward and reverse scans. This fifth-order polynomial is then adjusted for high frequency roll jitter components using ADS data from the PCD. Fifth-order mirror polynomials are also used to model the across-scan mirror deviation for forward and reverse scans. Thus, a total of four fifth-order polynomials characterize the scan mirror's repeatable deviation from nominal linear scanning: 1) along-scan deviation for forward scans, 2) across-scan deviation for forward scans, 3) along-scan deviation for reverse scans, and 4) across-scan deviation for reverse scans. This set of four polynomials constitutes the nonlinear portion of the scan mirror profile.

The ETM+ instrument contains two sets of Scan Mirror Electronics (SME) used to control the mirror motion. Either SME can be used to drive the mirror in either of its operational modes, Scan Angle Monitor (SAM) mode or Bumper mode. For each mode, each set of SME exhibits a characteristic set of mirror profile polynomials as well as scan

start and scan stop mirror angles. This leads to a total of four sets of mirror profile polynomials: 1) SME1 SAM mode, 2) SME2 SAM mode, 3) SME1 Bumper mode, and 4) SME2 Bumper mode. The appropriate mirror profile coefficients and scan start/stop angles must be selected for a particular data set based on the SME and mode settings in the PCD.

Within each scan, the scan mirror assembly measures the deviation from the nominal time of scan from scan start to mid-scan (first half scan error), and from mid-scan to scan stop (second half scan error) and records this information in the scan line data minor frames for the following scan. These scan time errors are measured as departures from nominal, in counts, with each count being 0.18845 microseconds.

The first half and second half scan errors are used to correct the nominal scan profile by adjusting the fifth-order along-scan polynomial to compensate for the actual mid-scan and end of scan times. This correction is applied by rescaling the polynomial coefficients to the actual scan time and by computing correction coefficients which are added to the linear and quadratic terms in the fifth-order polynomial. The calculation procedure is given in section 3.1.5.3.3.

3.1.5.1.3 Scan Line Corrector Mirror Model

The Scan Line Corrector (SLC) mirror rotates the ETM+ line of sight about the sensor Y axis to compensate for the spacecraft's along track motion during the scanning interval. Although the IAS algorithms support fifth-order correction polynomials for the SLC profile, in practice, no significant SLC non-linearity has been observed for Landsats 4, 5, and 6. Refer to section 3.1.5.3.4 for more information on the Scan Line Corrector Mirror Model.

3.1.5.2 Landsat 7 Platform Model

3.1.5.2.1 Sensor Pointing (Attitude and Jitter) Model

Sensor line of sight vectors constructed using the ETM+ instrument model must be related to object (ground) space by determining the orientation and position of the sensor coordinate system with respect to object space (ECI coordinates) as a function of time. The sensor orientation is determined using the sensor pointing model which includes the effects of sensor to spacecraft (navigation reference base) alignment, spacecraft attitude as determined by the on-board computer using the inertial measurement unit gyros and star sightings, and the high frequency attitude variations (jitter) measured by the angular displacement assembly. The inputs to this model are the attitude quaternions, gyro drift estimates, raw gyro outputs, and ADS outputs contained in the Payload Correction Data, and the sensor alignment matrix measured pre-launch and updated in flight by the Image

Assessment System using the sensor alignment calibration algorithm described in section 3.1.5.4.1.

The Landsat 7 attitude control system outputs estimates of the spacecraft attitude every PCD major frame (4.096 seconds). These estimates are provided in the form of attitude quaternions which describe the orientation of the spacecraft navigation reference system with respect to the ECI (J2000) coordinate system. These estimates are derived from the IMU gyro data combined with periodic star transit observations from the Celestial Sensor Assembly. As a byproduct of the integration of the gyro and star tracker observations the ACS also computes estimates of the gyro drift rates. A gyro drift rate estimate is also included in each PCD major frame, but only changes after a star sighting.

The raw outputs from each of the three gyro axes are recorded in the PCD every 64 milliseconds. In Landsats 4, 5, and 6 there was a 28 millisecond delay between the gyro sampling time and the PCD major frame start time (*i.e.*, gyro sampling was indexed from PCD start time - 28 milliseconds). From Reference 1, it appears that this offset does not apply for Landsat 7. The 15.625 Hertz gyro sampling rate is not sufficient to capture the high frequency spacecraft angular dynamic displacement (jitter). This sampling frequency will capture attitude variations up to the Nyquist frequency of 7.8125 Hz but will alias the higher frequencies to the extent the gyros respond to these higher frequencies. This response is expressed in the IMU transfer functions. For Landsats 4 and 5, the transfer functions for each IMU axis were taken to be the same.

The high frequency jitter information is measured by the angular displacement sensors (ADS) which are sampled at 2 millisecond intervals and are sensitive to frequency components between approximately 2 Hz and 125 Hz. Like the gyros, the ADS samples are offset from the PCD major frame start time. Unlike the gyros, the ADS axes are sampled at different times. The ADS samples begin at the PCD major frame time plus 375 microseconds for the X axis, plus 875 microseconds for the Y axis, and plus 1375 microseconds for the Z axis. The 500 Hz ADS sampling frequency could capture jitter frequencies up to 250 Hz, but the output of the ADS is band-limited to the maximum expected frequency of 125 Hz by a pre-sampling filter. Historically, the three ADS axes have had different transfer functions. For Landsats 4 and 5, the ADS transfer functions were not separated from the pre-sampling filter but were provided as a net response. For Landsat 6, the pre-sampling filter transfer function was provided separately.

The gyro and ADS transfer functions are used to blend the gyro/attitude and ADS/jitter data in the frequency region where their pass bands overlap from 2 to 7 Hz. The IAS uses the classical approach defined by Sehn and Miller (see Reference 10) to construct the crossover filters used to combine the gyro and ADS data. This is described in more detail in section 3.1.5.3.3.1.

3.1.5.2.2 Platform Position and Velocity

The spacecraft state vectors contained in the Payload Correction Data stream provide position and velocity information, in the Earth Centered Inertial of epoch J2000 coordinate system, every PCD major frame (unlike earlier Landsats which only provided new state vectors every other major frame). These state vectors are interpolated on-board using the uplinked predicted ephemeris, and may contain significant errors. Gross blunders (*i.e.*, transmission errors) are detected and removed during PCD pre-processing. The systematic errors which accumulate in the predicted ephemeris are estimated and removed as part of the Precision Correction algorithm described in section 3.1.5.3.8.

3.1.5.3 Level 1 Processing Algorithms

The diagrams that follow describe the high-level processing flows for the IAS level-1 processing algorithms. Figure 3.1.5-1 describes the process involved in initialization and creation of the Landsat 7 geometry model. Figure 3.1.5-2 shows the process of creating a geometric correction grid and the application of that grid in the resampling process. Figure 3.1.5-3 describes the process of refining the Landsat 7 geometry model with ground control, resulting in a precision geometry model. Figure 3.1.5-4 again describes the creation of a geometric correction grid (this time precision), and resampling with terrain correction.

Detailed algorithms for each of main process boxes in these diagrams are given in the sections that follow.

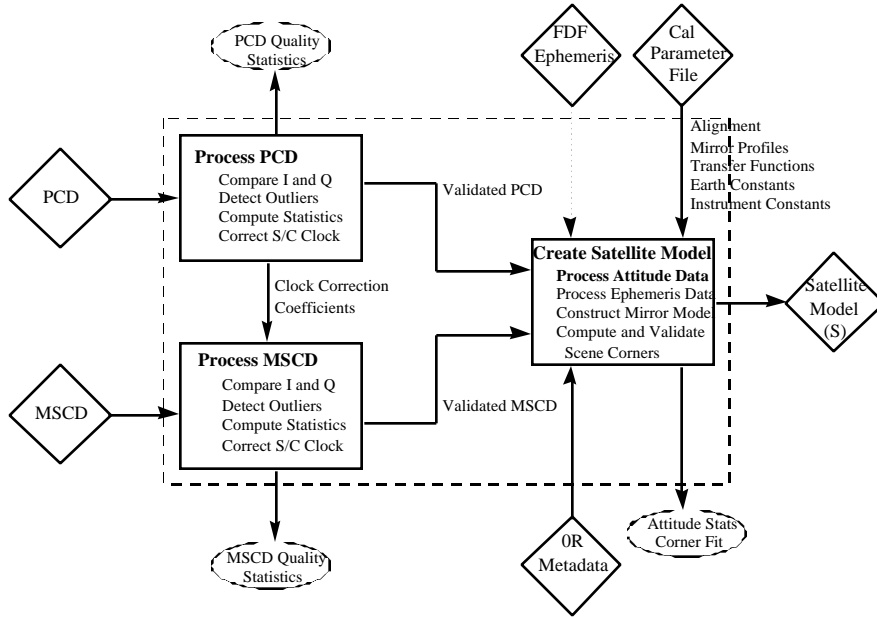


Figure 3.1.5- 1 Model Initialization

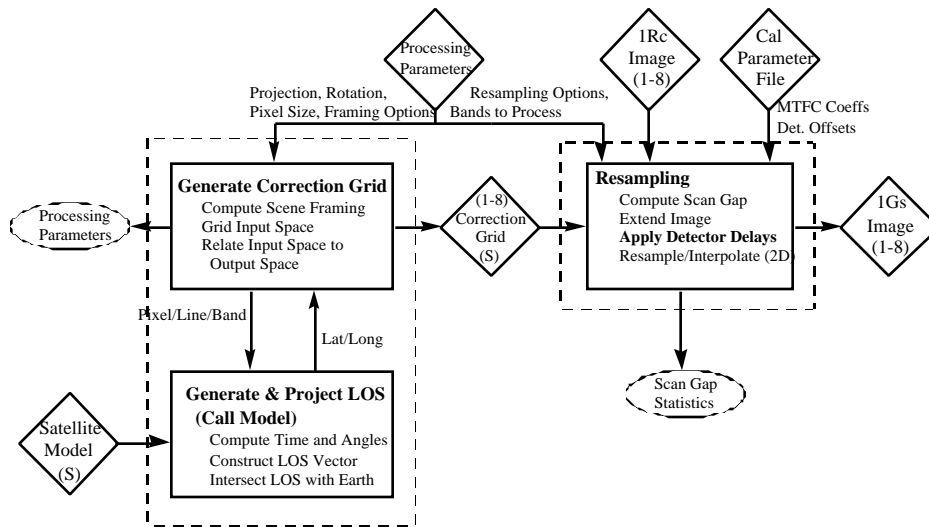


Figure 3.1.5- 2 Rectification and Resampling

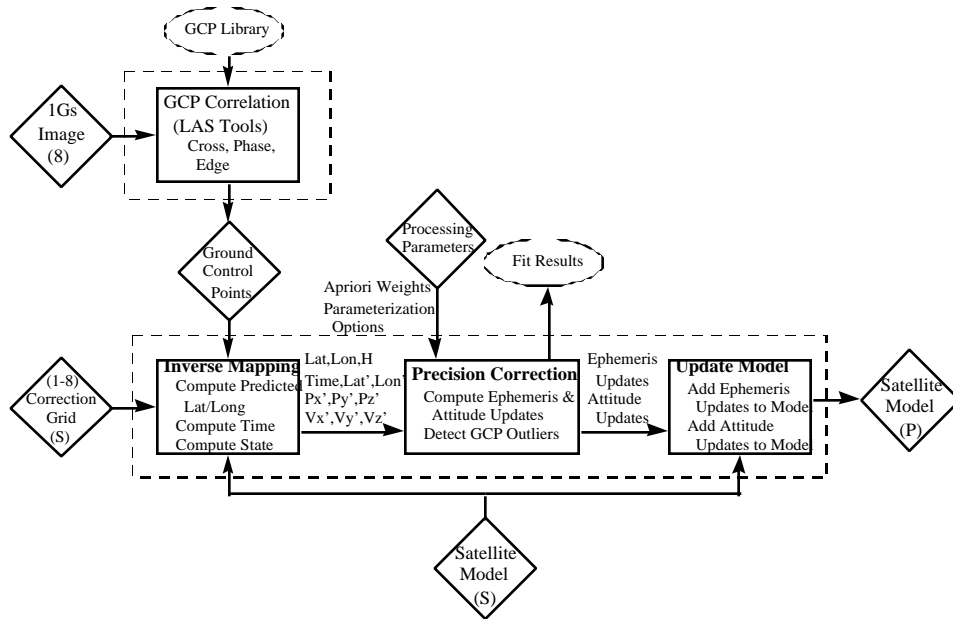


Figure 3.1.5- 3 Precision Correction Solution

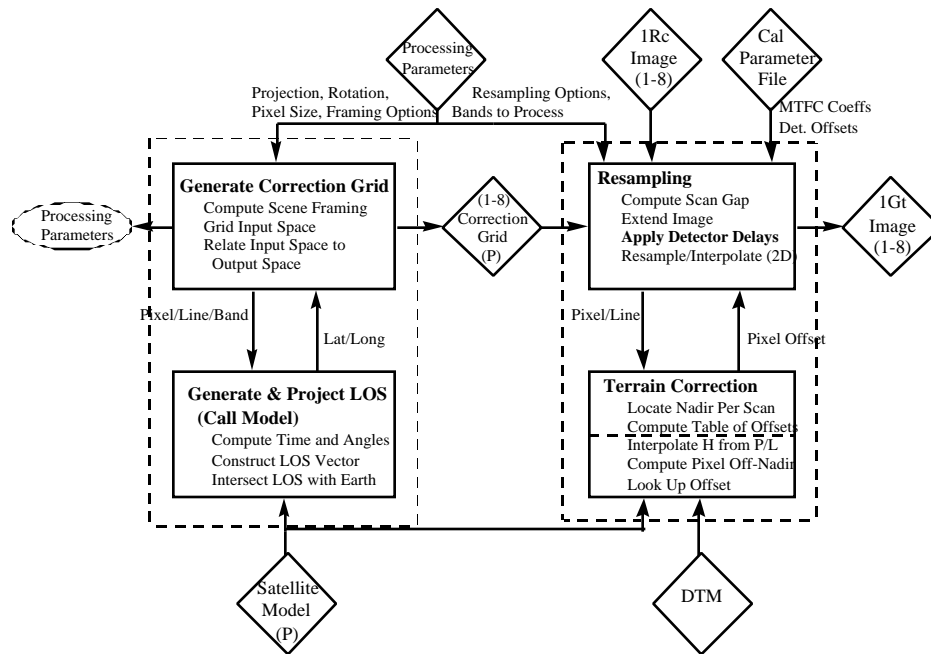


Figure 3.1.5- 4 Precision/Terrain Correction

3.1.5.3.1 PCD Processing

The PCD contains information on the state of the satellite and sensor. The PCD information is transmitted in both the In-Phase (I) and Quadrature (Q) channels of the wide-band data. The two PCD data streams are converted to engineering units and stored in the HDF format for the Level 0R product. The I channel is used as the default PCD for processing. The PCD is recorded for the entire sub-interval or full interval. The PCD information required for geometric processing includes: the ephemeris, the spacecraft attitude, the gyro data, the gyro drift rate data, the ADS data, the SME flag, the gyro unit flag, and the spacecraft clock corrections. The ephemeris and spacecraft attitude are updated every major frame, the gyro data is updated 64 times per axis in a major frame, and the ADS is updated 2048 times per axis in a major frame. There are 4 PCD major frames in a PCD cycle. Also included in the PCD are housekeeping values.

Validate Ephemeris Data

The PCD is transmitted in both the I and Q channels of the telemetry data. Under normal conditions, the I and Q channels should be identical. Therefore, a comparison between the ephemeris values contained in the I and Q channels is used as one of the validation tests. Any differences detected are flagged and reported in the processing history file. The I channel is assumed to be correct unless the other validation checks determine it to be in error.

The Landsat 7 orbit's semi-major axis, inclination and angular momentum calculated from the ephemeris data should not deviate substantially from their nominal values. A second validation compares these values to their nominal values and any large deviations are flagged. If a large deviation is detected, the Q channel's values are checked. If the Q channel values are correct, they are used instead of the I channel values. The ephemeris points that do not pass the I and Q channel tests are not used in the interpolation routine. The average and the standard deviation from the nominal value for the semi-major axis, inclination and angular momentum for the scene to be processed are saved for trending. The equations to calculate the satellite's semi-major axis, inclination, and angular momentum are as follows:

$$\text{Angular momentum} = | \mathbf{R} \times \mathbf{V} |$$

where \mathbf{R} is the satellite's position vector and \mathbf{V} is the satellite's velocity vector

$$\text{Inclination} = \text{acos}(|\mathbf{H} \cdot \mathbf{k}| / |\mathbf{H}|)$$

where $\mathbf{H} = \mathbf{R} \times \mathbf{V}$ and \mathbf{k} is the unit vector in the z-direction.

$$\text{Semi-major axis} = -\mu / (2.0 * E)$$

where $E = |\mathbf{V}|^2 / 2.0 - \mu / |\mathbf{R}|$ and $\mu = G * M$, where G is the Earth's gravity constant and M is the mass of the Earth.

Validate Spacecraft Attitude Data

The on-board computer (OBC) calculates a flight segment attitude estimate every 512 milliseconds. The OBC outputs one of eight sets of spacecraft attitude data in the telemetry every 4.096 seconds. The attitude information is output in the form of Euler parameters that specify the vehicle attitude relative to the Earth-centered inertial frame (J2000). The spacecraft's attitude is calculated using star crossings, gyro data and ADS data. Care must be taken when using the spacecraft's attitude data, because star crossing updates may cause discontinuities. The IAS converts the Euler parameters to roll, pitch, and yaw to be used in the model.

The I and Q channel values are compared and any differences flagged. The spacecraft's attitude data should not deviate greatly from a calculated value which was found using a linear interpolation of the values around the value to be checked. The linear interpolated value will be used to validate the spacecraft's attitude. Any large deviations are flagged. If a large deviation is detected, the Q channel is validated. If the Q channel value passes the validation test, it will be used instead of the I channel's value. If the attitude data in both the I and Q channels have large deviations, the interpolated value is used. The Euler parameters should satisfy the following equation.

$$EPA_1^2 + EPA_2^2 + EPA_3^2 + EPA_4^2 = 1 +/-$$

where EPA_1 , EPA_2 , EPA_3 , and EPA_4 are the Euler parameters which have been converted by the LPS. The \pm is some very small error term due to system noise.

The I channel values are validated using the above equation and any deviation is flagged. If a deviation occurs, the Q channel values are checked. If both channels fail the validation test, the interpolated value for each of the Euler parameters will be used.

The averages and standard deviations of the Euler parameters and the deviation from the equation above are stored for trending.

Validate Gyro Data

The I and Q channel values are compared and any differences flagged. The gyro data should not deviate greatly from a calculated value. This calculated value is found using a forward and backward differencing of the values around the value in question. The steps involved are:

- 1) Check the current gyro value against a tolerance.
- 2) Do a forward prediction for each point using the two previous points. Compare this predicted value against observed value.
- 3) Do a backward prediction for each point using the next two points. Compare this predicted value against observed value.

Any point that passes (1) and either (2) or (3) is a good point. If a deviation is detected in the I channel, the Q channel is checked. If the Q channel passes the validation test, it is used in the processing. If both the I and Q channel values fail, the value in question is flagged as an outlier. Once all values are checked the flagged values are replaced. Linear interpolation is used to replace all outliers. The first valid points before and after the outlier are found. These two values are then used to interpolate all outliers that lie in between. *Note: Care must be taken to account for counter resets in this check. The register resets after $(2^{23} - 1)$ positive and -2^{23} negative.*

Validate Gyro Drift Data

The I and Q channel values are compared and any deviations are flagged. The values for each major frame are compared. Any changes in the I channel are compared to the values in the Q channel to determine if the changes have occurred in the Q channel. If both channels display the same change and the change is determined to be within an acceptable level, then it is assumed that a star sighting has occurred. The PCD major frame that displays the change is flagged and the magnitude of the change is saved for trending.

Validate ADS Data

The I and Q channel values are compared and any differences flagged. The ADS data should not deviate greatly from a calculated value which was found using a linear interpolation of the values around the value in question. Any large deviations from the calculated value are flagged. If a large deviation is detected, the Q channel value is checked using the same interpolation method. If the Q channel's value passes the validation test, the Q channel's value replaces the I channel's value. If both channels fail the test, the value in question is corrected using the interpolated value.

The Linear interpolation test has been verified using an empirical test of Landsat 5 data. The results showed that the difference between linear predicted and actual ADS data points are typically within 10 counts. For a test scene over Iowa, once 5 actual outliers were removed which had deviations of several thousand counts, the maximum deviations in roll, pitch, and yaw were 12, 11, and 11 counts, respectively.

Validate Spacecraft Time Correction

The I and Q channels values are compared and any differences flagged; the number of occurrences will be saved for trending. The Mission Operations center will attempt to maintain the on-board spacecraft clock to 145 milliseconds. A validation test will calculate the correction of the clock and this value should not exceed the 145 millisecond value. If the absolute value of the clock correction is much greater than 145 milliseconds, the Q channel values are checked. If the Q channel clock correction values are less than 145 milliseconds, the Q channel's values are used. If both the I and Q channel values are greater than 145 milliseconds, then the clock coefficients are set to zero.

The clock correction is:

$$\text{dt} = \text{spacecraft time} - \text{clock update time}$$

$$\text{ClockCorrection}_t = \text{TimeCoef1}_I + \text{TimeCoef2}_I * \text{dt} + 0.5 * \text{TimeCoef3}_I * \text{dt}^2$$

Validate and Save Instrument Time On

The I and Q channels values for the instrument on-time are compared. Any differences are flagged and the values saved. The difference between the instrument on time and the start of the first major frame is saved for trending and analysis.

Correct PCD Spacecraft Time

Add the clock correction to the major frame times.

Other Geometric PCD Parameter Validations

Other PCD geometric processing parameters, such as the SME mode and gyro unit flags are validated by comparing the I and Q channel values. Any differences are flagged and reported. The I channel is used as the default value.

3.1.5.3.2 MSCD Processing

For Landsat 7, the MSCD data is contained in the HDF formatted Level-0R product. The counted line length, scan direction, First Half Scan Error (FHSERR) and Second Half Scan Error (SHSERR) are associated with the previous scan. The scan start time is, however, for the current scan. Due to the counted line length, scan direction, FHSERR and SHSERR being associated with the previous scan, the number of MSCD records must be one more than the number of scans. The MSCD for the output product is subsetted to match the imagery when the L0R product is generated.

The values from the MSCD required for ETM+ processing are:

- FHSERR (First Half Scan Error)
- SHSERR (Second Half Scan Error)
- Scan Direction

Scan Start Time
Counted line length

Validate Scan Direction

The I and Q channels are checked for consistency and any differences are flagged and reported in the processing history file. The IAS assumes the I channel has the correct value.

The flag for scan direction is a 1 or a 0. The scan direction is for the previous scan. The validation test checks the first scan direction flag and the direction flags there after. Any errors in the direction flags are corrected using the first valid direction flag as a reference. The errors are flagged and reported in the processing history file and are also saved for trending analysis.

Validate FHSERR and SHSERR

The MSCD is transmitted in both the I and Q channels of the telemetry data. Under normal conditions the I and Q channels should be identical. Therefore, a comparison of the FHSERR and SHSERR values contained in the I and Q channels will be used as one of the validation tests. Any differences detected are flagged and reported in the processing history file. The I channel is assumed to be correct unless the other validation check determines it to be in error.

The FHSERR and SHSERR values should not deviate greatly from their nominal values. Once these nominal values for the FHSERR and SHSERR have been characterized, the FHSERR and SHSERR are checked for deviations from their nominal value. Large deviations are flagged and the average difference and its standard deviation are saved for trending. If a large deviation is detected, the Q channel is validated. If the Q channel passes the validation check, the Q channel value is used in processing.

Validate Scan Start Time

The I and Q channels are checked for consistency and any differences are flagged and reported in the processing history file. The IAS assumes the I channel has the correct value.

The difference in time between start of scan times should not vary greatly from the nominal value. The start of scan time is validated by comparing the difference in time between scans. Any large variation from nominal is flagged and the Q channel is checked for its difference between start times. If the Q channel values pass the validation check, it will be used during processing. Otherwise, the scan start time is corrected using the

nominal value. The average difference and the standard deviation between the scans times for the scene being processed are saved for trending.

Validate Counted Line Length

The I and Q channel values are compared and any differences are flagged and reported in the processing history file. The IAS will assume the I channel has the correct value.

The counted line length is the number of minor frames sampled from the start of scan to the end of scan mark. The counted line length should be the same as the truncated calculated line length which is found using the FHSERR, SHSERR, DWELLTIME (and the conversion of counts to seconds). The counted line length should not deviate greatly from its nominal value. The validation algorithm for the counted line length checks the deviation of the counted line length from its nominal value and its deviation from the truncated calculated line length. Large deviations from the nominal counted line length and any deviation from the calculated line length are flagged. If a large deviation is detected, the Q channel counted line length is compared to the calculated line length and if it passes, the Q channel is used in the processing. The average counted line length and standard deviation of the counted line length are saved for trending.

Calculate the first half scan time, the second half scan time, and the total scan time using:

For each forward scan:

$$\begin{aligned} \text{first_half_time} &= T_{\text{fhf}} - \text{FHSERR} * T_{\text{unit}} \\ \text{second_half_time} &= T_{\text{shf}} - \text{SHSERR} * T_{\text{unit}} \\ \text{total_scan_time} &= \text{first_half_time} + \text{second_half_time} \end{aligned}$$

For each reverse scan:

$$\begin{aligned} \text{first_half_time} &= T_{\text{fhr}} - \text{FHSERR} * T_{\text{unit}} \\ \text{second_half_time} &= T_{\text{shr}} - \text{SHSERR} * T_{\text{unit}} \\ \text{total_scan_time} &= \text{first_half_time} + \text{second_half_time} \end{aligned}$$

Calculate the line length using:

$$\text{calculated_line_length} = \text{total_scan_time} / \text{DWELLTIME}$$

where:

T_{fhf}	The forward nominal first half scan time
T_{shf}	The forward nominal second half scan time
T_{fhr}	The reverse nominal first half scan time
T_{shr}	The reverse nominal second half scan time
T_{unit}	The conversion factor from counts to time

Correct Spacecraft Time in the MSCD

The correction value for the spacecraft time is found in the process PCD module. This value must be added to the MSCD start of scan times.

3.1.5.3.3 Platform/Sensor Model Creation

The Platform/Sensor model creation algorithm reads the telemetry data from the PCD and the MSCD. These data are converted to a form which is usable by the geometric model. The gyro and ADS data are combined and converted to the common Navigational Reference Base system to create a time ordered table of attitude information. The ephemeris data is converted to the ECEF coordinate system and fit with a polynomial which is a function of time. The mirror scan 5th order polynomial is corrected for each scan's variation in velocity.

Calculate Satellite State Vector

Transformation from J2000.0 system to the Earth Fixed system: For each valid ephemeris data point, the following coordinate transformation is used to convert the satellite position and velocity from the inertial system (J2000.0 system for Landsat 7; the true-of-date system was used for Landsat 4, 5) to the Earth Fixed system:

Transform the J2000.0 system to the mean-of-date system through the precession matrix (Landsat 7 only).

Transform from the mean-of-date system to the true-of-date system through nutation matrix (Landsat 7 only).

Transform from the true-of-date system to the Earth Fixed system through Earth rotation and polar-motion matrix. The Earth Orientation Parameters (UT1-UTC, xp, yp) are passed in from the Calibration Parameter File.

Generation of polynomial for orbit interpolation:

Two sets of polynomial coefficients are generated, one for the orbit position and velocity in the Earth Fixed system and the other for the orbit position and velocity in the Inertial system (J2000.0 for Landsat 7; true-of-date system for Landsat 5). The methods for generating the coefficients for the two sets are the same: solving the Vandermonde equation system using an algorithm given in Reference 6. The order of the polynomial is automatically chosen as the number of valid ephemeris data points in the scene, *i.e.*, an even-determined fit with no redundancy.

The polynomial in the Earth Fixed system is used to interpolate the orbit position and velocity at each (grid point) sensor time, for the purpose of constructing a look vector and intersecting the Earth model in the Earth Fixed system.

The polynomial in the Inertial system is used to interpolate the orbit position and velocity at each gyro data point time, for the purpose of correcting the portion of gyro observation caused by satellite motion.

Process Gyro Data

The Inertial Measurement Unit (IMU) which houses the gyroscopic units are sampled every 64 msec for each of the three axes. The sampled values are referred to as the gyro data. This results in 64 samples per axis per PCD major frame or 256 samples per axis per PCD cycle. The gyro data registers reset if a positive count occurs when the register's value is a positive $2^{23} - 1$, or if a negative count occurs when the register's value is a negative 2^{23} . The time of the gyro data samples are referenced from the start of a PCD cycle by the equation.

$$\text{Gyro_data_sample_time} = 64N \text{ milliseconds, where } N = 0 \dots 255$$

The OBC calculates the gyro drift rates for each of the axes, using the results of star sightings. The results of the OBC gyro drift calculations are in the ACS system. The gyro drift parameters are updated asynchronously at a rate of up to once per minute. When a gyro drift value changes, the value is updated at the PCD time code for the cycle minus 8.192 seconds.

Processing Summary

The high-level flow of gyro processing is as follows:

1. The register resets are accounted for.
2. For each axis, the first gyro value is subtracted from the rest.
3. The gyro data are rotated to the ACS system.
4. The orbital drift component are removed.
5. The gyro, gyro drift, and quaternion data are combined.
6. The data from step 5 are rotated to the ADS system.
7. The data from step 6 are filtered using the G-filter.
8. The data from step 7 are synchronized with the ADS data.
9. Synchronize the ADS data.
10. The data from step 8 are combined with the ADS data.
11. The combined data are filtered using the F-filter.
12. The combined data are rotated to the ACS system.

For more detail on step 5 see section 3.1.5.3.3.1 on Smoothing Low Frequency Information.

For more detail on steps 6, 8, 9, 10, 11 and 12, see section 3.1.5.3.3.2 on Combining Low and High Frequency Attitude Information.

Processing Gyro Data to a Common (ADS) Reference System

Processing of the gyro data to a common ADS reference system is as follows:

1. Since the LPS converts the gyro data counts to arc-seconds, the register reset correction must be accomplished using arc-seconds as the units. Thus, a positive reset occurs at 511705.027 arc-seconds and a negative reset occurs at -511705.088 arc-seconds. Once a reset is detected, the values following the reset are offset by the appropriate reset value.
2. Due to the gyro data measuring changes in attitude, the first value for each of the axes, which corresponds with the spacecraft's attitude values, is subtracted from the rest of the values.
3. Each axis of the gyro data is rotated to the ACS reference system using a pre-launch derived transformation matrix. This is accomplished using the following:

Define **A** as the rotation matrix due to roll. Define **B** as the rotation matrix due to pitch and define **C** as the rotation matrix due to a yaw. Then the Perturbation matrix **P** is defined as:

$$\mathbf{P} = \mathbf{CBA}$$

Use the Transformation matrix from the gyro axes to the ACS **[IMU2ACS]** and its inverse to find the **P** matrix in the ACS reference system or **P'**:

$$\mathbf{P}' = [\mathbf{IMU2ACS}] \mathbf{P} [\mathbf{IMU2ACS}]^{-1} = \begin{matrix} a & b & c \\ d & e & f \\ g & h & i \end{matrix}$$

Then the transformed roll (r') is:

$$r' = -\tan^{-1}(h / i) \quad \text{where } h \text{ and } i \text{ are elements of } \mathbf{P}'$$

Then the transformed pitch (p') is:

$$p' = \sin^{-1}(g) \quad \text{where } g \text{ is an element of } \mathbf{P}'$$

and the transformed yaw (y') is :

$$y' = -\tan^{-1}(d/a) \quad \text{where } d \text{ and } a \text{ are elements of } \mathbf{P}'$$

4. The drift of the gyro data due to the orbital motion is removed using the polynomial for the ephemeris data in the inertial system derived in the Calculate Satellite State Vector subroutine.
5. Combine the gyro, gyro drift and quaternion data into one data stream.

(Details of step 5 can be found in section 3.1.5.3.3.1, Smoothing Low frequency Attitude Information)

6. Each axis of the gyro data is transformed to the ADS reference system. This is accomplished by combining the ACS to ETM+ transformation matrix and the ETM+ to ADS transformation matrix. The ACS to ETM+ transformation matrix is the inverse of the ETM+ to ACS matrix. The ETM+ to ACS matrix is first determined pre-launch and is updated after launch. Its values will be contained in the Calibration Parameter file. The ETM+ to ADS matrix is determined pre-launch and its members are contained in the Calibration Parameter File.

The transformation from the ACS system to the ADS is accomplished using the following:

Define **A** as the rotation matrix due to roll. Define **B** as the rotation matrix due to pitch and define **C** as the rotation matrix due to a yaw. Then the Perturbation matrix **P** is defined as:

$$\mathbf{P} = \mathbf{CBA}$$

First combine the Transformation matrix from the ACS to the ETM+ **T** and the transformation matrix from the ETM+ to the ADS system **R**. Calculate the combined matrix **S** inverse. Then using **S** and its inverse to find the **P** matrix in the ADS reference system or **P'**:

$$\mathbf{S} = \mathbf{RT}$$

$$\mathbf{P}' = \mathbf{SPS}^{-1} = \begin{matrix} a & b & c \\ d & e & f \\ g & h & i \end{matrix}$$

Then the transformed roll (r') is:

$$r' = -\tan^{-1}(h / i) \quad \text{where } h \text{ and } i \text{ are elements of } \mathbf{P}'$$

Then the transformed pitch (p') is:

$$p' = \sin^{-1}(g) \quad \text{where } g \text{ is an element of } \mathbf{P}'$$

Then the transformed yaw (y') is:

$$y' = -\tan^{-1}(d / a) \quad \text{where } d \text{ and } a \text{ are elements of } \mathbf{P}'$$

7. Apply the G-filter. (Refer to Section 3.1.5.3.3.1).

Steps 7,8, 9, 10, and 11 are shown in more detail in the section on attitude processing, Section 3.1.5.3.3.2.

12. Calculate the inverse of step 7, $\mathbf{P}'' = \mathbf{S}^{-1}\mathbf{P}'\mathbf{S}$

Spacecraft Attitude Processing

The OBC calculates a flight segment attitude estimate every 512 milliseconds. The OBC outputs one of the eight sets of data in the telemetry every 4.096 seconds or once a PCD major frame. The attitude is output in the form of Euler parameters that specify the vehicle's attitude relative to the Earth-Centered Inertial reference frame. The Euler parameters (EPA₁, EPA₂, EPA₃, EPA₄) are components of the reference quaternion, as propagated from the gyro data, which defines the spacecraft's attitude. Components 1 through 3 define the Eigen axis of the rotation in ECI coordinates, and the fourth component defines the rotation about the Eigen axis.

There are four attitude estimates in each PCD cycle. The time associated with the attitude data contained within the PCD can be derived from the time code contained in the words 96 through 102 of the first PCD major frame in the cycle. The derivation for Landsat 7 (see Reference 1, page 3–29) is as follows:

PCD Major-Frame	Time Computation
0	PCD time code – 8.192 seconds
1	PCD time code – 4.096 seconds
2	PCD time code
3	PCD time code + 4.096 seconds

Processing

The PCD attitude quaternions define the attitude of the spacecraft at a reference time. This attitude measurement reflects the gyro information up to that point. The IAS determines the spacecraft low frequency attitude by processing the gyro, gyro drift and quaternions into one data stream by using a Kalman filter/smoothing. This integrates attitude measurements from all time into a single best estimate of the attitude over an entire interval. The average associated with this data stream serves as the scene reference attitude state. The average is removed from the data stream. This data stream is then combined with the ADS information to get the change in state of the attitude from this reference state. To accomplish this, the Euler parameters need to be converted to ACS roll, pitch, and yaw values.

The direction cosines (transformation) matrix from the ACS reference axis to the ECI reference system (**ACS2ECI**) is defined as:

ACS2ECI =

$$\begin{bmatrix} EPA_1^2 - EPA_2^2 - EPA_3^2 + EPA_4^2 & 2(EPA_1EPA_2 - EPA_3EPA_4) & 2(EPA_1EPA_3 + EPA_2EPA_4) \\ 2(EPA_1EPA_2 + EPA_3EPA_4) & -EPA_1^2 + EPA_2^2 - EPA_3^2 + EPA_4^2 & 2(EPA_2EPA_3 - EPA_1EPA_4) \\ 2(EPA_1EPA_3 - EPA_2EPA_4) & 2(EPA_2EPA_3 + EPA_1EPA_4) & -EPA_1^2 - EPA_2^2 + EPA_3^2 + EPA_4^2 \end{bmatrix}$$

The **ACS2ECI** transformation matrix can also be defined as the product of the inverse of the spacecraft's attitude perturbation matrix **P** and the transformation matrix from the orbital reference system to the ECI reference system (**ORB2ECI**).

$$\mathbf{ACS2ECI} = [\mathbf{ORB2ECI}][\mathbf{P}^{-1}]$$

The orbital reference system to ECI matrix must be defined at the same time as the spacecraft's attitude matrix. The **ORB2ECI** matrix is constructed of the negative of the spacecraft's position vector divided by its magnitude (z-direction vector), the cross of the z-direction vector with the spacecraft's velocity vector divided by its magnitude (y-direction vector) and the cross of the y-direction vector with the z-direction vector divided by its magnitude (x-direction vector).

The resulting **ORB2ECI** matrix is:

$$\mathbf{ORB2ECI} = \begin{matrix} X_x & Y_x & Z_x \\ X_y & Y_y & Z_y \\ X_z & Y_z & Z_z \end{matrix}$$

Where Z_x is the x component of the z-direction vector,
 Z_y is the y component of the z-direction vector,
 Z_z is the z component of the z-direction vector,
 X_x is the x component of the x-direction vector,
 X_y is the y component of the x-direction vector,
 X_z is the z component of the x-direction vector,
 Y_x is the x component of the y-direction vector,
 Y_y is the y component of the y-direction vector,
 Y_z is the z component of the y-direction vector.

The roll, pitch and yaw values are contained in the \mathbf{P}^{-1} matrix, thus:

$$\mathbf{P}^{-1} = [\mathbf{ORB2ECI}]^{-1}[\mathbf{ACS2ECI}] = \begin{matrix} a & b & c \\ d & e & f \\ g & h & i \end{matrix}$$

Then the spacecraft roll (r) is:

$$r = \tan^{-1}(h / i) \quad \text{where h and i are elements of } \mathbf{P}^{-1}$$

Then the spacecraft pitch (p) is:

$$p = -\sin^{-1}(g) \quad \text{where g is an element of } \mathbf{P}^{-1}$$

Then the spacecraft yaw (y) is:

$$y = \tan^{-1}(d / a) \quad \text{where d and a are elements of } \mathbf{P}^{-1}$$

Convert ADS to Common Reference System

The Attitude Displacement Sensor Assembly (ADSA) consists of three nominally orthogonal ADS sensors. The ADSA is mounted on the ETM+ telescope. A digital sample count of 0 is the maximum positive angular displacement and a digital count of 4095 is the maximum negative angular displacement. The LSB of each count is

$250 / 2^{11}$ microradians. The nominal zero angular displacement output of the ADSA is 2048 counts. Each axis of the ADSA is sampled every 2 milliseconds, resulting 8192 samples of each axis in a PCD cycle. The axes are sampled sequentially as given below:

ADSA AXIS	Sampling Times
roll	PCD Time Code + $(2N + 3/8)$ milliseconds
pitch	PCD Time Code + $(2N + 7/8)$ milliseconds
yaw	PCD Time Code + $(2N + 11/8)$ milliseconds

where $N = 0, 1, 2, \dots, 8191$ for the given axis

Each axis of the ADSA has a nominal 2.0 to 125.0 Hz bandwidth. The transfer function to rotational motion is measured pre-launch and is supplied in the Calibration Parameter File. The nominal relative alignment matrix between the ADS and the ETM+ Sensor is determined pre-launch and is also supplied in the Calibration Parameter File.

Processing

The first three steps are summarized here. Refer to Section 3.1.5.3.3.2, Combining Low and High Frequency Attitude Information, for more information.

1. Each of the samples for each axis is transformed to rotational motion using the transfer function.
2. Synchronize the ADS data
3. Combine the ADS data with the smoothed low frequency attitude data.
4. Rotate to the ACS system. Due to the ADSA being mounted on the ETM+ telescope, the transformation to the ACS reference system requires the ADSA measurements to be transformed to the ETM+ reference system and then transformed through the ETM+ sensor to ACS alignment matrix. Since the ETM+ to the ACS reference system matrix will be determined after launch, this transformation must be a two step process.

Define the transformation matrix from the ADSA to the ETM+ sensor as **ADS2ETM** and the transformation matrix from the ETM+ to the ACS as **ETM2ACS**. Then the transformation matrix between the ADSA and the ACS (**ADS2ACS**) is:

$$\mathbf{ADS2ACS} = [\mathbf{ETM2ACS}][\mathbf{ADS2ETM}]$$

To transform the axis of the ADSA, the perturbation matrix \mathbf{P} must first be calculated. To accomplish this, we must define a matrix \mathbf{A} as the rotation matrix due to roll, a matrix \mathbf{B} as the rotation matrix due to pitch and a matrix \mathbf{C} as the rotation matrix due to yaw. Thus, the perturbation matrix is:

$$\mathbf{P} = \mathbf{CBA}$$

Then using the transformation matrix $\mathbf{ADS2ACS}$ and its inverse, the perturbation matrix in the ACS reference \mathbf{P}' is found:

$$\mathbf{P}' = [\mathbf{ADS2ACS}]\mathbf{P}[\mathbf{ADS2ACS}]^{-1} = \begin{matrix} a & b & c \\ d & e & f \\ g & h & i \end{matrix}$$

Then the transformed roll (r') is:

$$r' = -\tan^{-1}(h / i) \quad \text{where } h \text{ and } i \text{ are elements of } \mathbf{P}'$$

Then the transformed pitch (p') is:

$$p' = \sin^{-1}(g) \quad \text{where } g \text{ is an element of } \mathbf{P}'$$

Then the transformed yaw (y') is:

$$y' = -\tan^{-1}(d / a) \quad \text{where } d \text{ and } a \text{ are elements of } \mathbf{P}'$$

Calculate Scan Mirror Correction

The scan mirror (as introduced in section 3.1.5.1.2) is modeled using a linear motion with a 5th order polynomial correction. A 5th order polynomial is determined during the ground testing of the instrument, this along with an adjustment due to high frequency roll jitter components combine to give an overall 5th order polynomial correction. Along with the high frequency jitter component, in orbit perturbations within the satellite causes the scan mirror velocity to change from scan to scan. The scan mirror has sensors attached to it to measure the mirror position at the start of scan, mid-scan, and end of scan. The data from these sensors are output in the form of counts, which are the deviation from nominal scan mirror position in time. For example, the scan mirror crossed the mid-scan detector so many counts ahead (or behind) of the nominal time. The unit of the counts are $16/84.9037e-6$ seconds or 0.18849 microseconds.

In the IAS model of the scan mirror motion, the mirror starts at a positive angle (A_{sm}) and becomes more negative as a function of time, until it reaches A_{me} , where A_{sm} is the angle from the start of scan to the mid-scan position and A_{me} is the angle of the mirror from

mid-scan to end of scan. This sign convention is used to place the scan mirror motion in the spacecraft coordinate system. *Note: This convention is different than the convention used in Reference 1 and 2.*

Remaining in the true time domain, for the forward and reverse scan direction, a positive result from the polynomial corresponds to the mirror being ahead of its linear location and a negative result corresponds to the mirror being behind its linear location. However, whether the results are added to the linear portion or subtracted depends on the slope of the linear motion. For example, using the IAS sign conventions, adding a positive polynomial value to the forward scan direction causes the scan mirror to be behind its linear location. Thus, for the forward scan direction, a positive polynomial value must be subtracted from the linear location or the sign of each of the coefficients must be changed. The latter was chosen. For a reverse scan, a positive polynomial value added to the linear location corresponds to the mirror being ahead of its linear location. Thus, adding the polynomial value is correct. *Note: The MSCD values of scan direction, counted line length, first half scan error and second half scan error are for the previous scan.*

Define:

$b_{j=0,5}$	The forward scan polynomial coefficients for the SME mode
$d_{j=0,5}$	The reverse scan polynomial coefficients for the SME mode
A_{smf}	The forward start to middle angle for the SME mode
A_{mef}	The forward middle to end angle for the SME mode
A_{smr}	The reverse start to middle angle for the SME mode
A_{mer}	The reverse middle to end angle for the SME mode
T_{fhf}	The forward nominal first half scan time
T_{shf}	The forward nominal second half scan time
T_{fhr}	The reverse nominal first half scan time
T_{shr}	The reverse nominal second half scan time
T_n	The nominal scan time
T_{unit}	The conversion factor from counts to time
$mprofile_{i,j}$	The corrected mirror polynomial for each scan

Compute the actual scan time--find true first half time (T_{fh}), true second half time (T_{sh}), and total scan time (t_s):

For a forward scan:

$$\begin{aligned} T_{fh} &= T_{fhf} - FHSERR_i * T_{unit} && \text{(The first half scan time)} \\ T_{sh} &= T_{shf} - SHSERR_i * T_{unit} && \text{(The second half scan time)} \\ t_s &= T_{fh} + T_{sh} && \text{(The total scan time)} \end{aligned}$$

For a reverse scan:

$$\begin{aligned} T_{fh} &= T_{fhr} - FHSERR_i * T_{unit} && \text{(The first half scan time)} \\ T_{sh} &= T_{shr} - SHSERR_i * T_{unit} && \text{(The second half scan time)} \end{aligned}$$

$$t_s = T_{fh} + T_{sh} \quad (\text{The total scan time})$$

Calculate the correction to the linear model needed to make the mid-scan angle equal to the observed value (zero) at time T_{fh} . (see Figure 3.1.5-5)

For a forward scan: $A_f = -(A_{mer}T_{fhf} + A_{smf}T_{shf}) / t_s$

For a reverse scan: $A_r = -(A_{mer}T_{fhr} + A_{smr}T_{shr}) / t_s$

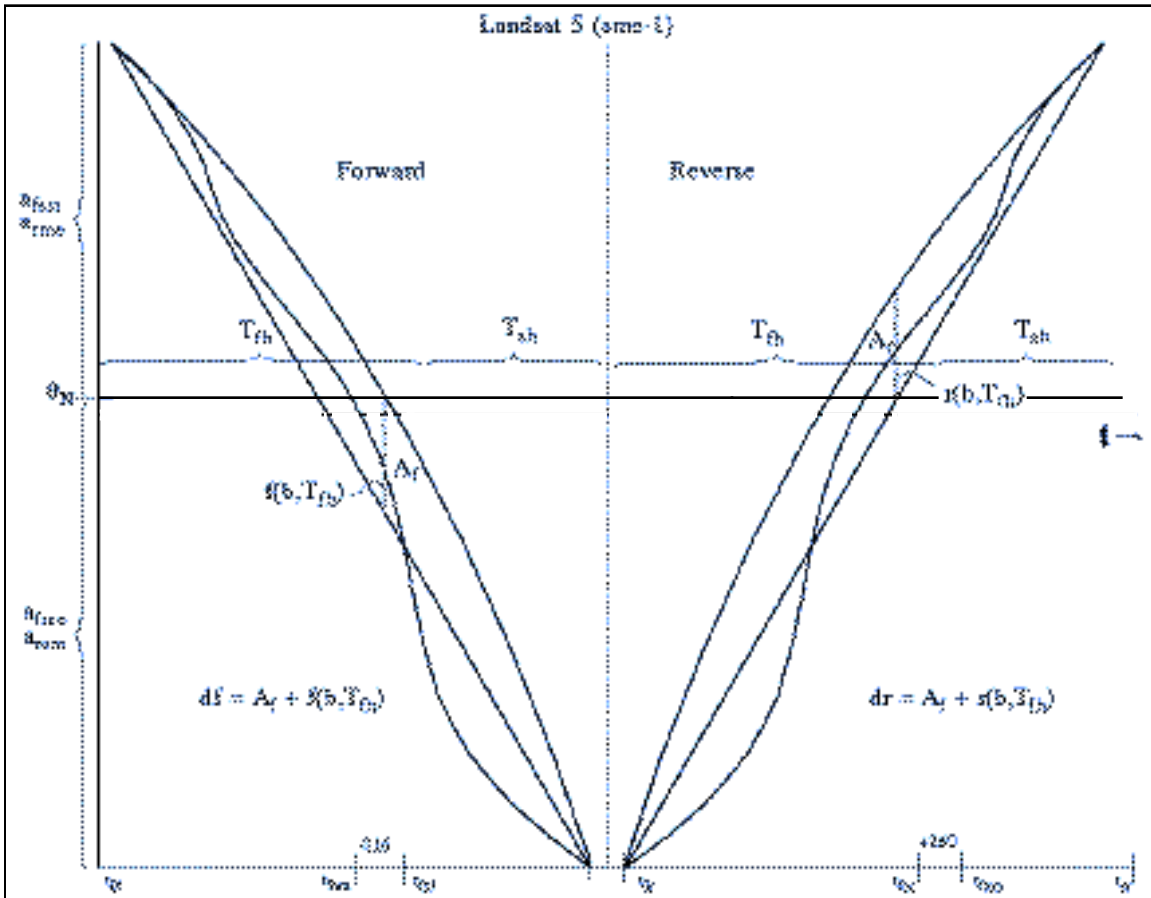


Figure 3.1.5- 5 Scan Mirror Profile Deviations

Rescale the fifth-order polynomial coefficients to account for the difference between the actual and nominal scan time:

For a forward scan: $b_j = b_j * (T_n / t_s)^j$ where $j = 0$ to 5

For a reverse scan: $d_j = d_j * (T_n / t_s)^j$ where $j = 0$ to 5

Calculate the amplitude component of the correction quadratic (B_f) due to the polynomial location of the mirror to the linear location. This is done by evaluating the rescaled fifth-order polynomial at time T_{fh} . ($f(b, T_{fh})$ in figure 3.1.5-5).

For a forward scan:

$$B_f = b_0 + (b_1 * T_{fhf}) + (b_2 * T_{fhf}^2) + (b_3 * T_{fhf}^3) + (b_4 * T_{fhf}^4) + (b_5 * T_{fhf}^5)$$

For a reverse scan: (Note: a (-) sign is applied to the d coefficients)

$$B_r = d_0 + (d_1 * T_{fhr}) + (d_2 * T_{fhr}^2) + (d_3 * T_{fhr}^3) + (d_4 * T_{fhr}^4) + (d_5 * T_{fhr}^5)$$

The net correction to the mirror profile at the mid-scan time (T_{fh}) is (D_f and D_r) is:

$$\text{For a forward scan: } D_f = A_f - B_f$$

$$\text{For a reverse scan: } D_r = A_r - B_r$$

Using the constraints $a(0) = a(t_s) = 0.0$, and $a(t_{sh}) = D$, the coefficients of the quadratic are:

$$\text{For a forward scan: } a_2 = -D_f / (T_{fhf} * T_{shf})$$

$$\text{For a reverse scan: } a_2 = -D_r / (T_{shr} * T_{fhr})$$

$$\begin{aligned} \text{For both scan directions: } a_1 &= -t_s * a_2 \\ a_0 &= 0.0 \end{aligned}$$

Integration of Roll Jitter into the Scan Mirror Model

The high frequency roll attitude components (jitter) must be considered together with the scan mirror profile since the scan mirror is not rigidly attached to the instrument structure in the along scan direction but, rather, is driven by a flex pivot. This acts as a mechanical buffer which does not transmit the high frequency along scan jitter directly to the mirror. The roll jitter terms therefore have two effects: the ETM+ instrument rotates relative to the orbital coordinate system and the scan mirror rotates relative to the ETM+ instrument (in the opposite direction). Effectively, the scan mirror does not “see” the high frequency roll jitter. The roll rotation of the ETM+ instrument (i.e., the focal planes) independent of the scan mirror causes the effective line of sight to be deflected in the opposite direction from that caused by a rigid rotation of the entire focal plane/scan mirror assembly. [Reference 35] This is depicted in Figure 3.1.5-6.

The scan mirror angle relative to the rest of the ETM+, and to the orbital coordinate system, is known at the three points where it is measured by the scan angle monitor (SAM): scan start, mid-scan, and scan end. The line of sight at these three times will be based on the known mirror angles at beginning, middle, and end of scan modified by the high frequency roll at the corresponding times, so the combined mirror/roll jitter model must match these known angles at these three times. This is accomplished by modifying the scan mirror profile for each scan to include the scan start, mid-scan, and scan end high frequency roll effects. This is implemented as a roll jitter correction to the scan mirror polynomial: $\hat{\theta}(t)$. The differential jitter relative to this profile is then: $\theta_t - 2\hat{\theta}(t)$ where θ_t is the measured roll jitter and $\hat{\theta}(t)$ is doubled to account for the fact that a scan mirror rotation of $\hat{\theta}(t)$ leads to a line of sight deflection of $2\hat{\theta}(t)$. As described above and depicted in Figure 3.1.5-6, this differential jitter leads to a deflection of the line of sight in the opposite direction, or: $-[\theta_t - 2\hat{\theta}(t)]$. So, the net deflection of the line of sight relative to the orbital coordinate system is: $-\theta_t + 2\hat{\theta}(t)$. We implement this deflection by inverting the sign on the roll jitter component (θ_t) and including the scan mirror profile adjustment ($\hat{\theta}(t)$) in the mirror model. All that remains is to determine what the scan mirror profile adjustment should be.

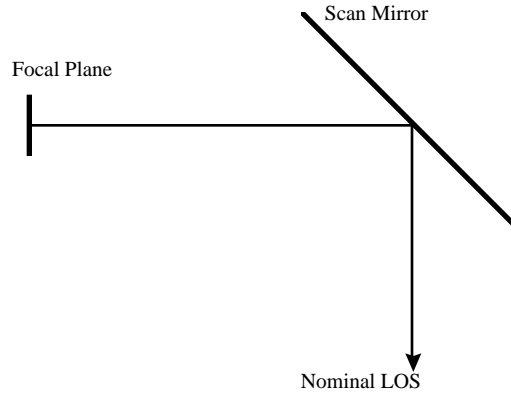
As noted above, the net line of sight deflection must account for the roll angles at scan start (θ_s), mid-scan (θ_m), and scan end (θ_e). If the mirror profile adjustment is constructed so that it is equal to the measured roll jitter at scan start, mid-scan, and scan end (i.e., it modifies the mirror profile to include roll jitter effects at those three points) then the net line of sight deflection at $T=0$, $T=t_{fh}$, and $T=T_s$ will be:

$$\theta_{net} = -\theta_t + 2\hat{\theta}_t = \theta_t \quad \text{where } t = s, m, \text{ or } e \text{ for scan start, mid-scan, and scan end.}$$

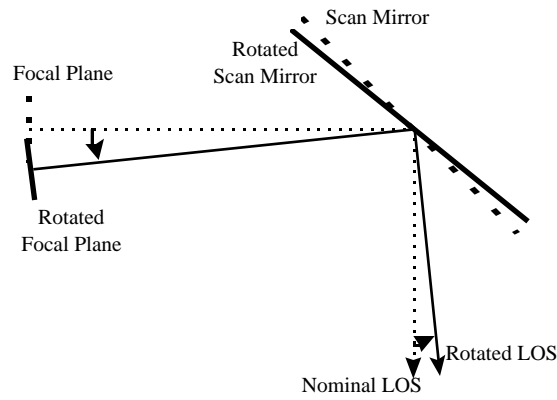
This is the desired result, so the mirror correction term, $\hat{\theta}(t)$, must be constructed so that:

$$\begin{aligned} \hat{\theta}(0) &= \theta_s \\ \hat{\theta}(t_{fh}) &= \theta_m \\ \hat{\theta}(T_s) &= \theta_e \end{aligned}$$

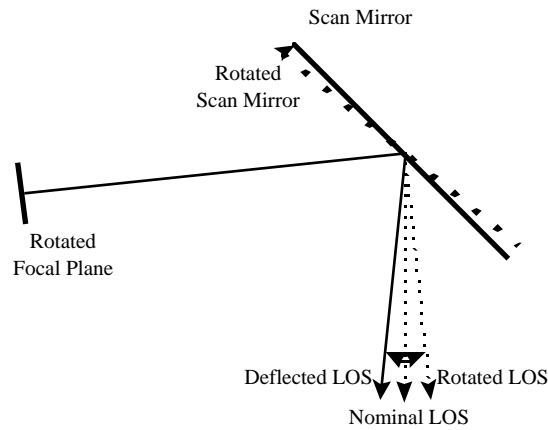
IAS Geometric ATBD Version 3



a) Nominal Focal Plane/Scan Mirror Geometry



b) Rigid Rotation of Focal Plane and Scan Mirror



c) Rotation of Focal Plane Independent of Scan Mirror

Figure 3.1.5-6 Effect of Roll Jitter on Line of Sight Direction

This can be accomplished using a correction quadratic similar to that used to perform the mid-scan correction. The coefficients of this polynomial can be shown to be:

$$c_0 = s$$

$$c_1 = \frac{e - s}{T_s} - \frac{(e - m)t_{fh} + (s - m)t_{sh}}{t_{fh}t_{sh}}$$

$$c_2 = \frac{(e - m)t_{fh} + (s - m)t_{sh}}{T_s t_{fh} t_{sh}}$$

This makes the net mirror profile:

$$b_0 = b_0 + a_0 + c_0$$

$$b_1 = b_1 + a_1 + c_1$$

$$b_2 = b_2 + a_2 + c_2$$

$$b_3 = b_3$$

$$b_4 = b_4$$

$$b_5 = b_5$$

where the b_i are the nominal mirror profile coefficients normalized for actual scan time, the a_i are the mid-scan correction quadratic coefficients computed from the first half and second half scan errors, and the c_i are the roll jitter correction quadratic coefficients defined above. Inverting the sign on the measured roll jitter data and using this modified mirror profile creates the desired net line of sight deflection.

3.1.5.3.3.1 Smoothing Low Frequency Attitude Information

Purpose:

In the IAS release 1 model the quaternion and gyro drift observations from the PCD major frame immediately preceding the scene was used as a reference point. All subsequent attitude data for the scene was referenced from this point, therefore if a stellar observation occurred later in the scene this change in reference frame was not be reflected in the model. This change can be thought of as an update in the reference frame of the system. The update could produce a discontinuity in the attitude data stream. To incorporate all of the stellar observation information in the PCD quaternion samples, a Kalman filter is used as a post processing filter of the attitude data stream. The Kalman filter is implemented in a forward-predictor, backward-smoother configuration. Under this scenario, the filtering serves as a forward recursive sweep while the smoothing serves as a backward sweep. The backward-smoother processing propagates the stellar observations, represented by the quaternion data, backward in time to provide a best estimate of the spacecraft attitude given data from all times in the sub-interval. The smoothed data stream will be a new attitude data stream representing the combined gyro, quaternion, and drift data. This smoothed data set will represent the low frequency

attitude information of the satellite. The data is then combined with the ADS information to produce the overall attitude of the sensor/satellite.

The rest of this section contains three parts. The first is a brief description of the filtering and smoothing equations. The reader is encouraged to pursue the references given later in the text for further details on the subject. The second portion will involve calculating the equations that are specific to this application. The final portion will explain the details of running the process with actual data.

Algorithm:

The discrete Kalman filter assumes a random process modeled as follows:

$$[X]_{K+1} = []_K [X]_K + [q]_K$$

Where

$[X]_K = (n \times 1)$ state vector at time t_K

$[]_K = (n \times n)$ state transition matrix relating X_K to X_{K+1}

$[q]_K = (n \times 1)$ process noise, white, uncorrelated, with covariance Q

Measurements of the process are modeled as:

$$[Z]_K = [H]_K [X]_K + [v]_K$$

Where

$[Z]_K = (m \times 1)$ measurement vector at time t_k

$[H]_K = (m \times n)$ observation matrix relating state vector at t_k to measurement vector

$[v]_K = (m \times 1)$ measurement error, white, uncorrelated, with covariance R

The first step involves using the Kalman filter as a forward prediction process. The Kalman filtering equations are (note all equations refer to the discrete domain):

(Note: superscript P refers to prediction)

Given an initial state vector and covariance matrix $[X]^P_0$ and $[P]^P_0$:

For $k=1, \dots, N$ (number of data points)

Filter data

$$[K]_K = [P]_K^p [H]_K^T \left([H]_K [P]_K^p [H]_K^T + [R]_K \right)^{-1}$$

$$[X]_K = [X]_K^p + [K]_K ([Z]_K - [H]_K [X]_K^p)$$

$$[P]_K = ([I] - [K]_K [H]_K) [P]_K^p$$

Predict

$$[X]_{K+1}^p = []_K [X]_K$$

$$[P]_{K+1}^p = []_K [P]_K []_K^T + [Q]_K$$

Where:

$[I]$ is the identity matrix

$[K]$ is the Kalman Gain matrix

$[P]$ is the state error covariance matrix.

$[Q] = E[qq]$

$[R] = E[vv]$

The second step involves using the filtered and predicted data to produce a smoothed data set. Let,

$[X]_K^p$ = estimate of $[X]$ given measurements through t_{K-1}

$[P]_K^p$ = error covariance associated with estimate $[X]_K$

$[X]_K$ = filtered estimate through t_K

$[P]_K$ = state error covariance associated with filtered estimate at t_K

Using the definitions above a new notation is:

$$[X]_{K|K-1} = [X]_K^p$$

$$[P]_{K|K-1} = [P]_K^p$$

$$[X]_{K|K} = [X]_K$$

$$[P]_{K|K} = [P]_K$$

Smooth data

For $K=N-1, N-2, \dots, 0$

$$[X]_{K|N} = [X]_{K|K} + [A]_K ([X]_{K+1|N} - [X]_{K+1|K})$$

$$[A]_K = [P]_{K|K} []_{K+1,K}^T [P]_{K+1|K}^{-1}$$

$$[P]_{K|N} = [P]_{K|K} + [A]_K ([P]_{K+1|N} - [P]_{K+1|K}) [A]_K^T$$

For more information on the Kalman filter and smoothing data refer to references 23 and 34.

This is all the background on the Kalman filtering that will be given here. If more information is desired the reader should refer to one of the references stated above. The rest of this document will focus on the how the matrix equations specific to the attitude processing were obtained and some of the processing flow issues.

The system will first be described for the continuous time case, then the corresponding discrete time case will be solved for. The equations for the continuous case are:

$$\dot{X} = FX + w$$

$$Y = CX$$

Where

X = state vector

F = state matrix

Y = output response vector

C = matrix relating state to measurement

w = vector of white noise processes

F,G,C may be time varying matrices.

The state matrix for the attitude processing contains three states. The states are attitude, gyro rate, and gyro drift. The state transition matrix is:

$$\begin{bmatrix} \dot{X} \\ X \end{bmatrix} = \begin{bmatrix} 0 & 1 & 0 \\ 0 & 0 & 0 \\ 0 & 0 & 0 \end{bmatrix} \begin{bmatrix} X_1 \\ X_2 \\ X_3 \end{bmatrix} + \begin{bmatrix} 0 \\ w_2 \\ w_3 \end{bmatrix}$$

X₁ = attitude

X₂ = gyro rate

X₃ = gyro drift

w = process noise (white)

The model above states that the gyro rate is the time derivative of the attitude and the time derivatives of the gyro rate and drift are independent white noise processes.

The output response vector has the following form:

$$[Y] = \begin{bmatrix} 1 & 0 & 0 \\ 0 & 1 & -1 \\ 0 & 0 & 1 \end{bmatrix} \begin{bmatrix} X_1 \\ X_2 \\ X_3 \end{bmatrix} + \begin{bmatrix} r_1 \\ r_2 \\ r_3 \end{bmatrix}$$

r = measurement noise (white)

The observation matrix above states that there are three kinds of measurements involved in the process:

- 1) Quaternion observations which measure the attitude.
- 2) Gyro/gyro rate observations which measure the attitude rate biased by the gyro drift.
- 3) Gyro drift observations which measure the bias in the gyro measurements.

The gyro measurements have no absolute origin, therefore they have meaning only relative to each other. By differencing the gyro samples and dividing by the sampling rate they can be converted to attitude rate measurements, the quaternions are then used as the reference. Once the gyro samples are converted into rate the drift can be directly applied since it is measured in units of radians per unit of time. The measurements then used by the process, as measured by the satellite, are quaternions, gyro rate, and gyro drift.

The matrix [F] does not contain any time varying elements and is small enough that the direct method can be used to determine the discrete transition matrix. The equation takes the form:

$$[X]_k = \mathcal{L}^{-1} \{ [I]_s - [F] \mathbb{I}^{-1} \} dt$$

Where

\mathcal{L}^{-1} is the inverse Laplace transform.

[I] = identity matrix

\mathbb{I}^{-1} = matrix inversion

dt = sampling interval

This gives the following

$$L^{-1} \{ [I]_s - [F] \mathbb{I}^{-1} \} = L^{-1} \begin{bmatrix} s & -1 & 0 \\ 0 & s & 0 \\ 0 & 0 & s \end{bmatrix}^{-1} = L^{-1} \begin{bmatrix} \frac{1}{s} & \frac{1}{s^2} & 0 \\ 0 & \frac{1}{s} & 0 \\ 0 & 0 & \frac{1}{s} \end{bmatrix} = \begin{bmatrix} 1 & t & 0 \\ 0 & 1 & 0 \\ 0 & 0 & 1 \end{bmatrix}$$

Substituting dt for t in the above matrix gives the discrete state transition matrix.

The discrete process noise matrix can also be solved directly. The discrete process noise is found from the equation:

$$[Q]_k = \int_0^{dt} \int_0^{dt} [G(u)] E [w(u)w^T(v)] [G(v)]^T [dt, v]^T dudv$$

Noting that w2 and w3 are uncorrelated and that σ^2 is the variance of the associated white noise process:

$$G(u) E [w(u)w^T(v)] G(v)^T = \begin{bmatrix} 0 & 0 & 0 \\ 0 & \sigma^2 & 0 \\ 0 & 0 & \sigma^2 \end{bmatrix}$$

Performing the remaining matrix operations:

$$\begin{bmatrix} 1 & u & 0 & 0 & 0 & 0 & 1 & 0 & 0 \\ 0 & 1 & 0 & 0 & 0 & v & 1 & 0 & 0 \\ 0 & 0 & 1 & 0 & 0 & 0 & 0 & 1 & 0 \end{bmatrix} \begin{bmatrix} uv \frac{\sigma^2}{2} & u \frac{\sigma^2}{2} & 0 \\ v \frac{\sigma^2}{2} & \frac{\sigma^2}{2} & 0 \\ 0 & 0 & \frac{\sigma^2}{2} \end{bmatrix}$$

Solving the double integral for the matrix above gives the discrete process noise matrix:

$$\begin{bmatrix} dt & dt & 0 & 0 & 0 \\ 0 & 0 & dt & dt & 0 \\ 0 & 0 & 0 & 0 & dt \end{bmatrix} \begin{bmatrix} uv \frac{\sigma^2}{2} & u \frac{\sigma^2}{2} & 0 \\ v \frac{\sigma^2}{2} & \frac{\sigma^2}{2} & 0 \\ 0 & 0 & \frac{\sigma^2}{2} \end{bmatrix} = \begin{bmatrix} \frac{dt^4}{4} & \frac{dt^3}{2} & 0 \\ \frac{dt^3}{2} & dt^2 & 0 \\ 0 & 0 & dt^2 \end{bmatrix}$$

The observation matrix relating the state vector to the output/measurement vector is the same for the continuous and discrete cases.

$$[H] = [C]$$

Under this system model, each axis can be processed independently. The attitude of the satellite will be contained in the first state of the state vector. The gyro and quaternion data for Landsat 7 is not sampled at the same instant in time or at the same rate. This will need to be accounted for prior to and during processing. The data will also have to be in a

common coordinate system. The drift is measured in the attitude control system (ACS). The quaternions are given as Euler parameters and can be converted to the ACS (ATBD section 3.1.5.3.3 Satellite Attitude Processing). The gyro data is measured in the inertial measurement unit (IMU) axis and can be converted to the ACS (ATBD section 3.1.5.3.3 Processing Gyro Data). The system therefore works in the ACS. The output will also be in the ACS. The time offset is accounted for by looking at the sampling times associated with each data source.

Gyro samples

PCD time code + 0.064N seconds N=0,1,2,...,255

Attitude

PCD

Major Frame

- 0 PCD time code – 8.192 seconds
- 1 PCD time code – 4.096 seconds
- 2 PCD time code + 0.0 seconds
- 3 PCD time code + 4.096 seconds

Drift

PCD

Major Frame

- 0 PCD time code – 8.192 seconds

At the first PCD cycle, PCD major frame 0, the gyro data will correspond to the quaternion value of the first PCD cycle, major frame 2. This will be the initial/start conditions for the filtering. The gyro drift value will be zero until the data stream reaches a point with valid drift data. The initial covariance error matrix, $[P]$, was set equal to the process noise matrix. This value may need to be changed after some test runs with different data sets. Due to the fact that the gyro, attitude and drift data have different sampling rates, there will be three different observation matrices. One observation matrix when only the gyro is present, a second when both the gyro and quaternions are present, and a third when all three measurements are available. When only the gyro is available, the observation matrix will be:

$$[Y] = \begin{bmatrix} 0 & 1 & -1 \end{bmatrix} \begin{matrix} X_1 \\ X_2 \\ X_3 \end{matrix} + [r]$$

When both the gyro and quaternions are available the observation matrix will be

$$\begin{array}{l} Y_1 = 1 \ 0 \ 0 \ X_1 + r_1 \\ Y_2 = 0 \ 1 \ -1 \ X_2 + r_2 \end{array}$$

When the gyro, quaternion, and gyro drift measurements are available the observation matrix will be:

$$\begin{array}{l} Y_1 \quad 1 \ 0 \ 0 \ X_1 \quad r_1 \\ Y_2 = 0 \ 1 \ -1 \ X_2 + r_2 \\ Y_3 \quad 0 \ 0 \ 1 \ X_3 \quad r_3 \end{array}$$

Note: Although it is stated that “gyro measurements are available” it is actually the gyro rate that the system is working with at this point.

The state transition matrix will be the same for all these cases. The final step is to determine the values associated with the measurement noise matrices and the standard deviations associated with the process noise matrix. The measurement error for the gyro corresponds to the increment associated with one gyro count or 0.061 arc-seconds. The measurement error for the gyro rate is found by dividing 0.061 arc-seconds by the sampling rate of the gyro, 0.064 seconds. The measurement error used for the quaternion corresponds to the error associated with the Celestial Sensor Assembly and is 4.2 arc-seconds [Reference 35]. The measurement error for the drift and the standard deviations for the process noise were determined by trial and error. The criteria for choosing values for trial however fell under the following premise.

The drift values were considered much less reliable than either the gyro or quaternion values.

The measurement error for the quaternion was chosen to be larger than the gyro (rate) measurement error. This allowed the quaternions to act as a very low frequency reference and the gyro (rate) to represent the higher frequency reference. This will keep the scan-to-scan consistency needed for processing. The attitude processing should not effect the scan-to-scan accuracy to any measurable degree.

The measurements for the gyro (rate) were considered to carry more weight than the model while the opposite was considered for the drift. The values were chosen such that more consideration was given to the model for the drift while for the gyro (rate) more consideration was given toward the measurements.

Through trial and error this led to a values of 50.0 arc-seconds for the drift measurement, a standard deviation of 0.1 for the process noise associated with the gyro rate, and a

standard deviation for 0.00001 for the process noise associated with the drift. It should be noted that these values were determined from data associated with the Landsat 4 satellite, the values may need to change slightly to reflect Landsat 7. These values were used to process one hundred consecutive major frames of Landsat 4 attitude data. Processing the quaternion, gyro and drift produced a change of less than one meter in the difference between adjacent gyro samples. This provided proof that the effect on between scan alignment was negligible.

Once all the data is processed, filtered and smoothed, the new attitude data can be used by the G and F filters, along with the ADS information, to get the overall satellite attitude. To be consistent with the old way of processing however, the output from the filtering and smoothing should have the first value kept as a frame of reference and subtracted from all other values.

3.1.5.3.3.2 Combining Low and High Frequency Attitude Information

Much of the premise for the design of the Attitude Data processing algorithm comes from the document Landsat Thematic Mapper Attitude Data Processing by G. J. Sehn and S. F. Miller [Reference 10]. References 38, 39, and 40 are also good sources on the subject.

The following symbols will be used throughout this section:

FFT	Fast Fourier Transform with a complex component of -1 on the exponent associated with the forward transform (1 for the reverse).
Hg	Frequency response of the gyro sensor
P	Frequency response of the ADS pre-filter
Ha	Frequency response of the ADS sensor
PHa	Frequency response of the ADS sensor combined with pre-filter
G(f)	Frequency response of G filter
F(f)	Frequency response of F filter
function	Magnitude response of function
<i>j</i>	Indicates the imaginary part of a complex number

The gyro has the following transfer function for Landsat 4 and 5:

$$H_g = a_k * (1.0 + K * s) / (1.0 + \tau * s) * [(s / \omega_n)^2 + (2.0 * \zeta * s) / \omega_n + 1.0]$$

where a_k , K , τ , ω_n , and ζ are measured constants and

$$s = 2j * \pi * \text{freq.}$$

The ADS and pre-filter combined have the following transfer function for Landsat 4 and 5:

$$H_{ads} = \frac{(A5 * s^5 + A4 * s^4 + A3 * s^3)}{(s^6 + B5 * s^5 + B4 * s^4 + B3 * s^3 + B2 * s^2 + B1 * s + B0)}$$

where A5, A4, A3, B5, B4, B3, B2, B1, and B0 are measured constants and

$$s = 2j * \pi * \text{freq.}$$

The Landsat 4 and 5 satellites have two sensors to measure satellite attitude perturbations. One of the sensors measures the low end frequencies while the other measures high end frequencies. These are called the gyro and attitude displacement sensor (ADS) respectively. The gyro is sampled every 64 milliseconds and the ADS is sampled every 2 milliseconds. The samples taken from these two systems cannot be simply added together to get the overall satellite attitude perturbations due to a discontinuity between the transition regions of the responses of the two systems and due to the sensor phase shift properties. A plot of the frequency responses of the two systems is shown in Figure 3.1.5-7.

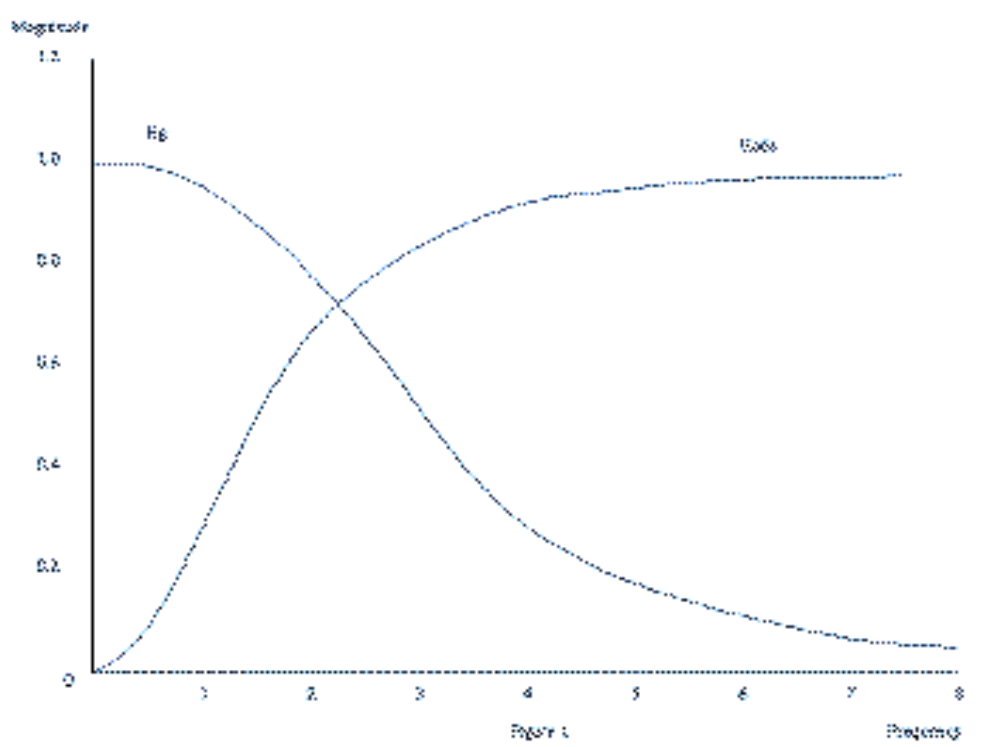


Figure 3.1.5- 7 Magnitude Response of Gyro and ADS

The magnitude of the sum $|H_g + P_H a|$ is shown in 8 Figure 3.1.5-8.

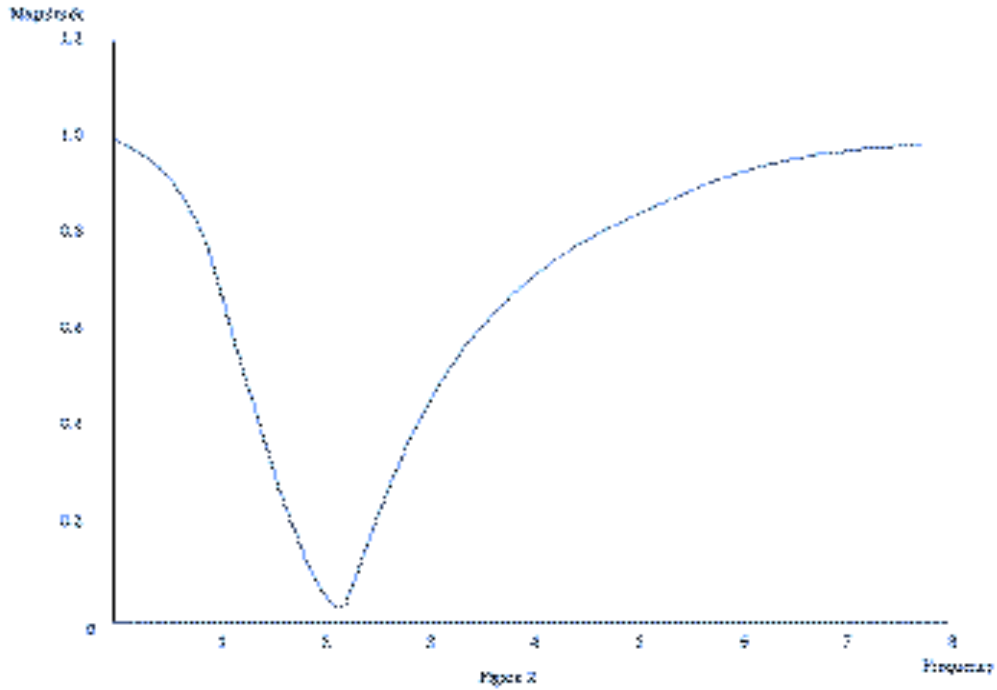


Figure 3.1.5- 8 Magnitude Response of Gyro Plus ADS

The magnitude of the sum $|H_g| + |P_{Ha}|$ is shown in Figure 3.1.5-9.

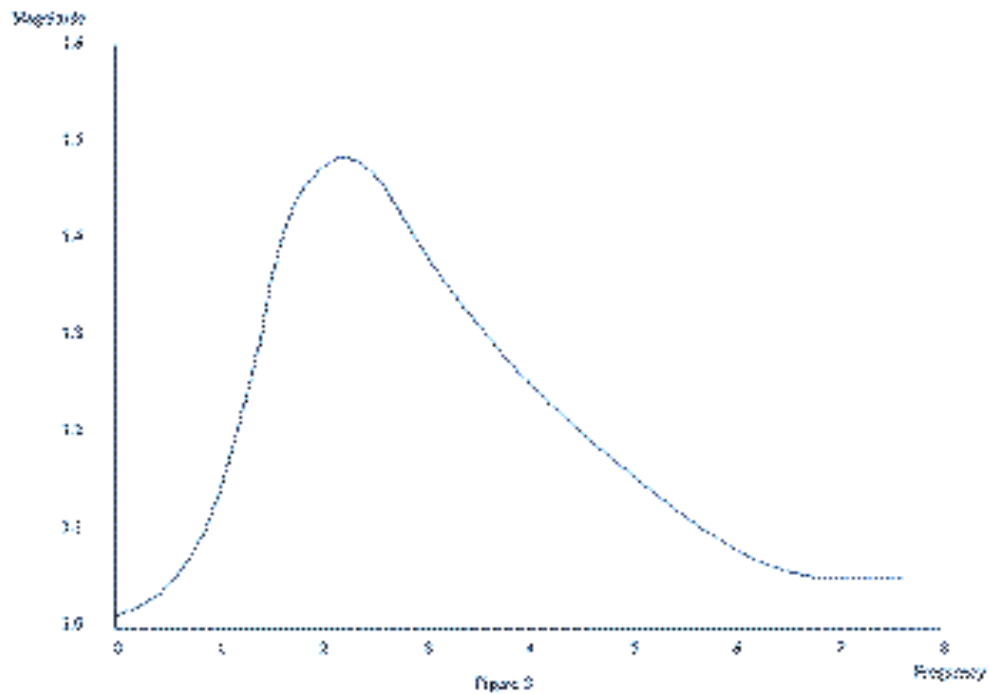


Figure 3.1.5- 9 Magnitude Response of Gyro + Magnitude Response of ADS

These figures help to explain the discontinuity between the system responses.

To combine these two signals, along with the quaternions and gyro drift values, a network is used that combines the traditional G.J. Sehn and S.F. Miller approach along with the Kalman filtering that was explained in section 3.1.5.3.3.1

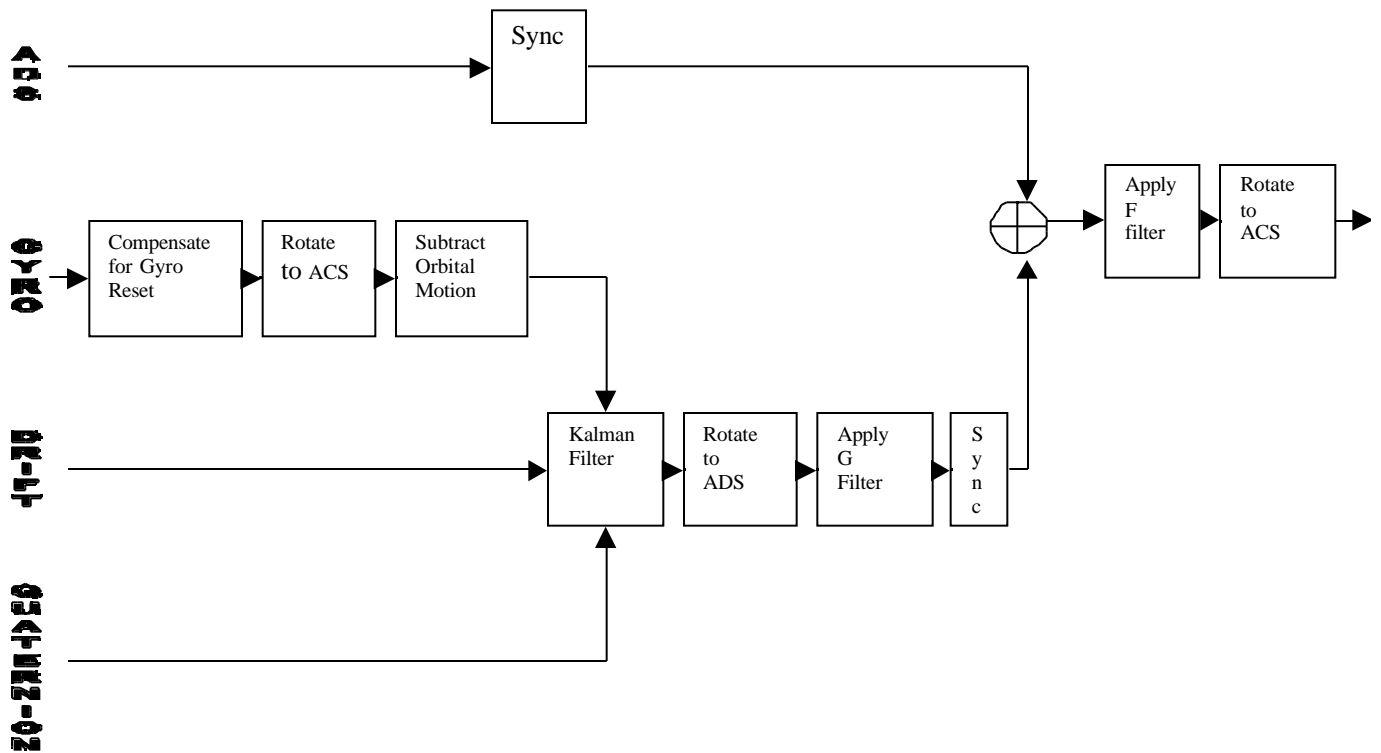


Figure 90 Attitude Processing Network

This algorithm combined with the necessary steps involved in implementing a workable system is listed below. A diagram of the algorithm steps is given in Figure 3.1.5-10.

1. The register resets are accounted for.
2. For each axis, the first gyro value is subtracted from the rest.
3. The gyro data is rotated to the ACS.

4. The orbital drift component is removed.

(Details of steps 1 through 4 can be found in section 3.1.5.3.3, Process Gyro Data)

5. Smooth gyro, gyro drift and quaternions.

(Details of step 5 can be found in section 3.1.5.3.3.1)

6. Rotate the data from step 5 to the ADS system.

(Details of step 6 can be found in section 3.1.5.3.3, Process Gyro Data)

7. Filter the data from step 6. This is done with a filter traditionally called the pre-summing G filter or just G filter. This filter will help to eliminate any frequencies above a predetermined cut-off while also providing an adequate transition for combining the gyro and ADS. The gyro data is not pre-filtered as the ADS data is, the G filter will serve this purpose. The requirements for the G filter are to provide unity gain at low frequencies and to allow the ADS system to provide the gain at high frequencies.

The G filter takes on the following values in the frequency domain:

Define: $F1 = 2.0$
 $F2 = 7.8125$
 $freq = \text{current frequency}$

Note: F1 was chosen as the frequency where Hads reaches -1.0 dB while F2 was chosen to be the Nyquist frequency associated with the sampling of the gyro data.

if $freq$ is less than $F1$ then $V_k = 1$

if $freq$ is greater than $F1$ but less than $F2$ then

$a = (F2 - freq) * (F2 - freq);$
 $b = (freq - F1) * (freq - F1);$
 $V_k = (a * |H_{pdf}| + b * |P_{Ha}|) / (a + b);$

(Note: This is just an interpolation over the crossover region of the two systems.)

if $freq$ is greater than $F2$ then

$V_k = P_{Ha}$
 $G(freq) = 0.0$

The G filter can then be solved for by looking at the response of the attitude processing system before the F filter is to be applied [Reference 10].

$$|GHg + PHa| = Vk$$

The G filter can be solved for by writing this equation as:

$$(GHg + PHa) * \text{conjugate}\{(GHg + PHa)\} = Vk * Vk$$

Multiplying this out and noting that G is real so that $G = \text{conjugate}\{G\}$ the equation becomes:

$$G^2|Hg|^2 + 2G\text{Re}\{Hg \text{conjugate}\{PHa\}\} + |PHa|^2 - Vk^2 = 0$$

The quadratic equation can then be used to solve for G, the solution is chosen for the minimum magnitude. This solution produces the following equations for the G filter.

$$Hc = \text{conjugate}\{PHa\}$$

$$Gpa = Hg * Hc$$

$$a = |Hg| * |Hg|;$$

$$b = 2.0 * Gpa.\text{re};$$

$$c = |PHa| * |PHa| - Vk * Vk;$$

$$\text{Re}\{G\} = (-b - (b * b - 4.0 * a * c)^{1/2}) / (2.0 * a);$$

$$\text{Im}\{G\} = 0.0;$$

Due to the fact that the gyro data is not pre-filtered there is aliasing associated with the measured signal. The G filter is applied in the spatial domain to try to remove some of the aliasing at frequencies above 2 Hz and also to provide for a smooth transition between the gyro and ADS transition region. Using the definition above of the G filter in the frequency domain a spatial domain filter is achieved as follows.

Define: Filter size = N
 Padded filter size = M

Note: This explanation assumes that values for the filter are stored in an array. If speaking in the frequency domain then the buffer location 0 in the array is the DC term and location N/2 is the Nyquist frequency.

7.1 Determine an appropriate size for the G filter. Sehn and Miller state that a G filter of length 31 guarantees less than 1% filter approximation error. It should

also be noted that since the G filter is determined in the frequency domain it makes sense to choose a value as close to a power of 2 as possible since this is what the FFT routine needs. If a routine was used that did not need powers of 2 then this would not be an issue. The IAS uses a value of 63.

- 7.2 Find the nearest power of 2 larger than the associated filter size N. Zero pad the data to this length (this will make the data of size M).
 - 7.3 Step through the number of values chosen (filter length padded to a power of 2) calculating the frequency response of the filter, the equations were given above. This will be calculated at frequency increments that are dependent on the gyro sampling rate and the number of samples from step 2. In practice, only one half plus one of the filter size needs to be calculated due to step 7.4.
 - 7.4 The G filter needs to be real in the spatial domain therefore the Fourier Transform must be the symmetrical complex conjugate with respect to the origin, or for in this case the Nyquist frequency. Reference 6 gives a good explanation on the Fast Fourier Transform and some of its properties which should further explain this process.
 - 7.5 Calculate the inverse FFT of the results from step 7.4.
 - 7.6 Adjust the data so that it is of the original desired filter length N. It should be symmetrical about the center of the filter.
 - 7.7 Apply the filter coefficients calculated in step 7.6 to the gyro data. When the filter coefficients are applied to the ends of the gyro data the data is mirrored about its end points.
8. Synchronize (up sample) the data from step 7 so that agrees with the 2 msec sampling rate of the ADS data. The prototype uses a series of filters that allows better control on the response of the overall interpolation (final sampling rate). A further understanding and explanation of this process can be found in Reference 33. The filtering coefficients used in the IAS are:

<u>Num</u>	<u>scale</u>	<u>h0</u>	<u>h1</u>	<u>h2</u>	<u>h3</u>	<u>h4</u>
Filter 1	1.0	1.0	0.0	0.0	0.0	0.0
Filter 2	2.0	1.0	0.0	0.0	0.0	0.0
Filter 3	16.0	9.0	-1.0	0.0	0.0	0.0
Filter 4	32.0	19.0	-3.0	0.0	0.0	0.0
Filter 5	256.0	150.0	-25.0	3.0	0.0	0.0
Filter 6	346.0	208.0	-44.0	9.0	0.0	0.0

IAS Geometric ATBD Version 3

Filter 7	512.0	302.0	-53.0	7.0	0.0	0.0
Filter 8	802.0	490.0	-116.0	33.0	-6.0	0.0
Filter 9	8192.0	5042.0	-1277.0	429.0	-116.0	18.0

These numbers are reflected around the point of interest (the point to be interpolated). The filter coefficients are multiplied by the corresponding pixel it is associated with and the sum is then divided by the scale factor. This will give an interpolated point. For example, if interpolating a point between n and n+1 with filter 4 (pix(n) defines gray value at point n).

$$\begin{aligned} \text{sum} = & \quad h1 * \text{pix}(n-1) + \\ & h0 * \text{pix}(n) + \\ & h0 * \text{pix}(n+1) + \\ & h1 * \text{pix}(n+2) \end{aligned}$$

$$\text{new pix} = \text{sum} / \text{scale}[4]$$

The sampling start time and the time between samples for the smoothed low frequency data is:

$$x,y,z \text{ axis} \quad \text{PCD} + 64N \quad N = 0, \dots, 255$$

while the ADS is sampled at increments of:

$$\begin{aligned} x \text{ axis} & \quad \text{PCD} + 2N + 3/8 \text{ msec} \\ y \text{ axis} & \quad \text{PCD} + 2N + 7/8 \text{ msec} \\ z \text{ axis} & \quad \text{PCD} + 2N + 11/8 \text{ msec} \\ & \quad \text{where } N = 0, \dots, 8191 \end{aligned}$$

To get the smoothed low frequency data to have a time difference of 0.002 secs between samples the data is interpolated 5 times with the coefficients listed above. To account for the offsets in the ADS data, interpolation with the coefficients above is performed 4 times. This will allow a time difference between samples to be chosen such that every 16th sample will fall on an even increment of 0.002N secs from a PCD cycle. Since there is no valid data at N=0 the first value for each axis of the time synchronized ADS will be zero. The offset is accounted for by stepping ahead by a set number of data points. The first valid synchronized ADS will occur at 0.002 secs.

(Note: Interpolating 4 times gives the ADS a time difference of 0.000125 secs)

$$x\text{-axis} \quad (0.002 - 0.000375) / 0.000125 = 13 \text{ samples}$$

$$y\text{-axis} \quad (0.002 - 0.000875) / 0.000125 = 9 \text{ samples}$$

$$z\text{-axis} \quad (0.002 - 0.001375) / 0.000125 = 5 \text{ samples}$$

Every 16th sample is then chosen after taking into account the offset. This will return the time difference between samples to 0.002 secs.

9. Sum the synchronized data from step 8.
10. Apply the F filter to the data obtained in step 9. Since the ADS data is pre-filtered and due to the fact that the gyro data has been G filtered, the F filter can be applied in the frequency domain (aliased frequencies have been suppressed). Both Sehn and Miller and EOSAT determine a spatial domain filter for the F filter in much the same way that the G filter was determined. This approach would apply the F filter in the spatial domain and would eliminate the need for the data in step 9 to be a power of 2.

The F filter takes on the following values in the frequency domain:

$$F(\text{freq}) = 1.0 / [\text{PHa} + G(\text{freq})\text{Hg}]$$

The following steps were taken to apply the F filter.

- 10.1 Calculate the FFT of the data from step 9. It should be noted that if the FFT is used then the number of data elements, when summed, must be a power of 2.
- 10.2 Step through the data from step 10.1 calculating the response of the F filter given the definition above. This will be calculated at frequency increments that are dependent on the ADS sampling rate and the number of samples from step 10.1.
- 10.3 Reflect complex conjugate of the data from step 10.2 around the Nyquist data point (this is analogous to what was done for the G filter). This will assure that the inverse FFT of this data set will be real.
- 10.4 Multiply the data from steps 10.1 and 10.3.
- 10.5 Calculate the inverse Fourier transform of the data
- 10.6 This data will be the roll, pitch, and yaw due to attitude perturbations as measured from the gyro, gyro drift, quaternions and ADS of the satellite.
11. The combined data is rotated to the ACS.

(Details of steps 6 and 11 can be found in section 3.1.5.3.3, Convert ADS to a Common Reference System)

Attitude Processing Sign Conventions

The PCD quaternions are used to construct an orientation matrix which rotates the ACS axes to ECI as described on page 39 of the ATBD. This is premultiplied by a matrix which rotates ECI to Orbital coordinates, constructed from the ephemeris data, to create an ACS to Orbital rotation matrix (body to orbit). This matrix is mapped to the roll, pitch, yaw perturbation matrix:

$$\begin{array}{ccc} \cos(p) \cos(y) & \sin(r) \sin(p) \cos(y) + \cos(r) \sin(y) & \sin(r) \sin(y) - \cos(r) \sin(p) \cos(y) \\ -\cos(p) \sin(y) & \cos(r) \cos(y) - \sin(r) \sin(p) \sin(y) & \cos(r) \sin(p) \sin(y) + \sin(r) \cos(y) \\ \sin(p) & -\sin(r) \cos(p) & \cos(r) \cos(p) \end{array}$$

From the last row and first column of this matrix:

$$\text{roll} = \tan^{-1}(-m_{32}/m_{33}) = -\tan^{-1}(m_{32}/m_{33})$$

$$\text{pitch} = \sin^{-1}(m_{31})$$

$$\text{yaw} = \tan^{-1}(-m_{21}/m_{11}) = -\tan^{-1}(m_{21}/m_{11})$$

These are the body to orbit rotation angles.

Orbital motion is removed from the gyro data as follows. The ephemeris data is used to construct the ECI to orbital rotation matrix at the first PCD major frame time (ECI2ORB₀). At each subsequent gyro point, the ephemeris is interpolated and used to construct the instantaneous ECI to orbital rotation matrix which is inverted to form the instantaneous orbital to ECI rotation matrix ORB_t2ECI. These arrays are multiplied (ECI2ORB₀ ORB_t2ECI) to form the rotation from the instantaneous orbital coordinate system to the orbital coordinate system at the beginning of the PCD interval, ORB_t2ORB₀. The same logic used above for the quaternions is used to extract roll, pitch, and yaw values from this composite matrix yielding body to orbit rotation angles where the “body” coordinate system is taken to be the ideal ACS which is perfectly aligned with the instantaneous orbital coordinate system, relative to the reference orbital coordinate system at PCD start. These “ideal” angles are subtracted from the gyro samples so that the gyro data reflects deviations from the ideal orbital coordinate system, or body to orbit rotation angles. These gyro body to orbit angles are combined with the body to orbit angles derived from the quaternions, in the Kalman filtering procedure.

After the quaternion and gyro data are combined the first filtered attitude sample value is subtracted from all of the samples and saved as a zero frequency (DC) reference. This DC reference is sign inverted to form an orbit to body rotation reference. The residual gyro samples are combined with the ADS data and, in the course of this filtering process, are sign inverted so that the blended high frequency attitude data represent orbit to body

perturbations. The orbit to body DC reference and the orbit to body high frequency perturbations are added to form the net orbit to body rotation which is used in the satellite model.

3.1.5.3.4 Line of Sight Generation and Projection

The algorithms that follow are used by the Geometric Correction Grid algorithm. The inputs to this algorithm are line, sample, and band. This algorithm also uses the information which was compiled and converted into a usable form in the Create Model algorithm. The result of this algorithm is the geodetic latitude and longitude for a point on the Earth, or a height h above the surface, which corresponds to the entered line, sample, and band of the input image.

Calculate Sample Time

The scan line number is found by subtracting 1 from the line number and then dividing by the number of lines per scan for the given band and then truncating.

The detector number is found by taking the decimal value remaining of the scan line number, before truncating, and multiplying by the number of lines per scan.

N = number of lines per scan

$$S = \text{remainder} \frac{\text{LineNumber} - 1}{N}$$

detector = $N - \text{floor}(S*N)$

The time into the current scan is found by:

For forward scans:

$$\text{time_in_scan} = (\text{sample} - 1.0 + \text{bandoffset}) * \text{DWELLTIME}$$

For reverse scans

$$\text{time_in_scan} = (\text{scan}[*\text{scan_line}].\text{counted_line_length} - \text{sample} + \text{bandoffset}) * \text{DWELLTIME}$$

For Landsat 7, the bands are aligned using left justified padding and so the padding must be removed from the calculation as a function of band. The LOR scan line offset (SLO) date are used to accomplish this.

The time from start of image is found using the MSCD start of scan value for the current scan minus the MSCD start of scan value for the first scan plus the time in scan.

Calculate Viewing Angles

Find the across-scan angle of a detector due to its location within the band. *Note: This example is for the multi-spectral bands.*

$$\text{detector_angle} = (\text{LINES_SCAN} / 2.0 - \text{detector} + 0.5) * \text{IFOVMS}$$

Find the along-scan 5th order polynomial correction. For forward scans use the time-in-scan value to determine the correction; for the reverse scans use the total scan time minus the time-in-scan value to determine the correction value. Do the same for the across-scan 5th order correction.

The polynomial coefficients and scan start and stop angles are provided as measures of mirror rotation. Since the instrument optical axis is being reflected off of the scan mirror the effect on the line of sight in object space is twice the mirror angle. The scan mirror model and the focal plane geometry must be combined to calculate object space along-scan angles in the sensor coordinate system. The IAS sign convention is defined so that positive scan angles are in the direction of the sensor Y axis (as described in section 3.1.2). The along-scan angle for band "BAND" is calculated as a function of time "TIME" as follows:

For forward scans:

$$s_{2m} = A_{fsm} = \text{start to midscan angle}$$

$$s_{2e} = A_{fsm} + A_{fme} = \text{start to end angle}$$

$$\text{along_angle} = 2.0 * (s_{2m} - s_{2e} * \text{TIME}/T_s + f(b, \text{TIME})) \\ + \text{bandoff_along[BAND]} - \text{odd_det_off[BAND]}$$

where $f(b, \text{TIME})$ is the corrected fifth-order polynomial model.

For reverse scans:

$$s_{2m} = A_{rsm}$$

$$s_{2e} = A_{rsm} + A_{rme}$$

$$\text{along_angle} = 2.0 * (-s_{2m} + s_{2e} * \text{TIME}/T_s + r(b, T_s - \text{TIME})) \\ + \text{bandoff_along[BAND]} - \text{odd_det_off[BAND]}$$

where $r(b, \text{TIME})$ is the corrected fifth-order polynomial model.

The across-scan angle is found using a linear interpolation of the Scan Line Corrector Mirror's position, which is a function of time in scan. Also accounted for is the Scan Mirror's across-scan 5th order correction, the detector angle, and the across-scan focal-plane offset.

Thus, the model for the SLC angle as a function of time in scan is:

$$\text{slc_angle} = \text{slc_start}[\text{SCANDIR}] - \text{slc_max}[\text{SCANDIR}] * \text{TIME}/\text{Ts}$$

where:

slc_angle = across-scan pointing angle (positive in the direction of flight)

slc_start = SLC angle at the beginning of scan (indexed by scan direction)

SCANDIR = index for scan direction (forward or reverse)

slc_max = total SLC angle (indexed by scan direction)

TIME = time in scan

Ts = total scan time

The same equation applies for forward and reverse scans, with the appropriate selection of the SLC start and SLC total angles. The sign convention and direction of SLC motion is the same in either case: positive angles are in the direction of flight (toward the sensor X axis) with the SLC rotating from a positive to a negative angle in each scan.

The SLC angle must be combined with the across-scan detector angle and the scan mirror across-scan correction polynomial to compute the total across-scan look angle for detector N in band BAND:

For forward scans:

$$\begin{aligned} \text{cross_angle} = & \text{slc_start}[\text{FWD}] - \text{slc_max}[\text{FWD}] * \text{TIME}/\text{Ts} \\ & + 2.0 * f(\text{b}, \text{TIME}) + \text{bandoff_cross}[\text{BAND}] \\ & + ((\text{ndets}[\text{BAND}] + 1)/2 - \text{N}) * \text{IFOV}[\text{BAND}] \end{aligned}$$

where $f(\text{b}, \text{TIME})$ is the scan mirror across-scan correction polynomial evaluated at the time of interest and all other components are as defined previously.

For reverse scans:

$$\begin{aligned} \text{cross_angle} = & \text{slc_start}[\text{REV}] - \text{slc_max}[\text{REV}] * \text{TIME}/\text{Ts} \\ & + 2.0 * r(\text{b}, \text{TIME}) + \text{bandoff_cross}[\text{BAND}] \\ & + ((\text{ndets}[\text{BAND}] + 1)/2 - \text{N}) * \text{IFOV}[\text{BAND}] \end{aligned}$$

where $r(\text{b}, \text{TIME})$ is the scan mirror across-scan correction polynomial evaluated at the time of interest. Note that the only difference between forward and reverse scans is the selection of the appropriate SLC parameters, as mentioned above, and the application of the scan mirror across-scan correction polynomial.

Calculate LOS Vector

This algorithm uses the time in which a pixel was imaged to find the attitude, position, and velocity of the spacecraft. The along and across-scan angles are used to construct a ideal line of sight (LOS) vector in sensor space. This LOS vector is transformed to the spacecraft navigation reference base and is then transformed using the attitude information to the Orbital Coordinate System (OCS). The OCS LOS vector is then transformed to the Earth centered coordinate system.

1. To find the attitude, this algorithm uses the time from first ADS value to the time of pixel imaging to look up the ADS and gyro combined attitude in the combined attitude table. This table was constructed in the Process Attitude module. Added to the roll, pitch, and yaw values from the table are the spacecraft's roll, pitch, and yaw values (the DC reference values).
2. The “move satellite” algorithm uses the time from the reference ephemeris point to the time of pixel imaging to interpolate a new, ECEF, satellite position and velocity. The polynomials for this interpolation were defined in the Create Model module in the Calculate Satellite State Vector algorithm.
3. The Find LOS algorithm uses the along and across-scan angles to construct a LOS vector in the sensor's coordinate system.

$$\text{los}_x = \sin(\text{across_angle}) * \cos(\text{along_angle})$$

$$\text{los}_y = \sin(\text{along_angle})$$

$$\text{los}_z = \cos(\text{across_angle}) * \cos(\text{along_angle})$$

4. The Attitude algorithm transforms the LOS vector to the spacecraft's ACS coordinate system. This vector is then transformed using the spacecraft's attitude to the OCS, and then the vector is transformed to the Earth Centered Earth Fixed (ECEF) coordinate system.

Transform the LOS from the sensor coordinate system to the ACS coordinate system:

$$\begin{matrix} ACS \\ LOS \end{matrix} = \begin{matrix} 3x3 \\ Transformation \\ Matrix \end{matrix} \begin{matrix} Sensor \\ LOS \end{matrix}$$

The 3 x 3 transformation matrix from the sensor to the ACS is determined pre-launch. As part of the IAS calibration activities, this matrix, from time to time will be checked

and, if required, updated. The members of this matrix will be contained in the Calibration Parameter File.

Transform the ACS LOS to the OCS using the attitude information by:

$$\begin{matrix} \text{Orbital} \\ \text{LOS} \end{matrix} = [\text{YAW}]^{-1} [\text{PITCH}]^{-1} [\text{ROLL}]^{-1} \begin{matrix} \text{ACS} \\ \text{LOS} \end{matrix}$$

Transform the Orbital LOS to the ECEF coordinate system.

$$\begin{matrix} \text{ECEF} \\ \text{LOS} \end{matrix} = \begin{matrix} 3 \times 3 \\ \text{Transformation} \\ \text{Matrix} \end{matrix} \begin{matrix} \text{Orbital} \\ \text{LOS} \end{matrix}$$

The 3X3 OCS to ECEF transformation matrix is found using the unit vectors of the axes for the Orbital Coordinate System (OCS) determined in the ECEF coordinate system. The Z axis of the OCS is defined as the negative of the spacecraft's position vector. The Y axis of the OCS is the negative of the spacecraft's angular momentum vector or (V X R). The X axis is the cross product of the Y axis with the Z axis (Y X Z).

Intersect LOS Vector With Earth

This algorithm finds the geocentric location on the ellipsoid of the intersection of the LOS vector to the ellipsoid or at a constant elevation for the entire scene above the ellipsoid.

The satellite's position vector, the LOS vector, and an elevation are the input to this algorithm and the geocentric location of the intersection is output in both the Cartesian and spherical coordinates.

This algorithm uses an iterative method to locate the intersection. The satellite's geocentric latitude is used as the first guess in this process. This latitude is used to find the geocentric radius of the ellipsoid plus the elevation at this latitude. Using the angle between the satellite's position vector and the LOS vector, the radius of the Earth, and the plane trigonometry's law of cosines, the magnitude of the LOS vector is found. The intersection is the addition of the satellite's position vector and the scaled LOS vector. However, this location was determined using a slightly incorrect latitude. Thus, the calculated intersection's geocentric latitude is used as the second guess. This process is continued until the LOS magnitude difference between iterations is small (< 0.01 meter).

Another approach is to use the reduced latitude in the calculation. This allows for a direct solution for a point on the surface of the ellipsoid. The solution is as follows:

Define \mathbf{R}_s as the position vector of the satellite, \mathbf{LOS} as the line of sight vector and \mathbf{R}_t as the position vector of the target in question. The position vector of the target using the reduce Latitude psi, its longitude Lt and the semi-major a and the semi-minor b axes is:

$$\mathbf{R}_t = X_t \mathbf{i} + Y_t \mathbf{j} + Z_t \mathbf{k}$$

$$X_t = a * \cos(\text{psi}) * \cos(\text{Lt})$$

$$Y_t = a * \cos(\text{psi}) * \sin(\text{Lt})$$

$$Z_t = b * \sin(\text{psi})$$

The solution requires the following equation to be true.

$$\mathbf{R}_t = \mathbf{R}_s + m * \mathbf{LOS}$$

Where m is the magnitude of the final LOS vector. The current LOS vector has a magnitude of 1.

or as separate components:

$$X_t = a * \cos(\text{psi}) * \cos(\text{Lt}) = X_s + m * X_{\text{los}}$$

$$Y_t = a * \cos(\text{psi}) * \sin(\text{Lt}) = Y_s + m * Y_{\text{los}}$$

$$Z_t = b * \sin(\text{psi}) = Z_s + m * Z_{\text{los}}$$

A vector \mathbf{R}_t' with a magnitude of 1 can be constructed by dividing the X_t and Y_t components by a and dividing the Z_t component by b .

$$\mathbf{R}_t' = X_t' \mathbf{i} + Y_t' \mathbf{j} + Z_t' \mathbf{k}$$

$$X_t' = X_t / a = \cos(\text{psi}) * \cos(\text{Lt}) = X_s / a + m * X_{\text{los}} / a$$

$$Y_t' = Y_t / a = \cos(\text{psi}) * \sin(\text{Lt}) = Y_s / a + m * Y_{\text{los}} / a$$

$$Z_t' = Z_t / b = \sin(\text{psi}) = Z_s / b + m * Z_{\text{los}} / b$$

Or

$$\mathbf{R}_t' = \mathbf{R}_s' + m * \mathbf{LOS}'$$

Using the law of cosines for a plane:

$$|\mathbf{R}_t'|^2 = m^2 * |\mathbf{LOS}'|^2 + |\mathbf{R}_s'|^2 - 2 * m * |\mathbf{LOS}'| * |\mathbf{R}_s'| * \cos(w) = 1$$

where w is the angle between the satellite's position vector and the line of sight vector. Due to \mathbf{R}_t' being defined to have a magnitude of 1, the only unknown left in the equation is m .

Re-arranging the equation to use the quadratic formula to solve for m results in:

$$0 = m^2 * |\mathbf{LOS}'|^2 - 2 * m * |\mathbf{LOS}'| * |\mathbf{R}_s'| + |\mathbf{R}_s'|^2 - 1$$

and thus, the solution for \mathbf{R}_t is:

$$\mathbf{R}_t = \mathbf{R}_s + m * \mathbf{LOS}$$

The geocentric location is then converted to a geodetic location. The theory behind this routine is found in Reference 20, page 398.

Speed of Light Correction

Due to the non-infinite velocity of light, the velocity of a point on the surface of the Earth and the velocity of the satellite, cause pixel location errors if not accounted for. The speed of light correction due to the Earth's rotation is sub-meter and is currently not accounted for. The speed of light correction for due to the satellite's velocity is approximately a constant for Landsat 7. The magnitude is about 15 meters and is in the along track direction and is applied in the model.

3.1.5.3.5 Correction Grid Generation

The ETM+ Geometric Correction Grid defines the piece-wise (gridded) geometric transformation of imagery in satellite perspective to corrected imagery in a user specified output projection of user-specified geographic extent. The grid is used by the geometric transformation function (the Resampler) to rectify the image data to the corrected image output space.

This algorithm assumes that the Landsat satellite model has been initialized using the input image's associated PCD and MSCD files. It also assumes that the output projection system is defined and read from a projection definition file. [Reference 19]. This algorithm also requires the frame (geographic extent) of the resulting output space

image, and the dimension of each pixel in the output coordinate space. Note: The PCD and MSCD files are used by the Landsat satellite model to define the input image's (0R or 1R) geometric space.

Note: Refer to the LAS Geometric Manipulation Overview Document [Reference 18] for more information on specific projection parameters for a given projection, and for information on the Projection Transformation Package, a coordinate transformation subroutine library based on the U.S. Geological Survey's General Cartographic Transformation Package (GCTP).

Defining the Frame

The first step in the gridding process is to determine the geographic extent of the output image to be generated by the resampler. This geographic extent of the output image space is referred to as the output space “frame”, and is specified in output image projection coordinates. There are four different methods that are used to determine the output frame.

Method 1:

The user defines the upper-left and lower-right corner coordinates of the area of interest in geographic (latitude/longitude) coordinates. These coordinates are then projected to the output projection coordinate system using the Projection Transformation Package. This usually results in a non-rectangular area so a minimum bounding rectangle is found (in terms of minimum and maximum X and Y projection coordinates) in the resulting output space. This minimum bounding rectangle defines the output space frame. The output image pixel size is then applied to the projection space to determine the number of lines and samples in the output space.

Method 2:

The user defines a rectangular area in the output space by specifying upper-left and lower right output space projection coordinates. The output image pixel size is then applied to the projection space to determine the number of lines and samples in the output space.

Method 3:

The user defines an upper-left output space projection coordinate, the output image pixel size, and the number of lines and samples in the output image. The coordinate pair must be the minimum X and maximum Y projection coordinate. The maximum X and minimum Y coordinates (the other end of the bounding rectangle) are then calculated.

Method 4:

The user allows the framing software to project the 4 corners of the input LOR data set to the Earth ellipsoid. This will produce the minimum bounding rectangle which contains all of the input image data.

Method 5:

The user specifies a path oriented Landsat product in either the Space Oblique Mercator (SOM) or Universal Transverse Mercator (UTM) projection. In this case, the framing coordinates are not user-specified. The frame is a preset number of lines and samples based on the Landsat World-wide Reference System (WRS) scene size and the maximum rotation needed to create a path oriented product. For a pixel size of 30 meters, a rectified image in the SOM or UTM projection is approximately 6440 lines by 6850 samples in size.

For diagrams and more information on the framing process, refer to the LAS Geometric Manipulation Package Overview Document [Reference 18].

Path Oriented Framing and Rotation

A path oriented projection is basically a rotation from a typical "map-north" up projection that better represents the near polar orbit of the Landsat satellite (nominal inclination angle of 98.2 degrees). The path oriented projection also does a better job of maintaining the scan line to the output space line.

The first step in generating a path oriented projection is to calculate the center location in the output space that the frame is to be rotated about. This is done by computing the nominal WRS scene center for the current path and row. The frame is centered in the output projection space at this projection coordinate and will be rotated about this point.

The procedure for computing the WRS scene center and the associated rotation angle is:

Given:

Parameter	Value	Source
Earth Parameters		
Semi-Major Axis	6378137.0 m	CPF:Earth_Constants:Semi_Major_Axis
Semi-Minor Axis	6356752.314 m	CPF:Earth_Constants:Semi_Minor_Axis
L7 Orbit Parameters		
Inclination	98.2 degrees	CPF:Orbit_Parameters:Inclination_Angle
L7 WRS Parameters		

Number of Paths	233	CPF:Orbit_Parameters:WRS_Cycle_Orbits
Number of Rows	248	CPF:Orbit_Parameters:Scenes_Per_Orbit
WRS Repeat Cycle	16 days	CPF:Orbit_Parameters:WRS_Cycle_Days
Desc Node Row	60	CPF:Orbit_Parameters:Descending_Node_Row
Long of 001/060	-64.6 degrees	CPF:Orbit_Parameters:Long_Path1_Row60
Input Parameters		
Path	Integer 1-233	User
Row	Float $0 < R < 249$	User

Find:

WRS Scene Center Latitude
WRS Scene Center Longitude
Scene Heading

Method:

Convert input angles to radians:

$$\text{Inclination_Angle} = \text{Pi} / 180 * \text{Inclination_Angle}$$

$$\text{Long_Path1_Row60} = \text{Pi} / 180 * \text{Long_Path1_Row60}$$

Compute the Earth's angular rotation rate:

$$\text{earth_spin_rate} = 2 * \text{Pi} / (24 * 3600)$$

Note: We use the solar rotation rate rather than the sidereal rate as called for in the General Electric Landsat D PIR which describes the Worldwide Reference System, in order to account for the orbital precession which is designed to make the orbit sun synchronous. Thus, the apparent Earth angular velocity is the inertial (sidereal) angular velocity plus the precession rate which, by design, is equal to the solar angular rate.

Compute the spacecraft's angular rotation rate:

$$\text{SC_Ang_Rate} = 2 * \text{Pi} * \text{WRS_Cycle_Orbits} / (\text{WRS_Cycle_Days} * 24 * 3600)$$

Compute the central travel angle from the descending node:

$$\text{Central_Angle} = (\text{Row} - \text{Descending_Node_Row}) / \text{Scenes_Per_Orbit} * 2 * \text{Pi}$$

Compute the WRS geocentric latitude:

$$\text{WRS_GCLat} = \text{asin}(-\sin(\text{Central_Angle}) * \sin(\text{Inclination_Angle}))$$

Compute the longitude of Row 60 for this Path:

$$\text{Long_Origin} = \text{Long_Path1_Row60} - (\text{Path} - 1) * 2 * \text{Pi} / \text{WRS_Cycle_Orbits}$$

Compute the WRS longitude:

$$\Delta_{\text{Long}} = \text{atan2}\left(\frac{\tan(\text{WRS_GCLat})}{\tan(\text{Inclination_Angle})}, \cos(\text{Central_Angle})/\cos(\text{WRS_GCLat})\right)$$

$$\text{WRS_Long} = \text{Long_Origin} - \Delta_{\text{Long}} - \text{Central_Angle} * \text{Earth_Spin_Rate} / \text{SC_Ang_Rate}$$

Make sure the longitude is in the range +/- Pi:

$$\text{While} (\text{WRS_Long} > \text{Pi})$$

$$\text{WRS_Long} = \text{WRS_Long} - 2 * \text{Pi}$$

$$\text{While} (\text{WRS_Long} < -\text{Pi})$$

$$\text{WRS_Long} = \text{WRS_Long} + 2 * \text{Pi}$$

Compute the scene heading:

$$\text{Heading_Angle} = \text{atan2}\left(\frac{\cos(\text{Inclination_Angle})}{\cos(\text{WRS_GCLat})}, -\cos(\Delta_{\text{Long}}) * \sin(\text{Inclination_Angle})\right)$$

Convert the WRS geocentric latitude to geodetic latitude:

$$\text{WRS_Lat} = \text{atan}\left(\frac{\tan(\text{WRS_GCLat}) * (\text{Semi_Major_Axis}/\text{Semi_Minor_Axis})}{(\text{Semi_Major_Axis}/\text{Semi_Minor_Axis})}\right)$$

Convert angles to degrees:

$$\text{WRS_Lat} = \text{WRS_Lat} * 180 / \text{Pi}$$

$$\text{WRS_Long} = \text{WRS_Long} * 180 / \text{Pi}$$

$$\text{Heading_Angle} = \text{Heading_Angle} * 180 / \text{Pi}$$

Round WRS lat/long off to the nearest whole arc minute:

$$\text{WRS_Lat} = \text{round}(\text{WRS_Lat} * 60) / 60$$

$$\text{WRS_Long} = \text{round}(\text{WRS_Long} * 60) / 60$$

Return the answers:

WRS_Lat

WRS_Long

Heading_Angle

The WRS heading angle, from geodetic north, will need to be converted from the WRS scene center to a frame orientation angle in map coordinates. This can be done by first converting the WRS scene center lat/long to map projection X1, Y1 and moving to a point slightly north of the WRS scene center. This is done by adding 1 microradian (0.2seconds) to the WRS scene center latitude and projecting this point to X2, Y2. Next the azimuth of this line is computed in grid space as the arctangent of the X difference (X2-X1) over the Y difference (Y2-Y1). This is the grid azimuth of geodetic north at the WRS scene center. Adding this angle to the geodetic heading to give the grid heading. A standard framed scene puts the satellite direction of flight at the bottom of the scene so the scene orientation angle is the grid heading plus or minus 180 degrees. If the grid

heading is less than zero add 180 degrees. If the grid heading is greater than zero subtract 180 degrees. This is the scene orientation angle to be used with the WRS scene center and the fixed standard scene size to calculate the frame corners.

It should be noted that the preceding approach does not take into account the skewing of the image data. Skewing of the image is due to the Earth's rotation relative to the spacecraft's absolute velocity.

A delta X and delta Y are calculated from the center of the projection space to the four corners of the output frame area using the output pixel size and the number of lines and samples in the output space.

Example: Calculation of the upper right delta X and delta Y

$$\begin{aligned}\text{delta_x} &= (\text{number_samples} - \text{center_sample}) * \text{pixel_size} \\ \text{delta_y} &= (\text{center_line} - 1.0) * \text{pixel_size}\end{aligned}$$

The deltas and the scene orientation angle are then used to calculate the rotated projection coordinate of each corner.

$$\begin{aligned}\text{ur_proj_x} &= \text{delta_x} * \cos(\text{angle}) + \text{delta_y} * \sin(\text{angle}) + \text{center_proj_x} \\ \text{ur_proj_y} &= -\text{delta_x} * \sin(\text{angle}) + \text{delta_y} * \cos(\text{angle}) + \text{center_proj_y}\end{aligned}$$

A least squares routine is used to generate a first order polynomial which maps output image (line, sample) coordinates to rotated output projection coordinates.

The output pixel size and projection coordinates are saved in the mapping grid file.

Gridding The Input Space

For the process of rectifying the ETM+ satellite imagery to a given projection, a regular grid is defined over the input space, one set per scan. This separate, forward mapping is necessary to properly correct for gaps between scans and because an inverse satellite model cannot be defined. The first and last lines from each scan are represented in the gridding of the input. The difference between the last line of a scan (line 16 for TM multi-spectral bands, line 8 for the thermal band, and line 32 for the Pan band) and the first line of the next scan, is used to determine the scan gap. These scan gaps are corrected in the ETM+ geometric resampling process. Refer to the Landsat 7 Wide Band Data Format Book (Reference 1) for more information about the Landsat 7 instrument and scan gap. The grid spacing in the along-scan (sample) direction 96 pixels--a factor that divides into the total number of input image samples and that coincides with the ADS sampling rate.

(The typical value used in for Landsat 4 and 5 was 128 pixels.) Figure 3.1.5-11 illustrates the gridding of an input image:

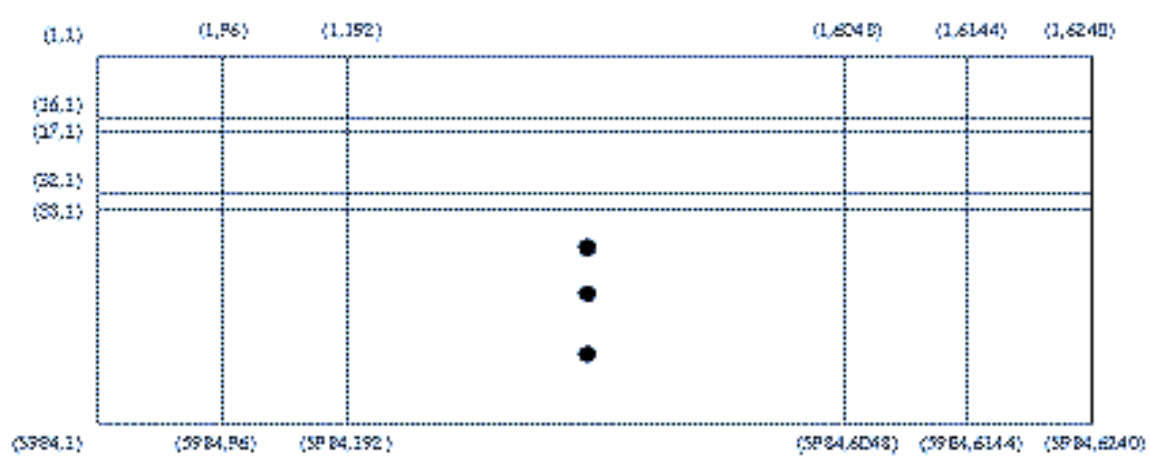


Figure 3.1.5- 11 Input Image Gridding Pattern

Relating Input to Output Space

The Landsat 7 mapping grids are defined in image (line, sample) coordinates which map input (level-0) line, samples to output, projected space line, samples. At each grid intersection (input line and sample) the initialized Landsat satellite model is called to calculate the geometric latitude and longitude at that point. Using the projection definition information as input to the Projection Transformation Package, the output projection coordinate is then calculated for each latitude and longitude point. From the output projection coordinates an output line and sample location, in the defined output frame, is calculated for each point. For a path oriented product, the polynomial is evaluated at each output projection coordinate. This mapping takes care of both the rotation of the projection space and the scaling from projection coordinates to image (line, sample) coordinates. The polynomial (called once for x coordinates and once for y coordinates) is of the form:

$$x' = a_0 + a_1x + a_2y$$

where: x' is the output line or sample and
 x and y are output space projection coordinates

For the other output projections (when there is no rotation between the image coordinate system and the projection coordinate system) the output line and samples are calculated directly using the following equations:

$$\begin{aligned} \text{out_line} &= (\text{ul_proj_y} - \text{proj_y}) / \text{pixel_size} + 1 \\ \text{out_samp} &= (\text{proj_x} - \text{ul_proj_x}) / \text{pixel_size} + 1 \end{aligned}$$

The input line and sample, output line and sample, and the projection information are written to a grid file. This geometric mapping grid file defines the transformation between the satellite image and the specified output projection. The grid file is used by the resampler to geometrically rectify the input image to the user-specified output image frame, projection, and pixel size.

The above process is done to create a grid for each band that is to be processed. The net effect is that there is a grid for each band in the grid file. This is necessary because of timing offset differences between bands.

3.1.5.3.6 Resampling

This section describes the IAS image resampling algorithm.

Calculate Scan Gap

This algorithm will calculate the scan gap and the sample shift between each grid cell of two consecutive scans. This information will be used to create a synthesized or extended image that will fill any gaps or "missing data" between two scans. A scan gap will refer to a line offset between consecutive scans that is larger than the nominal scan line spacing while a misalignment will refer to sample offset between consecutive scans in the image. A least squares routine is used in this algorithm to calculate mapping coefficients. The algorithm follows:

1. Loop through each grid cell calculating the scan gap and misalignment. This is done using the mapping equations for each grid cell:

Forward mapping equations:

$$\begin{aligned} S_o &= a_0 + a_1 * S_i + a_2 * L_i + a_3 * S_i * L_i \\ L_o &= b_0 + b_1 * S_i + b_2 * L_i + b_3 * S_i * L_i \end{aligned}$$

Where

S_i is the input sample

S_o is the output sample

L_i is the input line

L_o is the output line

$a_0, a_1, a_2, a_3, b_0, b_1, b_2, b_3$ are the bilinear mapping coefficients.

Inverse mapping equations:

$$S_i = c_0 + c_1 * S_o + c_2 * L_o + c_3 * S_o * L_o$$
$$L_i = d_0 + d_1 * S_o + d_2 * L_o + d_3 * S_o * L_o$$

Where

S_i is the input sample

S_o is the output sample

L_i is the input line

L_o is the output line

$c_0, c_1, c_2, c_3, d_0, d_1, d_2, d_3$ are the bilinear mapping coefficients.

The four corners of each grid cell are used to solve for the mapping coefficients.

By using the forward and inverse mapping equations for each grid cell of a scan along with the mapping equations for the grid cell of the scan directly below, the maximum gap is obtained. (If scan N cell M is being processed then it is compared with scan N+1 cell M). This is shown in figure 3.1.5 -12.

Also during this time the mapping coefficients are calculated (forward and inverse) for each grid cell and the inverse coefficients are stored in the grid structure.

These values are obtained from the following steps. (Scan N cell M is used to designate one grid cell):

1. Loop through each grid cell of each scan, except for the last scan since this scan cannot have a gap. Repeat steps 2-8 for number of grid cells.
2. Create a fictitious "extended" pixel 17E located directly (one line length) below scan N cell M.
3. Find the output to input (inverse coefficients) and input to output (forward coefficients) mapping coefficients for scan N cell M.
4. Store the inverse mapping coefficients into the grid structure.
5. Map pixel 17E to the output space using the forward mapping equations for scan N cell M.
6. Find the output to input mapping coefficients for scan N+1 cell M.
7. Map the output pixel created in step 5 back to the input space using the inverse mapping equations for scan N+1 cell M (call this point x_g, y_g).

8. The difference between (x_g, y_g) and sample one line one of scan $N+1$ cell M represents the misalignment and the scan gap for scan N cell M . See figure 3.1.5-12.
 9. Find inverse mapping coefficients for grid cells of last scan and store these coefficients into the grid structure.
2. The maximum scan gap in the image is found. The maximum scan gap and the resampling kernel size will determine the size of the intermediate extended image. These two parameters will determine the number of gap, or extended, lines needed (gap_lines).

A gap of greater than $1/32$ of a pixel is considered large enough to add one extra line to each scan. This number represents the pixel increments of the resampling kernel.

The image must also be extended according to the resampling kernel size. A value of kernel size minus one will make it possible to only need one scan of data at a time during resampling. If this was not done then at the bottom of each scan the resampling kernel would step into the scan directly below. Due to scan gap and misalignment this data would need to be resampled to "fit", evenly spaced pixels, the current scan being processed. To avoid a redundancy of this step it is only done once up front during extended image generation.

See Reference 26 and Reference 27 for more information about the characteristics of scan gap. Refer to Reference 28, Reference 29, and Reference 18 for more information about geometric corrections and transformations.

Creating the Extended Image

References 26 and 27 describe scan gap correction. It should be noted that these documents refer to LANDSAT 4 and 5. These documents also follow the traditional three pass approach for extending the gap and creating an output image.

Each scan is extended by both the maximum number of lines missing due to the scan gap and due to the resampling kernel size.

Algorithm:

1. Create weight tables. A set of cubic convolution weights are set up with $1/32$ pixel increments. This table will be used to resample the data in the sample direction. The weights are set up for a shift of 0.0 to 1.0 pixels at $1/32$ increments. A set of spline weights are set up with $1/32$ pixel increments. This table will be used to resample in the line direction. The weights are set up for a shift of 0.0 to the maximum gap

possible from the system. A value of 3.0 covers the maximum gap possible in the LANDSAT 5 satellite. A value of 6.0 will be needed for the LANDSAT 7 satellite, to cover the PAN band.

2. Loop through the image creating extra image data after each grid cell of every scan, except for last scan which does not need to be extended. (For the processing of scan N cell M); Repeat steps 3-6 for appropriate number of extended lines needed.
3. Get misalignment and scan gap for the current grid cell.
4. Determine data needed.
 - a) If the gap is zero then the lines are extracted only from the scan below and resampled to adjust for scan misalignment and detector delays.
 - b) If the scan gap is greater than zero then the first extended line is created from the last two lines from scan N and first two lines from scan N+1. These lines are used as long as an extended line falls in between their line locations. When the extended line starts to fall into scan N+1, going beyond line one of scan N+1, then the lines used must be incremented appropriately. This can be explained by looking at figure 3.1.5-12. If $x_1=1.0$, $x_2=2.0$, $x_3=4.5$, and $x_4=5.5$ corresponds to the line locations of the last two lines in scan N and the first two lines in scan N+1 respectively, then extended lines will be created at 3.0 and 4.0 using these four lines. In this case both extended lines fall between these four lines. However, when an extended line is created at 5.0 a new set of lines need to be chosen such that $x_1=3.0$, $x_2=4.0$, $x_3=5.5$, and $x_4=6.5$. At this point the first two lines are the previously created extended lines while the other two lines used will be from scan N+1 and will correspond to lines two and three. This pattern will then follow with two extended lines being used along with two lines from scan N+1 for all other lines created.
 - c) If the scan gap is less than zero then the first extended line is created with two lines from the scan N and scan N+1. The lines taken correspond to the last two from scan N and two from scan N+1 incremented by the appropriate offset. If the scan gap is -0.5 then lines 15 and 16 from scan N would be used along with lines 2 and 3 from scan N+1. After the first extended line is created it is used for further processing and only one new line from scan N+1 is needed. For the example just given the second iteration would include line 16 from scan N, the extended line created in the previous iteration, along with lines 3 and 4 from scan N+1.

5. The lines taken from scan N are resampled to adjust for detector delays. The data will be resampled using cubic convolution for a constant shift across the whole line, where the shift is equal to the detector delay of that line.
6. The lines taken from scan N+1 are resampled to adjust for detector delay and misalignment. The data will be resampled using cubic convolution so that it is scaled and shifted to account for geometric misalignment and scaling differences between the scan N cell M and scan N+1 cell M. It will also take into account detector delays. The transformation is treated as a linear relationship, mapping the lines from scan N+1 so that the samples line up in the sample direction.

This is done by the following relationship

$$\begin{aligned}
 S1N1 &= \text{seg} * \text{ns} + 1 \\
 S2N1 &= (\text{seg}+1)*\text{ns} + 1 \\
 \\
 S1N2 &= S1N1 - \text{misalignment}[\text{seg}]; \\
 S2N2 &= S2N1 - \text{misalignment}[\text{seg}+1]; \\
 \\
 m &= (S2N2 - S1N2) / (S2N1 - S1N1); \\
 b &= S1N2 - S1N1 * a1 + \text{delay}; \\
 \\
 \text{new_sample} &= m * \text{old_sample} + b;
 \end{aligned}$$

where

- S1N1 = first sample from scan N
- S2N1 = second sample from scan N
- S1N2 = first sample from scan N + 1
- S2N2 = second sample from scan N + 1
- m and b = mapping coefficients
- out_sample = newly mapped sample
- in_sample = sample from scan N+1
- delay = detector delay for line from scan N+1
- seg = current scan cell
- misalignment = scan misalignment between two cells
- ns = length of a cell

7. A new line is produced using the four lines created from steps 4 and 5. This is done using a cubic spline which will take into account the unequal spacing between pixels due to scan gap. The scan gap is treated as a linear function over the scan cell.

This is done by the following relationship

$$m = (\text{gap_at_end} - \text{gap_at_start}) / \text{ns};$$

$b = \text{gap_at_start};$

$\text{new_gap} = m * \text{sample} + b$

where

gap_at_start = size of scan gap at the start of grid cell

gap_at_end = size of scan gap at the end of grid cell

m and b = mapping coefficients

ns = length of a cell

sample = sample position of current resampling step. These values are from 0 to SAMP_RATE - 1.

new_gap = gap associated with sample

See figures 3.1.5-14 and 3.1.5-15.

Notes on the Cubic Spline

The cubic spline weights used were developed by Fischel [Reference 30] and take on the form of (See figure 3.1.5-13):

$$w1 = (U2/(3*h1*h2*h2))*(2*F-G);$$

$$w2 = (x3-x)/h2-(F/(3*h1*h2*h2*h2))*(2*U2*(h1+h2)+h1*V2) \\ + (G/(3*h1*h2*h2*h2))*(U2*(h1+h2)+2.0*V2*h1);$$

$$w3 = ((x-x2)/h2)+(F/(3*h2*h2*h2*h3))*(2*U2*h3+V2*(h2+h3)) \\ - (G/(3*h2*h2*h2*h3))*(U2*h3+2*V2*(h2+h3));$$

$$w4 = (V2/(3.0*h2*h2*h3))*(2.0*G-F);$$

where

$$h1 = x2 - x1;$$

$$h2 = x3 - x2;$$

$$h3 = x4 - x3;$$

$$F = (x3-x)*((x3-x)*(x3-x)-h2*h2);$$

$$G = (x-x2)*((x-x2)*(x-x2)-h2*h2);$$

$$U2 = h2/(h1+h2);$$

$$V2 = h2/(h2+h3);$$

Figure 3.1.5-16 shows the spline weights calculated for different size gaps. It should be noted that at larger gaps the weights show greater variations. When the PAN band is used for LANDSAT 7 this could cause some anomalies in cases of large varying grey values between pixels that are located in an area with a large scan gap.

The Pseudo-Inverse Model

Due to the fact that there is no inverse model a method is needed to find which output pixel correspond to which input pixel. This is done using the inverse mapping coefficients for each grid cell. To do this it must be determined which grid cell goes with what output pixel. A "rough" polynomial is set up which gives an approximate input pixel for a given output pixel. An approximate grid cell location can then be determined from this pixel. After this approximation is performed the correct grid cell can be found using a trial and error process with the inverse mapping coefficients for the grid cells.

Calculating the Rough Polynomial

A first order polynomial was used for the "rough" mapping polynomial. The data used to produce this polynomial was taken from the grid input and output pixel locations. The reasoning behind using the first order was mostly from a speed and computational stand point. The algorithm is as follows:

1. Read input and output lines/samples (not all are needed).
2. Use least squares routine to calculate a first order polynomial.

This creates a "rough" polynomial.

$$S_i = a_0 + a_1 * S_o + a_2 * L_o + a_3 * S_o * L_o$$

$$L_i = b_0 + b_1 * S_o + b_2 * L_o + b_3 * S_o * L_o$$

Where

S_i is the input sample

S_o is the output sample

L_i is the input line

L_o is the output line

a_0, a_1, a_2, a_3 are the polynomial mapping coefficients.

b_0, b_1, b_2, b_3 are the polynomial mapping coefficients.

Finding the Corresponding Grid Cell

The algorithm to determine the corresponding input grid cell for a given output grid cell is as follows: (Note: If the inverse mapping routine is caught or jumping back and forth between two scans then it is assumed that the output pixel falls in the gap between the two scans. In this case the scan above the gap is passed back as the appropriate grid cell.)

Map output pixel to current_input_space_point using "rough" polynomial.

Set current_grid_cell from the current_input_space_point.

Loop

Calculate the new_input_space_point using the inverse polynomial for the current_grid_cell.

Calculate the new_grid_cell from the new_input_space_point.

If

current_grid_cell and new_grid_cell are the same correct grid cell has been found, exit loop.

Else

Copy new_grid_cell to current_grid_cell.

Save current_grid_cell to history list.

If

Current_grid_cell is the same as the grid cell from previous iteration.

If

Matching grid cell is from the two iterations ago and the intervening grid cell was from the same row, use last grid cell as the correct grid cell.

Else

Set flag to indicate the output pixel maps to the gap, use the grid cell in the cycle from the upper most row as the correct cell.

Exit loop.

See figures 3.1.5-17, 3.1.5-18, and 3.1.5-19.

The Resampling Process

The output image is created by using the extended image and the image grid. Currently a two dimensional cubic convolution kernel is used for resampling.

This processing flow may need to be revised if a new weight table is needed due to detector delays or due to the MTF. This process does not contain any precision or terrain processing concerns.

The algorithm is as follows:

1. Create resampling table weights. (Refer to the section on detector delays [section 3.1.5.3.6.1] for more information).
2. Step through the output space (for each pixel); Repeat steps 3 - 8 for all output pixels
3. Use rough polynomial to map an output pixel to input space.
4. Use the "Find Corresponding Grid Cell" algorithm to determine which input image grid cell the output pixel falls in along with the input pixel location for the corresponding output pixel.
5. Determine (and get) data needed in extended image.
6. Determine correct resampling weights.

- If cubic convolution or MTF compensation is being used, find the fractional portion of the input line/sample to look up the correct set of resampling weights.
 - If nearest neighbor resampling is being used then find the nearest input pixel.
7. Perform resampling; Multiply each input pixel by the corresponding weight and sum the results.
 8. Store output pixel.

See References 12, 27, and 28 for more information about the resampling process.

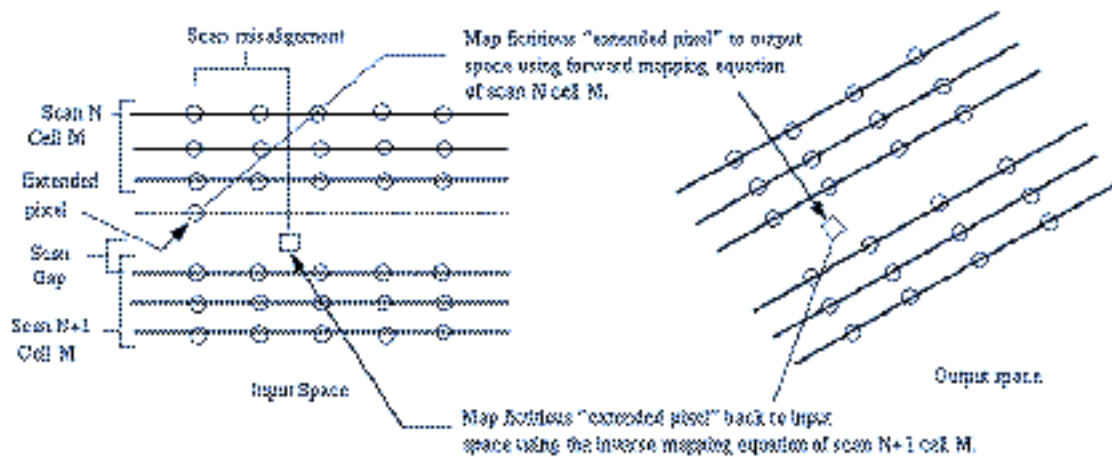


Figure 3.1.5- 12 Extended Pixels and Scan Alignment

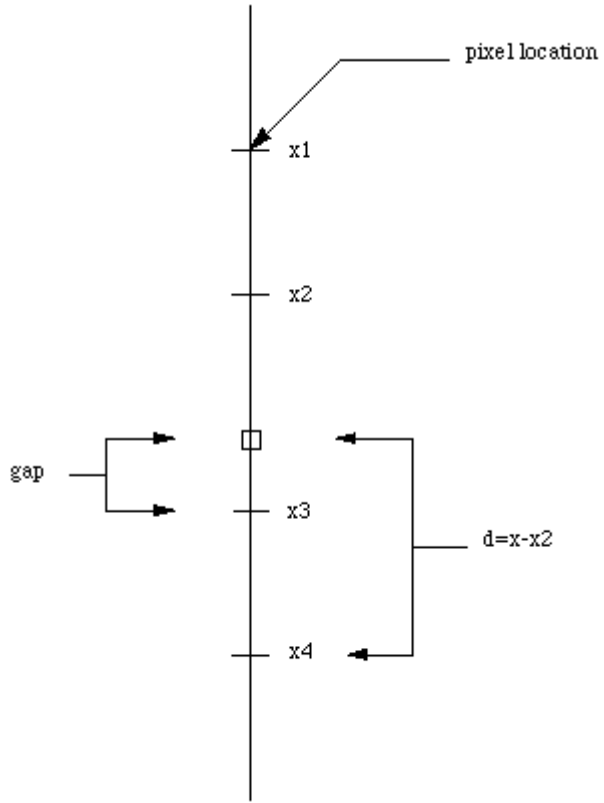
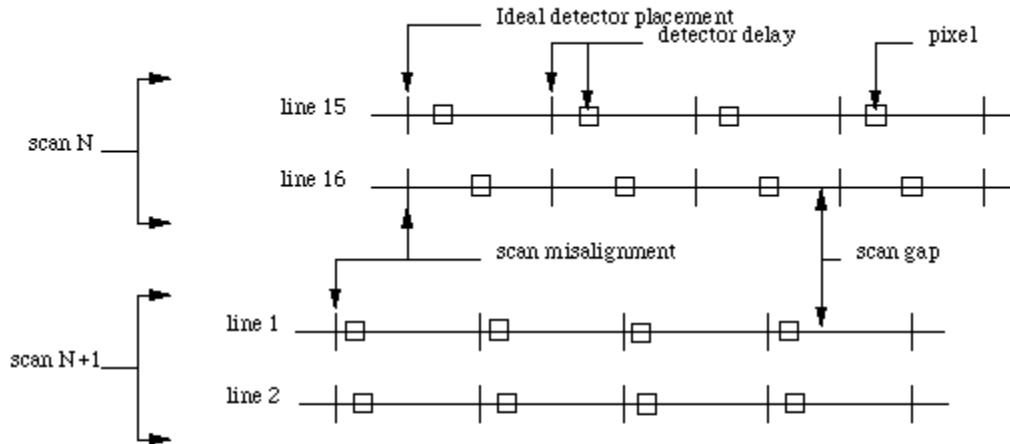
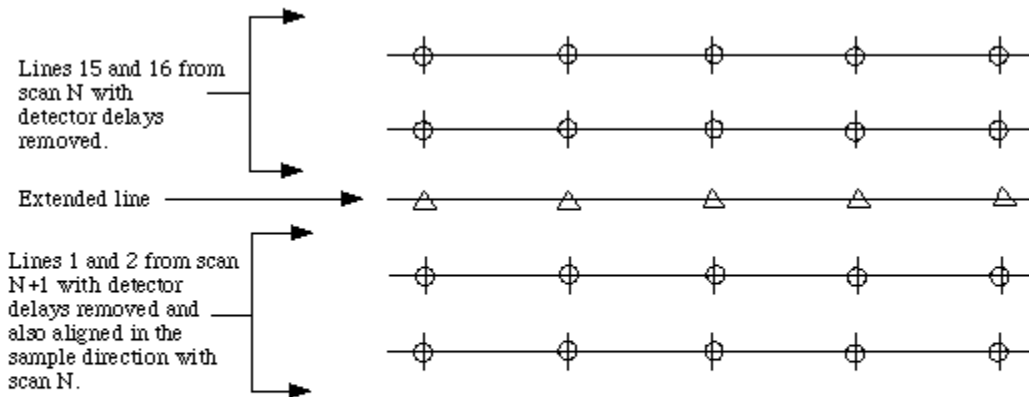


Figure 3.1.5- 13 Calculation of Scan Gap



The diagram above represents the last two lines of scan N and the first two lines of scan N+1. The diagram shows detector delays within a scan along with the scan misalignment and gap between the scans. These four lines will be used to create an extended line. The first step will be to resample the data in the sample direction. This will align the pixels in the sample direction. It should be noted that the pixels are equally spaced in the sample direction so cubic convolution can be used. Lines 15 and 16 from scan N need to be resampled to remove detector delays. Lines 1 and 2 from scan N+1 need to be resampled to remove detector delays and to remove the scan misalignment between it and scan N.

Figure 3.1.5- 14 Scan Misalignment and Gap



The diagram above shows the data from scan N and N+1 resampled so that the pixels align in the sample direction. It also shows the extended line that will be created by resampling the data in the line direction. It should be noted that the pixels are not evenly spaced in the line direction due to the gap, therefore a cubic spline is used for resampling.

Figure 3.1.5- 15 Extended Scan Lines

Gap size	w1	w2	w3	w3
0.000001	0.000000	0.000001	1.000000	0.0000000
0.3	-0.030100	0.206843	0.923591	-0.100334
0.6	-0.086538	0.425481	0.805288	-0.144231
1.0	-0.166667	0.666667	0.666667	-0.166667
1.3	-0.222661	0.810219	0.583720	-0.171278
1.6	-0.273504	0.928337	0.516108	-0.170940
2.0	-0.333333	1.055556	0.444444	-0.166667
2.3	-0.372798	1.133619	0.401264	-0.162086
2.6	-0.408213	1.200215	0.365003	-0.157005
3.0	-0.450000	1.275000	0.325000	-0.150000
3.3	-0.477841	1.322734	0.299907	-0.144800
3.6	-0.503106	1.364704	0.278153	-0.139752
4.0	-0.533333	1.413333	0.253333	-0.133333
4.3	-0.553759	1.445264	0.237276	-0.128781
4.6	-0.572511	1.473949	0.223021	-0.124459
5.0	-0.595238	1.507937	0.206349	-0.119048
5.3	-0.610785	1.530712	0.195315	-0.115242
5.6	-0.625199	1.551496	0.185346	-0.111643

Figure 3.1.5- 16 Cubic Spline Weights

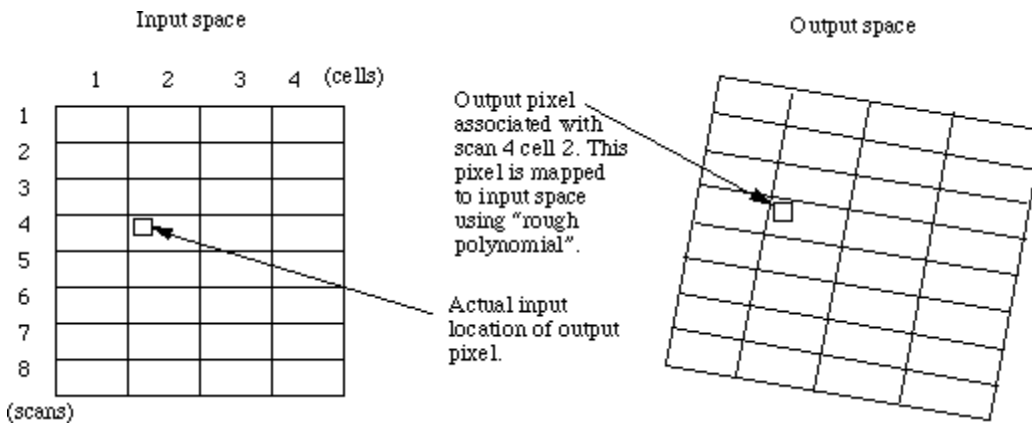


Figure 3.1.5- 17 Inverse Mapping with "Rough" Polynomial

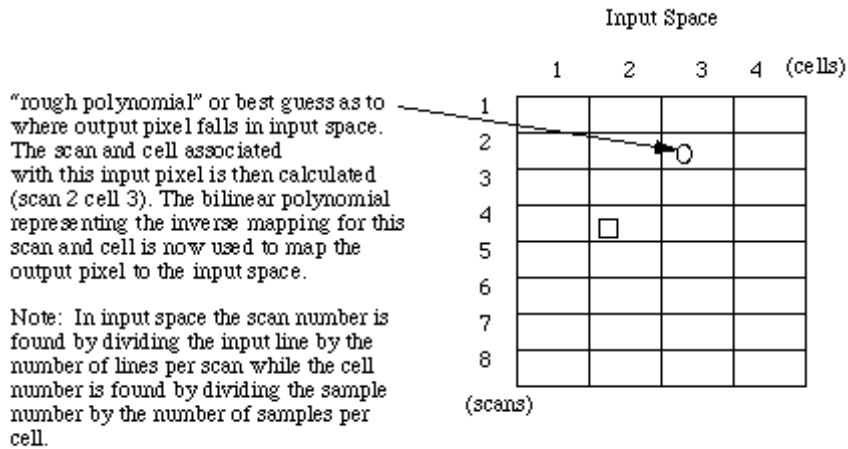


Figure 3.1.5- 18 “Rough” Polynomial – First Iteration

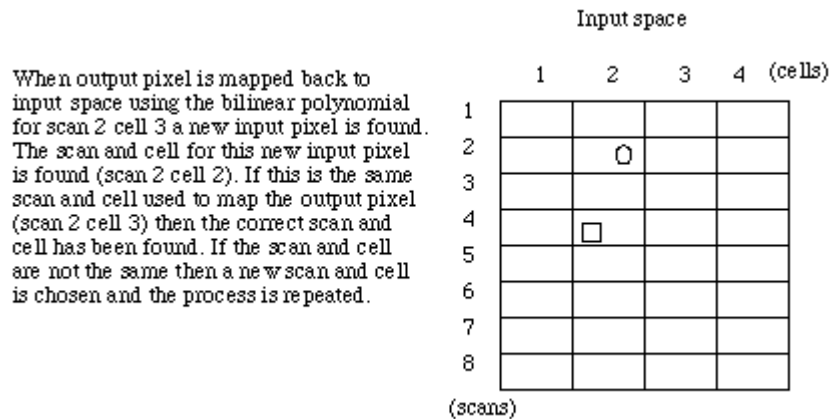


Figure 3.1.5- 19 Results Mapped back to Input Space

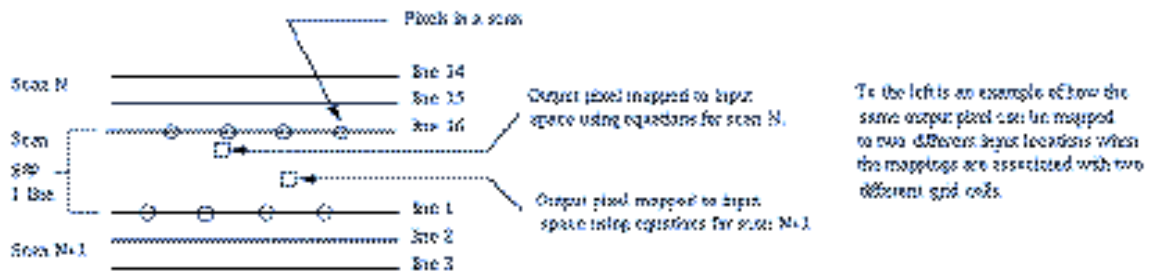


Figure 3.1.5- 20 Nearest Neighbor Resampling

Nearest Neighbor Resampling

To perform nearest neighbor resampling, changes to the algorithm described above must be made. To get the true nearest neighbor the scan gap is not extended. This presents two scenarios; one case where the pixel falls within a grid cell and the resampling follows the traditional nearest neighbor routine and the second case where the pixel falls in the scan gap area. In the second scenario there is extra work that must be performed to determine which pixel is really the true nearest neighbor. The confusion in determining the true nearest neighbor lies in the fact that each grid cell defines its own coordinate system. When a pixel falls within the gap the transformations between both grid cells must be used to determine which pixel is truly closest for nearest neighbor resampling. This is demonstrated in figure 3.1.5-20.

Linear Interpolation Resampling

Due to the effects of detector delays the linear interpolation employed is slightly different than the classical bilinear approach. Detector delay are shifts in the sample direction with respect to the raw imagery. When these offsets are taken into account during linear interpolation, the sample actually represents the centroid of the polygon that is made up of the four samples that surround the output sample location. These values are solved directly, there is not a table of values representing a set of offsets as there is for cubic convolution resampling.

Notes on the Correction Grid

Input lines in the grid must contain the top and bottom lines of a scan (for scan N line 1 and 16 must be contained in the input lines of the grid). This is made necessary by the way the scan gap is calculated. This algorithm expects the sample spacing between grid points to evenly divide into the total number of samples in the image. It should also be noted that the pixel locations given in the grid refer to the pixel center location. See Section 3.1.5.3.5, Correction Grid Generation, for more information on the Gridding process.

Notes on the Least Squares Routine

This algorithm uses the QR decomposition functions which are based on information in References 6 and 31.

3.1.5.3.6.1 Detector Delays

A detector delay represents the virtual distance of each detector from its respective band center. It contains the net effect of detector misplacement on the focal plane and the

effective sampling delays due to electronics and scan angle monitor delays. The manner in which they are defined is illustrated in Figure 3.1.5-21.

Since the delays are different for each detector of each band, they cannot be centered in the sparse geometric correction grid. Therefore, the detector delay information has been incorporated into the weight tables for resampling. The way in which they have been applied assumes that the nominal position of the detectors has been used in determining the along-scan angle in the forward satellite model (Figure 3.1.5-21). It is the difference between the real and ideal detector positions that is applied to the input sample when determining the resampling weight table. Following this method, the difference is added to the input samples of forward scans and subtracted from reverse scans. In order to simplify the application of detector delays in calculating the resampling weights, the minus sign has been included in the definition of the delay correction term for the reverse scan so that it can be added regardless of scan direction. So:

$$\text{new sample} = \text{old sample} + \text{delay correction}$$

where:

$$\text{delay correction} = \begin{cases} |(\text{delay} - \text{nominal})| & \text{Forward} \\ |-(\text{delay} - \text{nominal})| & \text{Reverse} \end{cases}$$

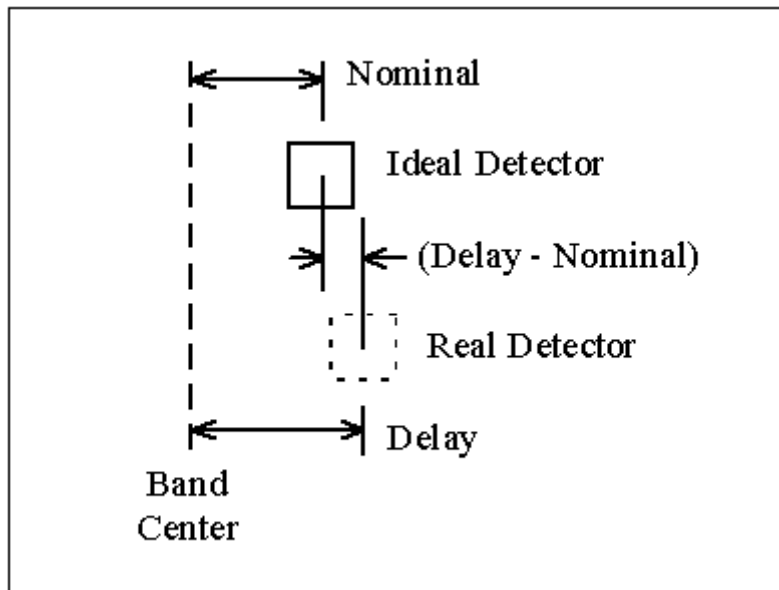


Figure 3.1.5- 21 Detector Delay Definition

Detector delays are defined as displacements relative to band center.

Prior to resampling, a set of weights are determined which will incorporate the non-ideal locations of the detectors. In Figure 3.1.5-22, the ideal line and sample locations are shown as dotted lines. When an output (line, sample) pair is mapped to input space, it generally falls on a non-integer (line, sample). Typically, the surrounding integer pixels are used to generate weights for resampling (*i.e.*, cubic convolution, MTF, bilinear, etc.). To incorporate detector delays, it is necessary to determine the weights based on the distance from the non-integer (line, sample) in input space to the actual detector location (see Figure 3.1.5-22). Weights for the synthetic “detectors” in the extended lines are calculated under the assumption that they act as ideally placed detectors.

The standard cubic convolution uses a four-segment, piece-wise third order polynomial over the range $[-2, +2]$ [see Reference 12]. It is defined so that beyond $[-2, +2]$ the weights are zero. From Fig. 3.1.5-22, note that if the detectors were ideally located at $S-1 \dots S+2$, then it would be necessary to calculate weights at these four samples only (for each of the four lines $L-1 \dots L+2$). However, since the detectors can be displaced from their nominal positions in either the positive or negative direction, it is necessary to calculate weights over the range $S-2 \dots S+3$. For every line, two of these weights will be zero, but which two weights are zero will depend on the magnitude and sign of the displacement and the location of the non-integer (line, sample).

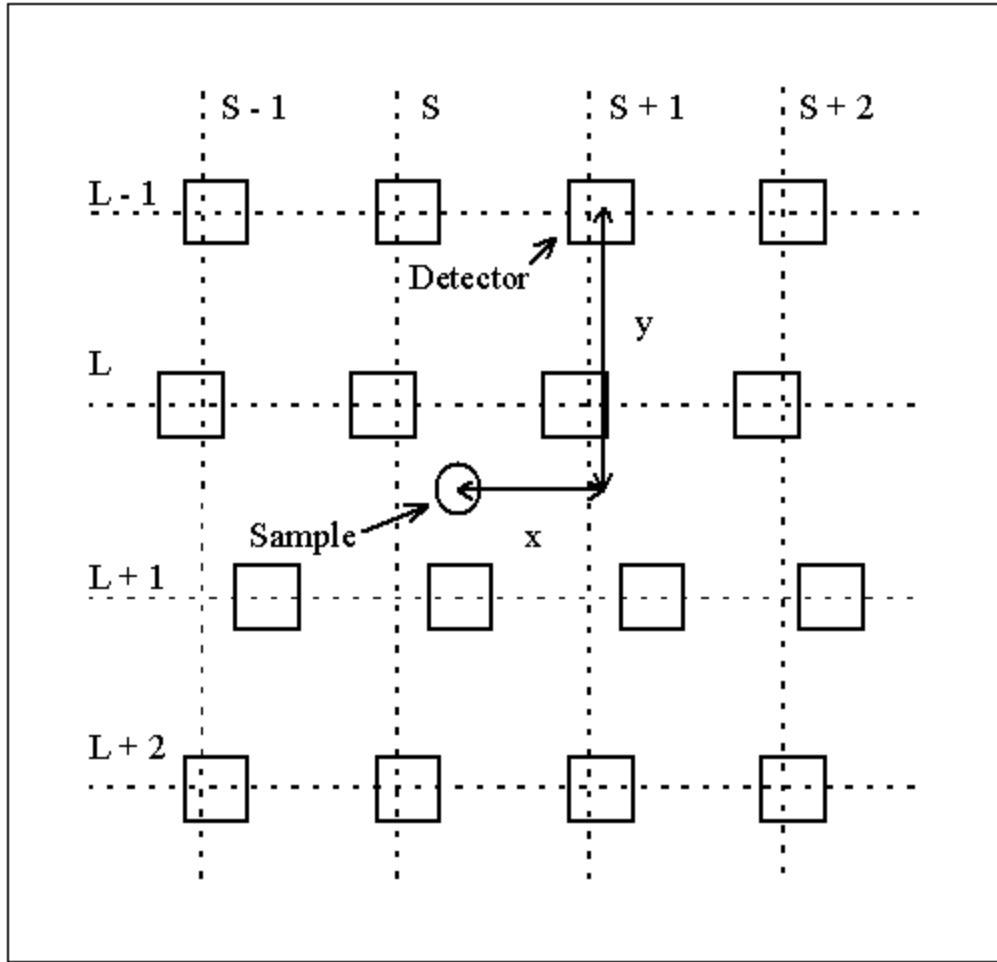


Figure 3.1.5- 22 Resampling Weight Determination

Resampling weights are determined based on the x and y distances between the non-integer (line, sample) and the real detector locations

3.1.5.3.7 Precision Correction

1. Defining the Precision Correction Problem

The geometric measurement in ETM sensor system can be regarded as the look vector, l_{sc} , in the spacecraft body-fixed system. This vector is transformed into the

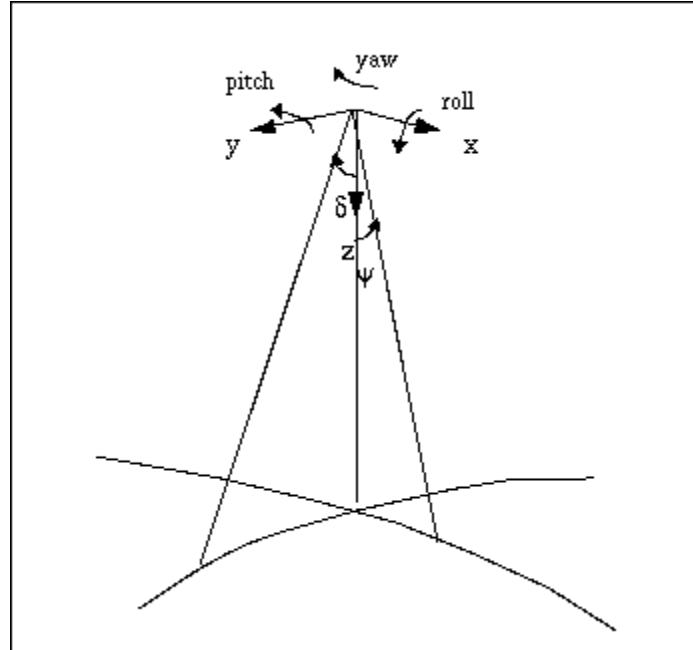


Figure 3.1.5- 23 Definition of Orbit Reference System

Orbit Reference Frame [Reference 2] (OB) system, [see Figure 3.1.5-23] through the spacecraft attitude parameters:

$$\mathbf{I}_{ob} = \mathbf{T}^T(\ r, \ p, \ y) \mathbf{I}_{sc}. \quad (1.1)$$

where r , p , and y are roll, pitch, and yaw angles, \mathbf{T} is the transformation matrix, and can be expressed as

$$\begin{aligned} \mathbf{T}(\ r, \ p, \ y) &= \mathbf{R}_3(y) \mathbf{R}_2(p) \mathbf{R}_1(r) \\ &= \begin{bmatrix} \cos p \cos y & \cos r \sin y + \sin r \sin p \cos y & \sin r \sin y - \cos r \sin p \cos y \\ -\cos p \sin y & \cos r \cos y - \sin r \sin p \sin y & \sin r \cos y + \cos r \sin p \sin y \\ \sin p & -\sin r \cos p & \cos r \cos p \end{bmatrix} \end{aligned}$$

the approximation for small angles r, p, y

$$\begin{bmatrix} 1 & & \\ -y & 1 & \\ p & -r & 1 \end{bmatrix} \quad (1.2)$$

where \mathbf{R}_1 , \mathbf{R}_2 , and \mathbf{R}_3 are the coordinate system transformation matrix for rotation around x, y and z axis respectively.

The vector \mathbf{l}_{ob} is further transformed into the Earth-fixed (EF system) system

$$\mathbf{l}_{ef} = \mathbf{T}_f(\mathbf{r}_{ef}, \mathbf{v}_{ef}) \mathbf{l}_{ob} \quad (1.3)$$

where \mathbf{T}_f is the forward transformation for vectors from the OB system to the EF system, as a function of the satellite position \mathbf{r}_{ef} and velocity \mathbf{v}_{ef} vectors in the EF system. Note that \mathbf{v}_{ef} should be the "inertial" velocity expressed in the EF system as described by Reference 13. This vector, \mathbf{l}_{ef} , together with the satellite position vector, \mathbf{r}_{ef} , is then used to intersect the ellipsoid Earth surface to define a point position, \mathbf{R}_{ef} , as the target point on the Earth. This is the common forward image pixel geolocation calculation.

Mathematically, \mathbf{R}_{ef} is a function of l_{sc} , r , p , y , \mathbf{r}_{ef} , and \mathbf{v}_{ef} .

$$\mathbf{R}_{ef} = F(l_{sc}, r, p, y, \mathbf{r}_{ef}, \mathbf{v}_{ef}) \quad (1.4)$$

Because of errors in the satellite orbit ephemeris and attitude data, this calculated \mathbf{R}_{ef} is different than the true location of the image pixel. If we know the true location of a landmark pixel, \mathbf{R}_{cp} , from other sources (*i.e.*, base map, survey etc.), this point can be taken as a Ground Control Point (GCP) to check the accuracy of the computed image pixel location. The precision correction process uses the Ground Control Point coordinates to estimate the correction to the satellite ephemeris and attitude data, so that with the corrected parameters in equation (1.4) the calculated image pixel location, \mathbf{R}_{ef} , will be close to its true location, \mathbf{R}_{cp} , (depending on the GCP positional accuracy).

To calculate the precision correction, the difference between \mathbf{R}_{ef} and \mathbf{R}_{cp} is taken as the observable, and the observation equation becomes:

$$d\mathbf{R} = \mathbf{R}_{cp} - F(l_{sc}, r, p, y, \mathbf{r}_{ef}, \mathbf{v}_{ef}) \quad (1.5)$$

according to equation (1.4). However, the actual calculation of \mathbf{R}_{ef} is usually not an explicit function of the orbit and attitude parameters, especially for the intersecting procedure. Therefore it is inconvenient to linearize equation (1.5) with standard estimation techniques. Instead, the calculation of look vector \mathbf{l}_{cp} corresponding to \mathbf{R}_{cp} , in the OB system, is much more explicit:

$$\mathbf{l}_{cp} = \mathbf{T}_i(\mathbf{r}_{ef}, \mathbf{v}_{ef}) \frac{(\mathbf{R}_{cp} - \mathbf{r}_{ef})}{|\mathbf{R}_{cp} - \mathbf{r}_{ef}|} \quad (1.6)$$

where $(\mathbf{R}_{cp} - \mathbf{r}_{ef})$ is the line-of-sight vector in the EF system corresponding to \mathbf{R}_{cp} , and $\mathbf{T}_i(\mathbf{r}_{ef}, \mathbf{v}_{ef})$ is the inverse transformation for the look vector from the EF system to the OB system. If all the satellite attitude and ephemeris parameters are accurate, the l_{cp} from equation (1.6) and l_{ob} from equation (1.1) should be equal. Since the measurement l_{sc} is accurate compared to the attitude and ephemeris information, any systematic difference between l_{cp} and l_{ob} can be attributed to the attitude and orbit errors. Thus we can use the difference between l_{cp} and l_{ob} as the observable

$$dl = l_{cp} - l_{ob} = \mathbf{T}_i(\mathbf{r}_{ef}, \mathbf{v}_{ef}) \frac{(\mathbf{R}_{cp} - \mathbf{r}_{ef})}{|\mathbf{R}_{cp} - \mathbf{r}_{ef}|} - \mathbf{T}(r, p, y) l_{sc} \quad (1.7)$$

The task of precision modeling is then to calculate the correction to those satellite ephemeris and attitude parameters (*i.e.*, \mathbf{r}_{ef} , \mathbf{v}_{ef} and θ 's) so that the residuals of dl after correction are minimized for all selected GCP's. The orbit correction is modeled as a linear function of time for each component in the OB system. Referred to as the short arc method, this purely geometric method shifts and rotates the short arc of orbit defined by the original ephemeris points to fit the GCP measurements.

2. Linearizing the Observation Equations

In equation (1.7), the calculation of l_{ob} can also be carried out through

$$l_{ob} = \mathbf{T}_i(\mathbf{r}_{ef}, \mathbf{v}_{ef})(\mathbf{R}_{ef} - \mathbf{r}_{ef}) / |\mathbf{R}_{ef} - \mathbf{r}_{ef}| \quad (2.1)$$

if \mathbf{R}_{ef} is more conveniently accessible. Since equation (2.1) is simply the inverse of equation (1.4) and equation (1.3), the l_{ob} calculated from equation (2.1) is the same as the one in equation (1.1) except for the possible inclusion of numerical errors. However, it should be mentioned that the true relationship between l_{ob} and the parameters is always equation (1.1). Equation (2.1) should not be confused with this because \mathbf{R}_{ef} in equation (2.1) is not an independent variable but a function of equation (1.4). So, in observation (1.7) information about the attitude parameters is contained in l_{ob} , and the information about orbit parameters comes from l_{cp} .

Since the measurement of l_{sc} is 2-dimensional in nature, only 2-dimensional information is contained in equation (1.7) though there are 3 components involved. If a look vector (either l_{cp} or l_{ob}) has the three components in the OB system

$$\mathbf{l} = \{xl, yl, zl\} \quad (2.2)$$

the real information in these three components can be summarized in two variables like the original look angle measurements. We chose the following two variables

$$= \text{atan}(yl / zl) \tag{2.3}$$

$$= \text{atan}(xl / zl) \tag{2.4}$$

So that the three components of equation (1.7) can be reduced to the two equations:

$$= \text{cp} - \text{ob} \tag{2.5}$$

$$= \text{cp} - \text{ob} \tag{2.6}$$

Note that in equation (2.3) and (2.4) the components of xl , yl , zl can be that of line-of-sight vector instead of unit look vector, so that cp and ob are explicit functions of orbit position. In that case zl is approximately the height of the satellite.

If we define

$$\text{true value} = \text{approximate value} + \text{correction}$$

and differentiate equations (2.3), (2.4) with respect to the orbit position (for cp and ob), differentiate equation (1.1) with respect to the satellite attitude (for ob and ob) at their corresponding approximate values, then equations (2.5) and (2.6) can be linearized as the function of correction parameters

$$(\cos^2 \text{cp} / h) dy - (\cos \text{cp} \sin \text{cp} / h) dz + d_r \tag{2.7}$$

$$(1.0 / h) dx - d_p + \tan \text{cp} d_y \tag{2.8}$$

where dx , dy and dz are the correction to satellite position vector \mathbf{r}_{ob} in the OB system, and d 's are the corrections to the satellite attitude angle 's. Other quantities are functions evaluated at the approximate values of \mathbf{r}_{ef} , \mathbf{v}_{ef} and 's.

The linearization above is done by directly differentiating equation (2.3) and (2.4), with transformation \mathbf{T}_1 regarded unaffected by the error in \mathbf{r}_{ef} and \mathbf{v}_{ef} . This, however, ignores the curvature of the satellite orbit and the Earth, resulting in about 10% of error in the coefficients of dx , dy and dz . A more accurate way to evaluate these coefficients is to examine the sensitivity terms d_{cp}/dx , d_{cp}/dy , and d_{cp}/dz through the geometry of the look vector (see Figure 3.1.5-24).

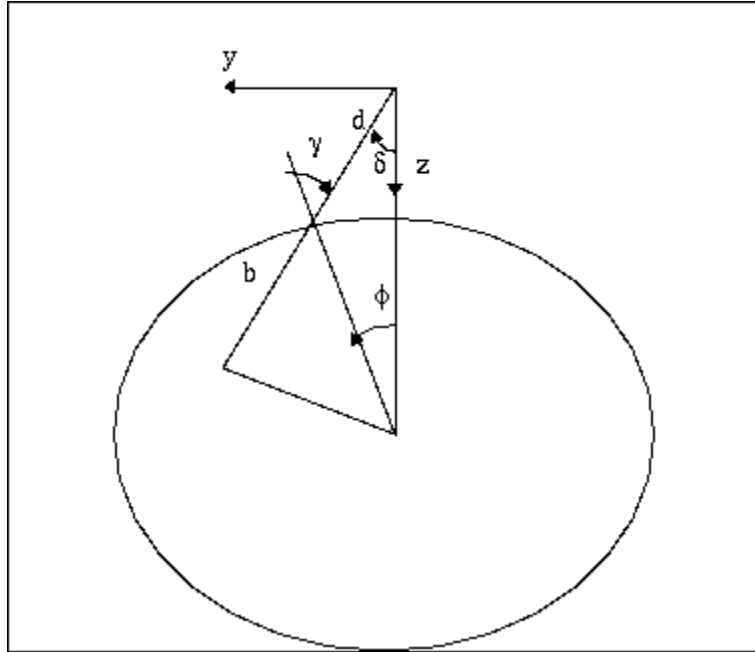


Figure 3.1.5- 24 Look Vector Geometry

Denote

- R – the Radius of the Earth;
- r – the radius of the satellite position;
- h – the altitude of the satellite;
- d – the magnitude of the look vector (from satellite to target);
- the along-scan angle of the look vector;
- the Earth centered angle between the satellite and the target;
- the zenith angle of the look vector at the target;
- x,y,z – the coordinates of the satellite position in the OB system

then we have

$$R \sin(\theta + \phi) = r \sin \gamma \tag{2.9}$$

Differentiating the equation (holding R and r constant) yield

$$R \cos(\theta + \phi)(d\theta + d\phi) = r \cos \gamma dd \tag{2.10}$$

Note that $\theta + \phi = \gamma$, and $d\theta = -dy / r$, we have

$$= dd = (-b / (r d)) dy \tag{2.11}$$

Similarly for the cross-scan direction, we have

$$= d_x = -(r - d \cos \theta) / (r d \cos \theta) dx \quad (2.12)$$

For the effect of altitude error, differentiate equation (2.9) with respect to θ and r (holding constant now) and noting $dr = -dz$, we have

$$= d_z = (\sin \theta / d) dz \quad (2.13)$$

Note that the dx , dy and dz in equations (2.11) through (2.13) are error terms, which are opposite in sign to the correction terms. With this in mind, we can replace the correction terms in equation (2.7) and (2.8) and rewrite the linearized observation equation as

$$= (b / (r d)) dy - (\sin \theta / d) dz + d_r \quad (2.14)$$

$$= ((r - d \cos \theta) / (rd \cos \theta)) dx - d_p + \tan \theta d_y \quad (2.15)$$

where

$$b = R \cos \theta = \text{sqrt}(R^2 - (r^2 \sin^2 \theta)) \quad (2.16)$$

$$d = r \cos \theta - b \quad (2.17)$$

3. Weighted Least Square Solution of the Parameters

The correction parameters in equations (2.14) and (2.15) can be expanded to include the correction to the change rates of the satellite attitude and position by defining

$$dx = dx_0 + dx_{\text{dot}} dt \quad \text{and} \quad d_r = d_{r0} + d_{r\text{dot}} dt \quad (3.1)$$

If the major random error source in computing θ and r is the error in the coordinates of the Ground Control Point, then the covariance matrix for the observation equations (2.14) and (2.15) should be the covariance matrix of \mathbf{R}_{cp} in equation (1.6) mapped through equations (1.6), (2.3) and (2.4).

Note that in the observation equations (2.14) and (2.15), θ is only related to parameters dy , dz and d_r , and r is only related to dx , d_p and d_y . The parameters are uncoupled in the two observations. In the simplified case where observational error of θ and r are uncorrelated, the observation equations can be separated into two independent equations and solved individually.

Define the parameter vectors as

$$\mathbf{X}_1' = \{d_{r0}, dy_0, dz_0, d_{rdot}, dy_{dot}, dz_{dot}\} \quad (3.2)$$

$$\mathbf{X}_2' = \{dx_0, d_{p0}, d_{y0}, dx_{dot}, d_{pdot}, d_{ydot}\} \quad (3.3)$$

where ' means transpose of a vector or matrix. Then, the two observation equations can be written as

$$= h_1 \mathbf{X}_1 + a \quad (3.4)$$

$$= h_2 \mathbf{X}_2 + b \quad (3.5)$$

where

$$h_1 = \{1.0, b/(d r), -\sin \theta/d, dt, b dt/(d r), -\sin \theta dt/d\} \quad (3.6)$$

$$h_2 = \{(r - d \cos \theta)/(r d \cos \theta), -1.0, \tan \theta, (r-d \cos \theta) dt/(r d \cos \theta), -dt, \tan \theta dt\} \quad (3.7)$$

a and b are the random error of θ and r respectively. With all GCPs included, the observation equation can be written as

$$\mathbf{A} = H_1 \mathbf{X}_1 + \mathbf{A}; \quad (3.8)$$

$$\mathbf{B} = H_2 \mathbf{X}_2 + \mathbf{B}; \quad (3.9)$$

and the parameters can be solved by Weighted Least Square estimation as

$$\mathbf{X}_1 = (H_1' W a H_1)^{-1} (H_1' W a \mathbf{A}) \quad (3.10)$$

$$\mathbf{X}_2 = (H_2' W b H_2)^{-1} (H_2' W b \mathbf{B}) \quad (3.11)$$

where \mathbf{A} and \mathbf{B} are the observation vectors, composed of θ and r for all the GCPs respectively, H_1 and H_2 are corresponding coefficient matrix with h_1 and h_2 as rows corresponding to each θ and r , $W a$ and $W b$ are the diagonal weight matrix for \mathbf{A} and \mathbf{B} respectively, composed of inverse of the variance of each individual a and b .

One problem in this solution is the nearly linear correlation between parameter dx and d_p in the observation equation (3.7). The along-track orbit error and the pitch angle error have the very similar effect on θ and the two parameters can not be well separated in the solution without additional information. Including both parameters in the observation equations results in a near-singular normal equation and therefore unstable solution of the

parameters. Similarly, high correlation exists between the cross-track position and the roll attitude errors in equation (3.6) and an ill-conditioned normal equation would result.

For the purpose of correcting the image, we do not have to distinguish between orbit position correction and attitude correction parameters. Letting either the orbit or attitude correction parameters absorb the existing errors will correct the image in a similar manner. Therefore, we can choose to estimate either dx and dy or d_p and d_r . This can be done by setting those coefficients in h_1 and h_2 corresponding to the unwanted parameters to zero. In practice the allocation of correction offsets to ephemeris and attitude terms is controlled by the selection of a priori weights for the correction parameters.

4. Separating Orbit Position and Attitude Errors

One of challenging tasks in the Landsat 7 Image Assessment System is to distinguish satellite attitude error from the orbit positional error. The purpose of precision correction estimation is not only to correct the image but also to extract information about the sensor alignment which is reflected in the attitude correction parameters. In order to separate the ephemeris error from the attitude error as much as possible, we should first use the most precise ephemeris data available and correct systematic errors with available models. Second we should use available a priori information in addition to the observation to cure the ill-condition of the normal equation in statistical estimation.

Let the observation equation be

$$\begin{aligned} Y &= HX + \epsilon; \\ [\epsilon] &= 0, \text{Cov}[\epsilon] = s^2 C \end{aligned} \quad (4.1)$$

and the a priori information of the parameters be

$$\begin{aligned} X &= X_0 + \epsilon_x; \\ [\epsilon_x] &= 0, \text{Cov}[\epsilon_x] = q^2 C_x \end{aligned} \quad (4.2)$$

then the normal equation for the Best Linear Unbiased Estimate (BLUE) [Reference 14], \hat{X} of X is

$$((1/s^2)H'WH + (1/q^2)W_x)X^\wedge = (1/s^2)H'WY + (1/q^2)W_x X_0 \quad (4.3)$$

where W and W_x are weight matrices

$$\begin{aligned} W &= C^{-1}; \\ W_x &= C_x^{-1} \end{aligned} \quad (4.4)$$

The covariance matrix of $\hat{\mathbf{X}}$ is

$$\text{Cov}[\hat{\mathbf{X}}] = ((1/s^2)H'WH + (1/q^2)W_x)^{-1} \quad (4.5)$$

Usually, however, the $\text{Cov}[\hat{\mathbf{X}}]$ and $\text{Cov}[\hat{\mathbf{x}}]$ can not be exactly known. In the case of ground control points, for example, the position error involves many factors like base map error, and human marking error, etc. If there are unknown scale factors s^2 and q^2 , we can still obtain the Weighted Least Square (WLS) estimate from the normal equation

$$(H'WH + W_x)\hat{\mathbf{X}} = H'WY + W_x\mathbf{X} \quad (4.6)$$

In such case, the inverse of the normal matrix can not be taken directly as the $\text{Cov}[\hat{\mathbf{X}}]$. Factor s^2 and q^2 should be estimated with appropriate variance component estimation from the residual of the solution of equation (4.6). The weighted residual square summation can be calculated as

$$\mathbf{V}'W\mathbf{V} = \mathbf{Y}'W\mathbf{Y} - 2\hat{\mathbf{X}}'M + \hat{\mathbf{X}}'N\hat{\mathbf{X}} \quad (4.7)$$

$$\mathbf{V}_x'W_x\mathbf{V}_x = \mathbf{X}'W_x\mathbf{X} - 2\hat{\mathbf{X}}'W_x\mathbf{X} + \hat{\mathbf{X}}'W_x\hat{\mathbf{X}} \quad (4.8)$$

where

$$\mathbf{V} = \mathbf{Y} - H\hat{\mathbf{X}} \quad (4.9)$$

$$\mathbf{V}_x = \mathbf{X} - \hat{\mathbf{X}} \quad (4.10)$$

$$N = H'WH \quad (4.11)$$

$$M = H'WY \quad (4.12)$$

5. Estimating the Weight Factor for Observation and a priori Information

When the factors s^2 and q^2 are appropriately estimated, the weight matrix \mathbf{W} and \mathbf{W}_x should be correspondingly corrected by factors $1/s^2$ and $1/q^2$ respectively, and equation (4.6) should be resolved with the new weight matrices. In the new solution, information from the observation and the a priori information are appropriately combined and the $(H'WH + W_x)^{-1}$ is the $\text{Cov}[\hat{\mathbf{X}}]$.

One of the estimate of s^2 and q^2 is the Helmert type estimate. For the problem here, the equation for the estimate can be derived following Helmert's variance component analysis [Reference 15],

$$E s^2 + D q^2 = \mathbf{V}'W\mathbf{V} \quad (5.1)$$

$$D s^2 + G q^2 = \mathbf{V}_x' \mathbf{W}_x \mathbf{V}_x \quad (5.2)$$

where

$$E = n - 2 \operatorname{tr}\{Q N\} + \operatorname{tr}\{Q N Q N\} \quad (5.3)$$

$$G = m - 2 \operatorname{tr}\{Q W_x\} + \operatorname{tr}\{Q W_x Q W_x\} \quad (5.4)$$

$$D = \operatorname{tr}\{Q N Q W_x\} \quad (5.5)$$

$$Q = (H' W H + W_x) \quad (5.6)$$

n = number of observations

m = number of parameters

Equation (5.1) and (5.2) do not guarantee positive solution of s^2 and q^2 . In some cases, especially for small s^2 and q^2 , noise can drive the solution negative. Another type of estimate, the iterative Maximum Likelihood Estimate (MLH) guarantees positive solution [Reference 16], though the estimate s^2 and q^2 may not be statistically unbiased. The MLH solution is obtained by iteratively solving equation (4.6) and

$$s^2 = \mathbf{V}' \mathbf{W} \mathbf{V} / n \quad (5.7)$$

$$q^2 = \mathbf{V}_x' \mathbf{W}_x \mathbf{V}_x / m \quad (5.8)$$

$$W = W / s^2 \quad (5.9)$$

$$W_x = W_x / q^2 \quad (5.10)$$

until s^2 and q^2 converge.

Note: The weight factor estimates procedure is very sensitive to the presence of blunders in the input data and therefore should not be used until the outlier rejection procedure, section 3.1.5.3.7.1, has been performed.

6. Propagating the Parameter Errors into Look Vector Error

The solution above provides the estimate of the corrections to the ephemeris and attitude data as well as to their covariance matrix. The covariance information can be used as a measure of precision for assessing the alignment errors of the sensor system. It can also

be propagated to any pixel in the scene to evaluate the pixel location error after the precision correction.

Given the sample time and along-scan look angle of a pixel, the coefficients h_1 and h_2 can be calculated for \hat{x} and \hat{y} according to equation (3.6) and (3.7). The variance of \hat{x} and \hat{y} are then calculated as

$$\sigma_{\hat{x}}^2 = h_1 \text{Cov}[\mathbf{X}^{\wedge}]h_1' \quad (6.1)$$

$$\sigma_{\hat{y}}^2 = h_2 \text{Cov}[\mathbf{X}^{\wedge}]h_2' \quad (6.2)$$

respectively. These are the variance of the pixel location in sample and line directions due to the uncertainty of the estimated precision correction parameters, they are in angles but can be easily converted into IFOV according to the sensor system specifications.

3.1.5.3.7.1 Precision Correction Outlier Detection Algorithm

Background

Outlier detection for the IAS precision correction solutions seeks to identify GCPs which are likely to be in error due to miscorrelation. This is done by analyzing the GCP residuals, taking into account the relative importance of the GCP as reflected in the precision solution normal equation matrix. [References 36, 37]

Definitions:

\mathbf{A} = matrix of coefficients (partial derivatives) relating parameters to observations

\mathbf{p} = parameter vector

\mathbf{X} = observation vector

\mathbf{V} = residual vector

\mathbf{C} = observation covariance matrix

n = the number of observations

p = the number of parameters

\mathbf{A} is $n \times p$, \mathbf{p} is $p \times 1$, \mathbf{X} and \mathbf{V} are $n \times 1$, and \mathbf{C} is $n \times n$

Observation Equation:

$$\mathbf{A}\mathbf{p} = \mathbf{X} - \mathbf{V}$$

$$\mathbf{X} = \mathbf{X}_{\text{true}} + \mathbf{E} \quad \text{where } \mathbf{E} = \text{error vector} \sim G(0, \mathbf{C})$$

$\mathbf{A}_{\text{true}} = \mathbf{X}_{\text{true}}$ where $\underline{\mathbf{x}}_{\text{true}}$ is the “true” parameter vector

$$\mathbf{A}_{\text{est}} = \mathbf{X}_{\text{true}} + \mathbf{E} - \mathbf{V}$$

so $\mathbf{V} = \mathbf{E}$ if $\underline{\mathbf{x}}_{\text{est}} = \underline{\mathbf{x}}_{\text{true}}$

Minimum Variance Parameter Estimate:

$$\underline{\mathbf{x}}' = [\mathbf{A}^T \mathbf{C}^{-1} \mathbf{A}]^{-1} \mathbf{A}^T \mathbf{C}^{-1} \mathbf{X}$$

Estimated Residual Error:

$$\mathbf{V}' = \mathbf{X} - \mathbf{A}[\mathbf{A}^T \mathbf{C}^{-1} \mathbf{A}]^{-1} \mathbf{A}^T \mathbf{C}^{-1} \mathbf{X}$$

Define Projection matrix \mathbf{P} :

$$\mathbf{P} = \mathbf{A}[\mathbf{A}^T \mathbf{C}^{-1} \mathbf{A}]^{-1} \mathbf{A}^T \mathbf{C}^{-1}$$

This matrix projects the observation vector into the parameter subspace (the column space of \mathbf{A}).

This projection is only orthogonal if \mathbf{C} has the special structure described below.

Substituting:

$$\mathbf{V}' = \mathbf{X} - \mathbf{P}\mathbf{X} = [\mathbf{I} - \mathbf{P}]\mathbf{X}$$

$[\mathbf{I} - \mathbf{P}]$ projects \mathbf{X} into the parameter null space.

Looking at the Error Estimate \mathbf{V}' :

$$\mathbf{V}' = [\mathbf{I} - \mathbf{P}]\mathbf{X} = [\mathbf{I} - \mathbf{P}][\mathbf{X}_{\text{true}} + \mathbf{E}] = [\mathbf{I} - \mathbf{P}]\mathbf{X}_{\text{true}} + [\mathbf{I} - \mathbf{P}]\mathbf{E}$$

but $[\mathbf{I} - \mathbf{P}]\mathbf{X}_{\text{true}} = \mathbf{0}$ since \mathbf{X}_{true} lies entirely within the parameter subspace.

$$\text{so } \mathbf{V}' = [\mathbf{I} - \mathbf{P}]\mathbf{E} = \mathbf{E} - \mathbf{P}\mathbf{E}$$

Some comments about \mathbf{V}' and \mathbf{E} :

1. For a given precision solution the elements of \mathbf{E} are not random variables, they are realizations of random variables.
2. \mathbf{V}' is an estimate of the actual (realized) error \mathbf{E} which includes an estimation error equal to $\mathbf{P}\mathbf{E}$.

3. We cannot exactly recover \underline{E} from $[\mathbf{I} - \mathbf{P}]^{-1}\underline{V}'$ because $[\mathbf{I} - \mathbf{P}]$ is singular (it is an $n \times n$ matrix of rank $n-p$).
4. We can attempt to predict how accurate our estimate (\underline{V}') of \underline{E} is likely to be by looking at the estimation error $\underline{R} = \mathbf{P}\underline{E}$.
5. Since we want the predicted accuracy to apply in general, we treat \underline{R} as a random vector which is a function of another random vector \underline{E} .

$$\begin{aligned} \text{Expected Value: } & E[\underline{R}] = E[\mathbf{P}\underline{E}] = \mathbf{P}E[\underline{E}] = \mathbf{P}\underline{0} = \underline{0} \\ \text{Variance: } & E[\underline{R}\underline{R}^T] = E[\mathbf{P}\underline{E}\underline{E}^T\mathbf{P}^T] = \mathbf{P}E[\underline{E}\underline{E}^T]\mathbf{P}^T = \mathbf{P}\mathbf{C}\mathbf{P}^T \end{aligned}$$

Special Structure of Observation Covariance Matrix for IAS Precision Correction:

$$\mathbf{C} = \sigma^2 \mathbf{I}$$

since the observation errors are realizations of independent and identically distributed zero mean Gaussian random variables with variance σ^2 .

Substituting into the equation for \mathbf{P} yields:

$$\mathbf{P} = \mathbf{A}[(1/\sigma^2)\mathbf{A}^T\mathbf{I}\mathbf{A}]^{-1}\mathbf{A}^T\mathbf{I}(1/\sigma^2) = \mathbf{A}^{-2}[\mathbf{A}^T\mathbf{A}]^{-1}\mathbf{A}^T(1/\sigma^2) = \mathbf{A}[\mathbf{A}^T\mathbf{A}]^{-1}\mathbf{A}^T$$

And the equation for the variance of \underline{R} :

$$\begin{aligned} E[\underline{R}\underline{R}^T] &= \sigma^2 \mathbf{P}\mathbf{I}\mathbf{P}^T = \sigma^2 \mathbf{P} \\ \text{noting that } &\mathbf{P}^T = \mathbf{P} \text{ and } \mathbf{P}\mathbf{P} = \mathbf{P} \\ \text{so } &\underline{R} \sim G(\underline{0}, \sigma^2 \mathbf{P}) \end{aligned}$$

For a particular component of \underline{R} r_i :

$$\begin{aligned} E[r_i] &= 0 \\ E[r_i^2] &= \sigma^2 p_{ii} \\ \text{where } &p_{ii} \text{ is the } i^{\text{th}} \text{ diagonal component of } \mathbf{P} \end{aligned}$$

Looking at the equation for \mathbf{P} we see that:

$$\begin{aligned} p_{ii} &= \underline{\Delta}_i^T [\mathbf{A}^T\mathbf{A}]^{-1} \underline{\Delta}_i \\ \text{where } &\underline{\Delta}_i^T \text{ is the } i^{\text{th}} \text{ row of } \mathbf{A} \end{aligned}$$

Considering a particular component of the Residual Error Vector \underline{V}' :

$$\begin{aligned} v_i &= e_i - r_i \\ \text{where } &e_i \text{ is the corresponding component of the observation error vector} \\ \text{so } &v_i \text{ is an unbiased estimate of } e_i \text{ with variance } \sigma^2 p_{ii} \end{aligned}$$

Outlier Detection

If we knew what e_i was we could test it against a probability threshold derived from its standard deviation, σ , to determine if it is likely to be an outlier. Instead of e_i we have v_i which includes the additional error term r_i . Including the additional estimation error in the threshold computation leads to:

$$v_i^2 = \sigma^2 + \sigma^2 p_{ii}$$

where σ^2 is the term due to the actual error variance and $\sigma^2 p_{ii}$ is the term due to the estimation error variance.

This may seem like cheating since e_i and r_i are not independent for a given realization. In fact:

$$E[v_i^2] = E[(e_i - r_i)^2] = E[e_i^2 - 2e_i r_i + r_i^2] \quad \text{and } r_i = \sum_j p_{ij} e_j$$

$$E[v_i^2] = \sigma^2 (1 - p_{ii})$$

It is tempting to use $v_i / (1 - p_{ii})^{1/2}$ for e_i in the outlier test (or, equivalently, to test v_i against a threshold based on $\sigma^2 (1 - p_{ii})$) but this becomes dangerous as p_{ii} approaches 1. The factor p_{ii} can be interpreted as a measure of the uniqueness of or as the information content of the i^{th} observation. As p_{ii} approaches 1 the i^{th} observation lies almost entirely within the parameter subspace which implies that it is providing information to the solution which the other observations do not. Note that such “influential” observations can be identified from the structure of the coefficient matrix, \mathbf{A} , without reference to the observation residuals. Attempting to use $1/(1 - p_{ii})^{1/2}$ to rescale the residual v_i to better approximate e_i will, in a sense, punish this observation for being important. Instead, we view p_{ii} as a measure of how poor an estimate of the actual error, e_i , the residual, v_i , is and ignore the fact that v_i will tend to be an underestimate of e_i . We therefore use $v_i^2 = \sigma^2 (1 + p_{ii})$ as shown above) to construct the outlier detection threshold.

One remaining problem is that we do not know exactly what σ^2 is and must estimate it from the observation residuals. This is done by scaling the apriori observation variance using the variance of unit weight computed in the precision solution. The fact that we are using an estimated variance to establish our outlier detection threshold modifies the algorithm in two ways: 1) we compensate for the fact that removing a point as an outlier will alter the computation of the variance of unit weight by removing one residual and reducing the number of degrees of freedom; and 2) we base the detection threshold computation on Student’s t-distribution rather than the Gaussian distribution.

The variance of unit weight is computed as:

$$\text{var}_0 = \underline{\mathbf{V}}^T \mathbf{C}^{-1} \underline{\mathbf{V}} / (n - p) = \underline{\mathbf{V}}^T \underline{\mathbf{V}} / \sigma^2 (n - p) = v_j^2 / \sigma^2 (n - p)$$

where: n = number of observations,
 p = number of parameters, and

σ_0^2 is the apriori variance.

The estimated variance is:

$$\text{var} = \text{var}_0 \sigma_0^2 = v_j^2 / (n - p)$$

Removing the k^{th} observation makes this:

$$\begin{aligned} \text{var}_k &= (v_j^2 - v_k^2) / (n - 1 - p) = (n - p) / (n - p - 1) * (v_j^2 - v_k^2) / (n - p) \\ \text{var}_k &= (n - p) / (n - p - 1) * \text{var} - v_k^2 / (n - 1 - p) \end{aligned}$$

To normalize the k^{th} residual we divide it by the estimated standard deviation $\hat{\sigma}_k = (\text{var}_k)^{1/2}$:

$$w_k = v_k / \hat{\sigma}_k$$

We can rescale this normalized residual to reflect the removal of this observation from the variance estimate without having to actually compute a new variance:

$$\begin{aligned} w_k' &= v_k / \hat{\sigma}_k' = w_k \hat{\sigma}_k / \hat{\sigma}_k' = w_k (\text{var} / \text{var}_k)^{1/2} \\ \text{var} / \text{var}_k &= 1 / [(n - p) / (n - p - 1) - v_k^2 / \text{var} (n - p - 1)] = (n - p - 1) / (n - p - v_k^2 / \text{var}) \\ \text{var} / \text{var}_k &= (n - p - 1) / (n - p - w_k^2) \\ &\text{noting that } v_k^2 / \text{var} = w_k^2 \\ w_k' &= w_k [(n - p - 1) / (n - p - w_k^2)]^{1/2} \end{aligned}$$

Finally, we include the $(1 + p_{kk})$ factor discussed above and our normalized and reweighted residual becomes:

$$\begin{aligned} w_k' &= w_k [(n - p - 1) / (1 + p_{kk})(n - p - w_k^2)]^{1/2} \\ &\text{where: } w_k = v_k / \hat{\sigma}_k \end{aligned}$$

This normalized and reweighted residual is compared against a probability threshold computed using Student's t-distribution with $(n - p)$ degrees of freedom.

3.1.5.3.7.2 Inverse Mapping

For the precision correction process the information needed from the systematic ground control point includes the satellite position and velocity vectors in earth centered inertial coordinates along with the latitude and longitude associated with the point. From the reference ground control point the precision process needs the latitude and longitude along with the height of the control point above the WGS84 ellipsoid. The steps involved in the process include:

1. Use Geometric Correction Grid to find an input line and sample for an associated output line and sample of the systematic Ground Control Point (GCP) (see the Resampling algorithm description).
2. Determine the scan time associated with the systematic GCP. Since the model truncates to determine the scan number from the input line, the input line has a value of 0.5 added to it so that it can be rounded to the nearest integer line.
3. Use an interpolating polynomial for satellite position and velocity to get the position and velocity vectors for the time associated with the input line and sample of systematic GCP.
4. Call the Projection Transformation Package to convert the projection coordinate of the systematic image GCP to latitude and longitude.
5. Call the Projection Transformation Package to convert the projection coordinate of the base image GCP to latitude and longitude.

3.1.5.3.7.3 Precision Ephemeris Update

The purpose of this algorithm is to update the systematic orbit model with the information from the precision correction solution parameters, so that a precision image can be generated.

Given:

t_{ref}	reference time for the precision correction;
x_{ob}	orbit position correction in the Orbit System x (along-track) direction
y_{ob}	orbit position correction in the Orbit System y (cross-track) direction
z_{ob}	orbit position correction in the Orbit System z (altitude) direction
$v_{x_{ob}}$	orbit velocity correction in the Orbit System x (along-track) direction
$v_{y_{ob}}$	orbit velocity correction in the Orbit System y (cross-track) direction
$v_{z_{ob}}$	orbit velocity correction in the Orbit System z (altitude) direction

For each ephemeris data point, the algorithm takes the following ephemeris information:

t_{eph}	time for the ephemeris data point
x	orbit position in the Earth Fixed system x direction
y	orbit position in the Earth Fixed system y direction
z	orbit position in the Earth Fixed system z direction
v_x	orbit velocity in the Earth Fixed system x direction
v_y	orbit velocity in the Earth Fixed system y direction

vz orbit velocity in the Earth Fixed system z direction

and performs the following steps:

1. Calculate the orbit position correction in Orbit System at the time

$$\begin{aligned} dx_{ob} &= x_{ob} + vx_{ob} * (t_{eph} - t_{ref}) \\ dy_{ob} &= y_{ob} + vy_{ob} * (t_{eph} - t_{ref}) \\ dz_{ob} &= z_{ob} + vz_{ob} * (t_{eph} - t_{ref}) \end{aligned}$$

2. Calculate the transformation matrix from the Orbit System to the Earth Fixed system at the time

- 2.1. First, compose the transformation matrix, T_{eo} , from the Earth Fixed system to the Orbit System:

\underline{W}_z , unit vector in negative radial direction, pointing to the Earth center:
(denoting $\underline{X} = \{x, y, z\}$ and $\underline{V} = \{v_x, v_y, v_z\}$)

$$\underline{W}_z = - \underline{X} / |\underline{X}|$$

\underline{W}_y , unit vector in cross-track direction (- angular momentum);

$$\underline{W}_y = \underline{W}_z \text{ cross } \underline{V} / |\underline{W}_z \text{ cross } \underline{V}|$$

\underline{W}_x , unit vector in along-track direction;

$$\underline{W}_x = \underline{W}_y \text{ cross } \underline{W}_z$$

$$T_{eo} = \begin{matrix} \underline{W}_x(1) & \underline{W}_x(2) & \underline{W}_x(3) \\ \underline{W}_y(1) & \underline{W}_y(2) & \underline{W}_y(3) \\ \underline{W}_z(1) & \underline{W}_z(2) & \underline{W}_z(3) \end{matrix}$$

- 2.2 Transpose the T_{eo} matrix to get the transformation from the Orbit System to the Earth Fixed system:

$$T_{oe} = \begin{matrix} \underline{W}_x(1) & \underline{W}_y(1) & \underline{W}_z(1) \\ \underline{W}_x(2) & \underline{W}_y(2) & \underline{W}_z(2) \\ \underline{W}_x(3) & \underline{W}_y(3) & \underline{W}_z(3) \end{matrix}$$

3. Calculating the orbit position correction in the Earth Fixed system:

$$\begin{aligned} dx &= \underline{W}_x(1) \underline{W}_y(1) \underline{W}_z(1) dx_{ob} \\ dy &= \underline{W}_x(2) \underline{W}_y(2) \underline{W}_z(2) * dy_{ob} \\ dz &= \underline{W}_x(3) \underline{W}_y(3) \underline{W}_z(3) dz_{ob} \end{aligned}$$

4. Calculating the orbit velocity correction in the Earth Fixed system:

$$\begin{aligned} dvx &= \underline{W}_x(1) \underline{W}_y(1) \underline{W}_z(1) vx_{ob} \\ dvy &= \underline{W}_x(2) \underline{W}_y(2) \underline{W}_z(2) * vy_{ob} \\ dvz &= \underline{W}_x(3) \underline{W}_y(3) \underline{W}_z(3) vz_{ob} \end{aligned}$$

5. Update the orbit position and velocity in the Earth Fixed system:

$$\begin{aligned} x &= x + dx; \\ y &= y + dy; \\ z &= z + dz; \\ vx &= vx + dvx; \\ vy &= vy + dvy; \\ vz &= vz + dvz; \end{aligned}$$

This algorithm computes the orbit correction for each ephemeris data point in the Earth Fixed system and adds to yield the new ephemeris data point information.

3.1.5.3.8 Terrain Correction

The terrain correction algorithm uses elevation data from a digital elevation model (DEM) to generate offsets which will correct for the effect of terrain parallax. These corrections are only required in the along-scan (sample) direction.

To avoid having to call the Projection Transformation Package for every point in the output space, the DEM is processed to the same pixel size, projection, and frame as the precision image and its elevations are relative to the WGS84 ellipsoid rather than mean sea level or some other vertical datum. It is also expected that the precision corrections have already been applied to the forward model. The process is as follows:

1. Read the DEM and get minimum and maximum elevations present in the scene.
2. Determine the location of nadir in terms of raw space input sample. The secant method of root finding is used to determine the sample location at which the y-component of the line of sight vector (LOS) in orbital coordinates goes to zero for

each scan. It stores these in an array. This segment also stores the latitude and magnitude of the satellite position vector (in meters) for the center of the scene.

3. Using the minimum and maximum elevations found in Step 1, determine the sample displacement due to terrain for every (off-nadir-sample, elevation) pair. Off-nadir-sample should range from zero to 3600 (or some number which guarantees that all possible input samples will be covered). Elevation should be in meters and range from the minimum to the maximum in the scene. The algorithm steps elevation in increments of 1 meter.
4. For every line, sample pair in the output image space, the terrain correction algorithm needs the corresponding line, sample in input space. (See the inverse model, section 3.1.5.3.6).
5. Given the current output line and sample, the elevation is read from the DEM buffer from Step 1.
6. Given the corresponding input sample, it's distance from nadir in pixels is determined from the calculation of nadir pixel in Step 2.

$$\text{off_nadir_pixel} = \text{in_sample} - \text{nadir_sample}$$

7. From the ($|\text{off_nadir_pixel}|$, elevation) pair determined in Steps 6 & 7, the value of the terrain offset is looked up from the table generated by Step 3.
8. The next step in terrain correction, (applied in the Resampler) is to adjust the input sample locations by the terrain offset and resample.

Note that the algorithm assumes a DEM is available in the same projection, datum and framing as the output space as defined by the precision corrected grid; and that it has been resampled to the same pixel size. It also assumes that for every line, sample in output space, the corresponding line, sample can be found in input space. The offsets due to terrain are applied in the resampler.

This algorithm was investigated using the $1^\circ \times 1^\circ$ (3arc-sec) DTED-1 (Digital Terrain Elevation Data Level-1) available via anonymous FTP from the EROS Data Center. Slightly better accuracy could be achieved using higher spatial resolution 7.5×7.5 arc-min (30m) USGS Digital Elevation Model (DEM) data; vertical accuracy is better than 15m RMSE.

Terrain Correction Algorithm

The terrain correction algorithm will generate a table of terrain induced sample offsets, corresponding to (off-nadir-sample, elevation) pairs, as generated in Step 3 above. The method used for determining these terrain corrections comes from Reference 22. The following summarizes that document. A schematic of the geometry is shown in Figure 3.1.5-25.

Given distance in pixels of a sample in input space from the nadir pixel location, the ground range, S , is given by:

$$S = \text{pixel_size} * \text{off_nadir_pixel}$$

Where pixel_size is the nominal pixel size in meters for the given band.

This is associated with an Earth centered angle, s :

$$s = S/Re$$

Where Re is the radius of the Earth reference ellipsoid at the scene center latitude.

The magnitude and direction of the line of sight vector relative to nadir can then be found as:

$$\begin{aligned} \text{LOS} &= \sqrt{Re^2 + (Re + \text{Alt})^2 - 2*Re(Re + \text{Alt})*\cos(s)} \\ d &= \text{asin}(Re*\sin(s)/\text{LOS}) \end{aligned}$$

Where Alt is the altitude of the satellite above the ellipsoid.

Looking at Figure 3.1.5-25, elevation, h , at location S , will cause the information at the top of the hypothetical mountain to be mapped to the location $S + dS$ on the ellipsoid used by the forward sensor model. What the terrain correction will do is determine the offset, dS , so that when the time comes to resample, we can grab the information projected on the ellipsoid at location $S + dS$ and move it back to the mountain top at location S . This is done by first determining the angular difference between the LOS to a spot on the ellipsoid below the terrain feature and the LOS' to the projected location of that feature on the ellipsoid.

$$dd = \text{atan}\left\{ \frac{(Re+\text{Alt}) * \sin(d) * (1-(Re+h)/Re)}{[(Re+h) * \sqrt{1-(Re+\text{Alt})^2 * \sin^2(d)/Re^2} - (Re+\text{Alt})*\cos(d)]} \right\}$$

$$z'' = \text{asin}[(Re+\text{Alt}) * \sin(d+dd)/Re]$$

$$ds = z'' - s - (d+dd)$$

$$dS = Re * ds$$

$$\text{terrain_offset} = dS / \text{pixel_size}$$

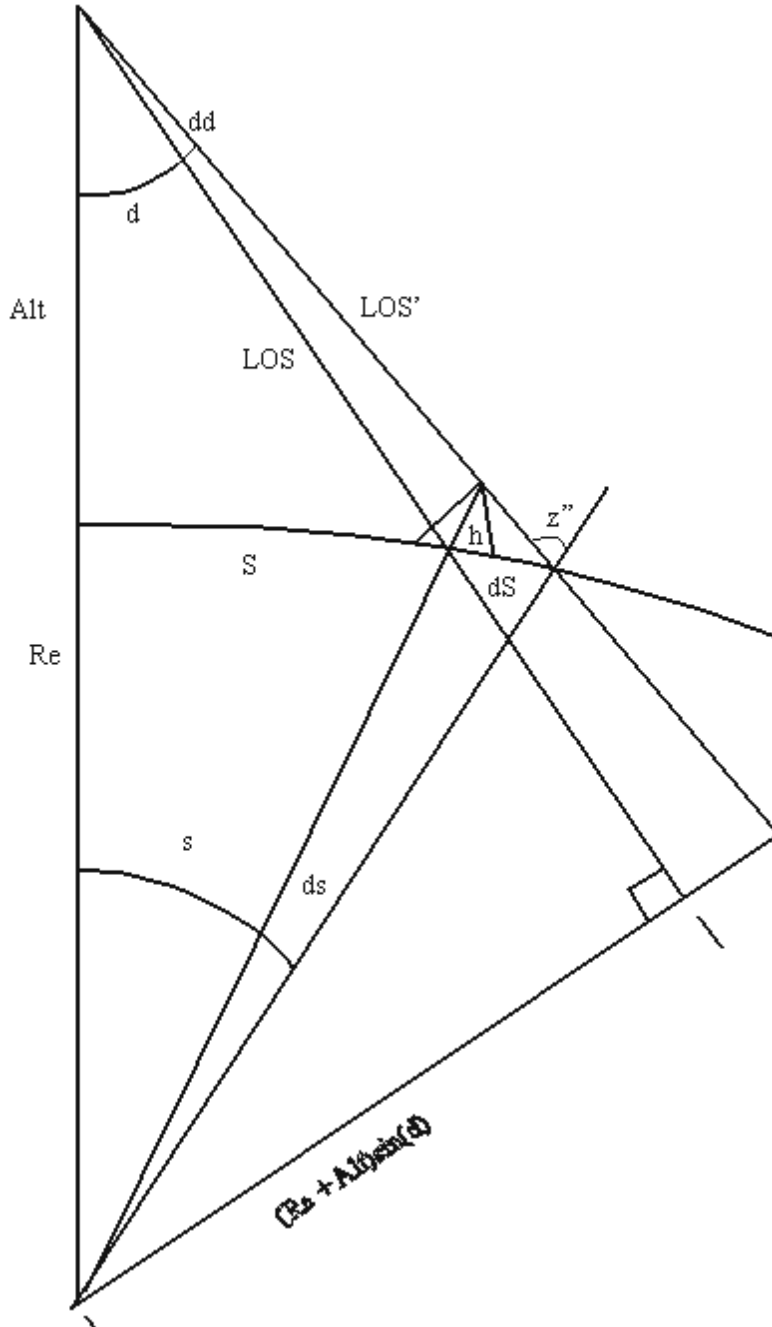


Figure 3.1.5- 25 Terrain Correction Geometry

Then for resampling, rather than getting data from input(sample), the data for the location in output space should be taken from input (sample + terrain_offset * (sign of off_nadir_pixel)).

The assumption of a constant satellite altitude above the geoid for one Landsat scene was tested with an absolute worst case scenario. A terrain feature with an elevation of 8,850m (the height of Mt. Everest) was placed near the equator at the end of a scan line. The orbit was modeled using the highest eccentricity allowed within specifications and in the vicinity of the greatest rate of change of orbit radius. In this case, the maximum error introduced was only ~0.03 panchromatic pixels. This is approximately the same size as the resampling increment, 0.03125 pixels. In a test case using Landsat 5 data from an actual test site, (path 28, row 30), the error from the altitude assumption for an elevation of 500m at the end of scan was ~0.001 pixels. For these reasons, the assumption of a constant satellite altitude over a scene was considered valid.

3.1.5.4 Geometric Calibration Algorithms

3.1.5.4.1 Sensor Alignment Calibration

The purpose of this algorithm is to use a sequence of precision correction solutions, including both correction parameter estimates and estimated covariance information, to estimate the underlying ETM+ instrument to Landsat 7 navigation reference base alignment. A Kalman filter implementation is used to isolate the systematic alignment trend from the attitude and ephemeris knowledge error which varies from scene to scene.

This algorithm is one step of the Kalman filter [Reference 23] for a linear dynamic model (constant rate model). It takes one precision correction solution file (generated from one scene) and updates the estimate of the alignment state parameters. It appends the newest state parameter estimate to the orbit parameter sequence file, attitude parameter sequence file, and also appends an innovation sequence file. This algorithm does not make a decision on whether the alignment is anomalous or whether it should be corrected. This algorithm provides the information (the sequence files) for an analyst to make that decision.

This algorithm would be applied each time a calibration scene is processed through the precision correction software, to update the alignment estimate. Operationally, the precision correction processing will include the use of definitive ephemeris data, obtained from the GSFC Flight Dynamics Facility (FDF), to help separate ephemeris position errors from angular alignment and attitude errors. Error propagation analyses and simulations run with the algorithm prototype software suggest that it will require 4 or 5 precision corrected calibration scenes to drive the alignment knowledge from its pre-

launch accuracy of approximately 240 arc seconds per axis (1 sigma) to the IAS calibrated specification value of 24 arc seconds per axis.

Algorithm Description

Defining the Filter:

The state vector of this filter is a 12x1 vector:

$\mathbf{X} =$	roll	roll attitude angle, in microradians (urad);
	pitch	pitch attitude angle, in urad;
	yaw	yaw attitude angle, in urad;
	x	along-track orbit position error, in meters (m);
	y	cross-track orbit position error, in m;
	z	radial orbit position error, in m;
	r_dot	roll angle rate, in urad/day;
	p_dot	pitch angle rate, in urad/day;
	yaw_dot	yaw angle rate, in urad/day;
	vx	velocity in x, in m/day;
	vy	velocity in y, in m/day;
	vz	velocity in z, in m/day;

See the precision correction algorithm description for the definition of above parameters, but note the units for the rate and velocity terms are different here. In fact, the rate and velocity state vector components represent long term linear trends in the bias data rather than the short term rate of change errors estimated by the precision correction process. The covariance matrix for \mathbf{X} is a 12x12 matrix \mathbf{P} .

The observation vector for this filter is a 6x1 vector:

$\mathbf{Y} =$	roll	roll attitude angle, in urad;
	pitch	pitch attitude angle, in urad;
	yaw	yaw attitude angle, in urad;
	x	along-track orbit position error, in m;
	y	cross-track orbit position error, in m;
	z	radial orbit position error, in m;

The covariance matrix for \mathbf{Y} is a 6x6 matrix \mathbf{R} . The observation is from the precision correction solution, but with the velocity and attitude rate parameters discarded. The velocity and rate estimated from precision correction are short term variations in a scene, what is to be monitored in the alignment calibration is the long term drift.

The precision correction estimates for the attitude bias terms: roll, pitch, and yaw; are actually estimates of the combination of long term alignment error (what we are looking for) plus short term alignment and attitude errors. These short term errors appear to be constant, or nearly constant, biases over time intervals of minutes to hours, but will decorrelate over the time intervals between calibration scenes (days). These short term variations thus appear to be random noise superimposed on the alignment bias observations taken from each calibration scene. This will manifest itself in the calibration scene precision correction results as sequences of attitude bias estimates whose dispersion is greater than would be expected based on the a posteriori covariance estimates computed in the precision correction process. Any systematic linear trend present in the attitude error will be indistinguishable from alignment and will be incorporated into the alignment bias estimated by the Kalman filter.

The random attitude and dynamic alignment errors are, in effect, an additional measurement error vector, added to the estimation error from the precision correction solution, in the Kalman filter formulation. The observation covariance matrix, \mathbf{R} , is therefore the sum of the a posteriori covariance matrix from the precision correction solution and the expected covariance of the “random” attitude and dynamic alignment errors. According to the Landsat 7 System Specification [Reference 5], the expected variance of the additional random attitude and dynamic alignment errors is less than or equal to the sum of the squares of 45 arc seconds of attitude knowledge error (Reference 5, section 3.7.1.3.9), 8 arc seconds of dynamic ETM+ to Navigation Base Reference alignment error (Reference 5, section 3.7.1.3.10), and 15 arc seconds of line of sight to ETM+ reference dynamic alignment error (Reference 5, section 3.7.8.1.16.7). This yields a net random component of 48 arc seconds. Since these errors are assumed to be uncorrelated with each other, they are added to the diagonal elements of the \mathbf{R} matrix corresponding to the alignment biases.

Although we do not expect to detect any systematic offset in the position bias terms: x, y, and z; they are included because of their high correlation with the attitude biases. This is reflected in the observation covariance matrix where significant off-diagonal terms will exist for x-pitch and y-roll. Any particular precision correction solution will resolve the correlation between the parameters by allocating the along track and across track errors between the ephemeris and attitude parameters based on their a priori weights. Thus, some of the systematic alignment bias could end up allocated to the ephemeris correction terms. Over multiple precision correction solutions the net ephemeris bias should be very close to zero, so we establish small a priori state variances for the ephemeris bias terms and allow the Kalman filter to reallocate systematic trends in the ephemeris corrections back to the alignment parameters. In practice, since accurate post-pass ephemeris will be available for the calibration test scenes, most of the correction will be allocated to the attitude terms in the precision correction solutions anyway.

The dynamic model used for this filter is the constant rate (velocity) model:

$$\mathbf{X}_k = \mathbf{F}(t_k, t_{k-1})\mathbf{X}_{k-1}$$

where the state transition matrix is:

$$\mathbf{F}(t_k, t_{k-1}) = \begin{bmatrix} \mathbf{I} & dt \mathbf{I} \\ \mathbf{0} & \mathbf{I} \end{bmatrix}$$

\mathbf{I} is a 6x6 identity matrix and $dt = t_k - t_{k-1}$ is the time difference between epoch t_{k-1} and t_k .

The observation equation is

$$\mathbf{Y} = \mathbf{H}*\mathbf{X} + \mathbf{v};$$

where $\mathbf{H} = [\mathbf{I} \ \mathbf{0}]$ and \mathbf{v} is the net measurement error with covariance \mathbf{R} .

Process noise can be added, with constant covariance matrix \mathbf{Q} . \mathbf{Q} is diagonal with 12 components. The process noise will initially be assumed to be zero. After several precision correction solution sets are available for analysis, the innovation sequence and a posteriori state covariance will be assessed to decide whether process noise should be added to better model the dynamic behavior observed in the data.

Procedure:

For each run this algorithm performs the steps described in the following sub-paragraphs.

1. Setup option

Read in the input option file to define the input and output file names, options and process noise variance.

2. Initialization

Read in the previous epoch time t_p , state vector \mathbf{X}_p , and covariance matrix \mathbf{P}_p . For a regular run this is read from the output state file of the previous run. For the first run, this is read from an initial observation file, which contains the a priori knowledge of the state vector

(alignment terms are zero plus or minus 240 arc seconds, ephemeris terms are zero plus or minus one meter).

3. Read and preprocess an observation as follows:

3.1 Extract the observation data from the precision correction solution

Read in the current epoch time t_c , precision correction observation \mathbf{Z} , and covariance matrix \mathbf{R} . This is read from a solution file output by the precision correction algorithm. The precision correction solution file contains both bias and rate correction terms whereas the Kalman filter observation only uses the bias components. The terms corresponding to roll, pitch, yaw, x, y, and z bias are extracted from the precision correction solution vector and covariance matrix to assemble \mathbf{Y} and \mathbf{R} , respectively. The additional observation noise due to scene to scene attitude and dynamic alignment error is accounted for by adding the expected error variance (48 arc seconds)² to the diagonal elements of \mathbf{R} corresponding to the roll, pitch, and yaw bias correction parameters.

3.2 Convert the attitude observation to an absolute pointing error observation

The precision correction solution contains updates to the alignment knowledge from the Calibration Parameter File (CPF) used to process the test scene. We want the Kalman filter to model the absolute alignment angles so that observations processed with different versions of the CPF can be combined. To make this possible we must construct the composite CPF alignment/precision correction angles for input to the Kalman filter.

The precision correction roll (r), pitch (p), and yaw (y) update values can be composed into an alignment correction rotation matrix as follows:

$$\mathbf{A} = \begin{bmatrix} \cos(p) \cos(y) & \sin(r) \sin(p) \cos(y) + \cos(r) \sin(y) & -\cos(r) \sin(p) \cos(y) + \sin(r) \sin(y) \\ -\cos(p) \sin(y) & -\sin(r) \sin(p) \sin(y) + \cos(r) \cos(y) & \cos(r) \sin(p) \sin(y) + \sin(r) \cos(y) \\ \sin(p) & -\sin(r) \cos(p) & \cos(r) \cos(p) \end{bmatrix}$$

The Calibration Parameter File (CPF) alignment matrix is defined as the rotation from the Navigation Base Reference (NBR) coordinate system to the ETM+ sensor coordinate system. To convert a look vector constructed in ETM+ sensor coordinates (\mathbf{X}_{ETM}) to the orbital coordinate system (\mathbf{X}_{orb}), where the precision correction solution is performed, the following rotations must be performed:

$$\mathbf{X}_{\text{orb}} = \mathbf{T}_{\text{att}}^T \mathbf{A}^T \mathbf{X}_{\text{ETM}}$$

where: \mathbf{T}_{att} is the attitude rotation matrix, and \mathbf{A} is the alignment matrix.

Note that the transpose of \mathbf{A} is used assuming that \mathbf{A} is an orthogonal rotation matrix so that its transpose is the same as its inverse.

The precision correction solution computes updates to the composite $\mathbf{T}_{\text{att}} \mathbf{A}^T$ rotation to best fit the observed ground control. This update takes the following form:

$$\mathbf{X}_{\text{orb}} = \mathbf{A} \mathbf{T}_{\text{att}}^T \mathbf{A}^T \mathbf{X}_{\text{ETM}}$$

where: \mathbf{A} is the alignment correction matrix defined above.

For small rotations, the \mathbf{A} and \mathbf{T}_{att} commute to a good approximation. Using the maximum off-nadir attitude pointing of 1080 arc seconds (900 arc seconds maximum off-nadir commanded pointing per the Landsat 7 System Specification section 3.7.1.3.8.2 plus 180 arc seconds of pointing error per section 3.7.1.3.8) and the maximum expected alignment error of 720 arc seconds (ibid. section 3.7.1.3.11), the error in commuting these rotations is less than 0.01 arc seconds. This allows the equation above to be rewritten as:

$$\mathbf{X}_{\text{orb}} = \mathbf{T}_{\text{att}}^T \mathbf{A} \mathbf{A}^T \mathbf{X}_{\text{ETM}}$$

The composite rotation $\mathbf{A}' = \mathbf{A} \mathbf{A}^T$ captures the net measured alignment offset. We extract roll, pitch, and yaw angles from this composite matrix using the following equations, where a'_{ij} indicates the element from the i th row and j th column of \mathbf{A}' .

$$\begin{aligned} \text{roll}' &= \tan^{-1}(-a'_{32}/a'_{33}) \\ \text{pitch}' &= \sin^{-1}(a'_{31}) \\ \text{yaw}' &= \tan^{-1}(-a'_{21}/a'_{11}) \end{aligned}$$

These composite angles are inserted into the observation vector, \mathbf{Y} , replacing the precision correction output values.

4. Propagate \mathbf{X}_p and \mathbf{P}_p to the current epoch time t_c .

Calculate:

$$\begin{aligned} dt &= t_c - t_p; \\ \mathbf{X}_c &= \mathbf{F}(t_c, t_p) * \mathbf{X}_p; \\ \mathbf{P}_c &= \mathbf{F}(t_c, t_p) * \mathbf{P}_p * \mathbf{F}^T(t_c, t_p); \end{aligned}$$

Because of the special structure of \mathbf{F} , the computation can be simplified if we divide the \mathbf{X} vector into 2 blocks:

$$\mathbf{X} = \begin{array}{|c|} \hline \mathbf{X}_1 \\ \hline \end{array}$$

$$\begin{bmatrix} \mathbf{X}_2 \end{bmatrix}$$

and \mathbf{P} into 4 sub-matrices:

$$\mathbf{P} = \begin{bmatrix} \mathbf{P}_{11} & \mathbf{P}_{12} \\ \mathbf{P}_{21} & \mathbf{P}_{22} \end{bmatrix}$$

Then:

$$\begin{aligned} \mathbf{X}_{c1} &= \mathbf{X}_{p1} + dt * \mathbf{X}_{p2} \\ \mathbf{X}_{c2} &= \mathbf{X}_{p2} \\ \mathbf{P}_{c11} &= \mathbf{P}_{p11} + dt * \mathbf{P}_{p12} + dt * \mathbf{P}_{p21} + dt * dt * \mathbf{P}_{p22} \\ \mathbf{P}_{c12} &= \mathbf{P}_{p12} + dt * \mathbf{P}_{p22} \\ \mathbf{P}_{c21} &= \mathbf{P}_{p21} + dt * \mathbf{P}_{p22} \\ \mathbf{P}_{c22} &= \mathbf{P}_{p22} \end{aligned}$$

And add the process noise if that option is selected:

$$\mathbf{P}_c = \mathbf{P}_c + \mathbf{Q}$$

5. Calculate the Kalman gain matrix \mathbf{K} :

$$\mathbf{K} = \mathbf{P}_c * \mathbf{H}^T * [\mathbf{H} * \mathbf{P}_c * \mathbf{H}^T + \mathbf{R}]^{-1}$$

Because of the structure of \mathbf{H} :

$$\mathbf{H} * \mathbf{P}_c * \mathbf{H}^T = \mathbf{P}_{c11}$$

and:

$$\mathbf{P}_c * \mathbf{H}^T = \begin{bmatrix} \mathbf{P}_{c11} \\ \mathbf{P}_{c21} \end{bmatrix}$$

which gives the Kalman gain matrix the following structure:

$$\mathbf{K} = \begin{bmatrix} \mathbf{K}_1 \\ \mathbf{K}_2 \end{bmatrix} = \begin{bmatrix} \mathbf{P}_{c11} \\ \mathbf{P}_{c21} \end{bmatrix} * [\mathbf{P}_{c11} + \mathbf{R}]^{-1}$$

6. Update the current state with the filtered innovation to create a new estimate and update the new filtered state covariance:

$$\begin{aligned} \mathbf{X}_n &= \mathbf{X}_c + \mathbf{K} * (\mathbf{Y} - \mathbf{H} * \mathbf{X}_c) = \mathbf{X}_c + \mathbf{K} * (\mathbf{Y} - \mathbf{X}_{c1}) \\ \mathbf{P}_n &= \mathbf{P}_c - \mathbf{K} * \mathbf{H} * \mathbf{P}_c \end{aligned}$$

which reduces to:

$$\mathbf{P}_n = \mathbf{P}_c - \begin{array}{|c|} \hline \mathbf{K}_1 * \mathbf{P}_{c11} \quad \mathbf{K}_1 * \mathbf{P}_{c12} \\ \hline \mathbf{K}_2 * \mathbf{P}_{c11} \quad \mathbf{K}_2 * \mathbf{P}_{c12} \\ \hline \end{array}$$

7. Append the orbit elements in \mathbf{X}_n to the orbit sequence file.
8. Append the attitude elements in \mathbf{X}_n to the attitude sequence file.
9. Append the innovation $\mathbf{Y} - \mathbf{H} * \mathbf{X}_c$ to the innovation sequence file.
10. Write out \mathbf{X}_n and \mathbf{P}_n to the new state file.
11. Update the Calibration Parameter File alignment matrix

Periodically, the analyst will decide that the alignment knowledge has improved sufficiently to justify modifying the Calibration Parameter File. This would typically occur after the first 5 or 6 calibration scenes have been processed post-launch and then at least once every quarter after the initial on orbit calibration. The update would be performed using the most current roll, pitch, and yaw correction estimates in the attitude sequence file.

The current filter estimates of roll (r), pitch (p), and yaw (y) are composed into a net alignment correction rotation matrix, as was done for the differential corrections above, as follows:

$$\mathbf{A}_{net} = \begin{array}{ccc} \cos(p) \cos(y) & \sin(r) \sin(p) \cos(y) + \cos(r) \sin(y) & -\cos(r) \sin(p) \cos(y) + \sin(r) \sin(y) \\ -\cos(p) \sin(y) & -\sin(r) \sin(p) \sin(y) + \cos(r) \cos(y) & \cos(r) \sin(p) \sin(y) + \sin(r) \cos(y) \\ \sin(p) & -\sin(r) \cos(p) & \cos(r) \cos(p) \end{array}$$

The net alignment rotation \mathbf{A}_{net} is the transpose of the new alignment matrix, so the updated alignment matrix for the CPF is computed as follows:

$$\mathbf{A}_{new} = \mathbf{A}_{net}^T$$

Once this update is incorporated into the CPF, subsequent calibration scenes will be processed with the improved alignment knowledge. Since this alignment knowledge is combined with the precision correction observation, as described in section 2.2.3.2 above, for input to the Kalman filter, the filter need not be reset after CPF updates. The state covariance would also not be reset since it accurately reflects the confidence of the current alignment knowledge.

After a sufficient number of precision correction results have been collected, an analyst may come up with some idea about the process noise by looking at the innovation sequence and the output filter covariance. The process noise sigma can be fed back to the filter through the input option file. Without the additional process noise, the filter may begin to diverge after a certain time (the filtered state covariance will begin to grow). Tuning the process noise is a difficult part of Kalman filtering practice, and some experimentation will be needed to optimize the algorithm.

3.1.5.4.2 Focal Plane Calibration

Focal Plane - Band Placement Calibration Algorithm Description

The objective of this algorithm is to estimate updates to the focal plane locations of the eight ETM+ band centers to improve band to band registration as specified in Reference 3.

Input to this algorithm includes the band to band comparison point correlation results from the band to band characterization algorithm, with outliers detected and removed as described in section 3.1.5.5.1. These are used in conjunction with the resampling grid file (used to produce the level 1Gs test image) as input to the band to band calibration process.

Algorithm:

The band location parameter vector is of the form:

$$\mathbf{X} = \begin{bmatrix} \mathbf{b}_{1x} \\ \mathbf{b}_{1y} \\ \dots \\ \mathbf{b}_{8x} \\ \mathbf{b}_{8y} \end{bmatrix}$$

where:

\mathbf{b}_{ix} = band offset in the focal plane x (along scan) direction for band i, in microradians

\mathbf{b}_{iy} = band offset in the focal plane y (across scan) direction for band i, in microradians

The band to band characterization test point correlation output data are assembled, point by point, to construct a band to band calibration measurement vector:

$$\mathbf{Y} = \begin{matrix} \mathbf{m}_{21P1} \\ \mathbf{m}_{21L1} \\ \dots \\ \mathbf{m}_{21PN} \\ \mathbf{m}_{21LN} \\ \mathbf{m}_{31P1} \\ \dots \\ \mathbf{m}_{81LN} \\ \mathbf{m}_{32P1} \\ \dots \\ \mathbf{m}_{87LN} \end{matrix}$$

where: m_{jiPk} = observed offset for point k, in output space pixels, between band j and band i (reference band) = pixel_{jk} - pixel_{ik}
 m_{jiLk} = observed offset for point k, in output space lines, between band j and band i (reference band) = line_{jk} - line_{ik}

The parameter vector and measurement vector are related by the following observation equation:

$$\begin{aligned}
 \mathbf{A}_{jik} \mathbf{X} &= \begin{matrix} 0 & \dots & -\frac{dp}{dx_{ik}} & -\frac{dp}{dy_{ik}} & \dots & 0 & \dots & \frac{dp}{dx_{jk}} & \frac{dp}{dy_{jk}} & \dots & 0 \\ 0 & \dots & -\frac{dl}{dx_{ik}} & -\frac{dl}{dy_{ik}} & \dots & 0 & \dots & \frac{dl}{dx_{jk}} & \frac{dl}{dy_{jk}} & \dots & 0 \end{matrix} \mathbf{X} \\
 &= \begin{matrix} \mathbf{m}_{jiPk} \\ \mathbf{m}_{jiLk} \end{matrix} + \mathbf{V}_{jik} = \mathbf{Y}_{jik} + \mathbf{V}_{jik}
 \end{aligned}$$

where: \mathbf{V}_{jik} is the 2x1 vector of measurement residuals for point k, assumed to be zero mean Gaussian errors with covariance matrix \mathbf{C}_{jik} . Typically, the \mathbf{C}_{jik} would be assumed to be the same for all k, so $\mathbf{C}_{jik} = \mathbf{C}_{ji}$.

$$\mathbf{C}_{ji} = \begin{matrix} 2 & 0 \\ p & \\ 0 & 2 \\ & p & 1 & 0.25 \\ & & & 1 \end{matrix}$$

The partial derivatives in the observation coefficient matrix \mathbf{A}_{jik} , are computed numerically using the resampling grids for bands j and i, from the input grid file, as follows:

For band i partials:

If band i was resolution adjusted for correlation with a lower resolution band, adjust the measured pixel, line to match the grid:

If $i=8$ (i.e., this band is panchromatic)

$$p_{ik} = 2 * p_{ik} - 1$$

$$l_{ik} = 2 * l_{ik} - 1$$

If $j=6$ (i.e., the other band is thermal)

$$p_{ik} = 2 * p_{ik} - 1$$

$$l_{ik} = 2 * l_{ik} - 1$$

Use $GRID_i$ to inverse map the test point pixel line coordinates: p_{ik}, l_{ik} to input image space pixel, line coordinates s_{ik}, d_{ik}

Add a small epsilon value, e_s , to s_{ik}

Use $GRID_i$ to map $(s_{ik} + e_s, d_{ik})$ to output space (p_{ix}, l_{ix})

Add a small epsilon value, e_d , to d_{ik}

Use $GRID_i$ to map $(s_{ik}, d_{ik} + e_d)$ to output space (p_{iy}, l_{iy})

Compute the partials numerically, dividing by the band IFOV in microradians to rescale the partial derivatives from output pixels per input pixel to output pixels per microradian:

$$dp/dx_{ik} = (p_{ix} - p_i)/e_s/IFOV_i$$

$$dl/dx_{ik} = (l_{ix} - l_i)/e_s/IFOV_i$$

$$dp/dy_{ik} = (p_{iy} - p_i)/e_d/IFOV_i$$

$$dl/dy_{ik} = (l_{iy} - l_i)/e_d/IFOV_i$$

If band i was resolution adjusted for correlation with a lower resolution band, adjust the partial derivative to match the actual measurements:

If $i=8$ (i.e., this band is panchromatic)

$$dp/dx_{ik} = (dp/dx_{ik})/2$$

$$dl/dx_{ik} = (dl/dx_{ik})/2$$

$$dp/dy_{ik} = (dp/dy_{ik})/2$$

$$dl/dy_{ik} = (dl/dy_{ik})/2$$

If $j=6$ (i.e., the other band is thermal)

$$dp/dx_{ik} = (dp/dx_{ik})/2$$

$$\begin{aligned} dl/dx_{ik} &= (dl/dx_{ik})/2 \\ dp/dy_{ik} &= (dp/dy_{ik})/2 \\ dl/dy_{ik} &= (dl/dy_{ik})/2 \end{aligned}$$

The same procedure is used with the grid file for band j, GRID_j, to yield the band j partials: dp/dx_{jk} , dl/dx_{jk} , dp/dy_{jk} , and dl/dy_{jk} . In this case, i and j are interchanged in the procedure above.

The normal equations can be constructed directly from a sequence of observation equations:

$$\begin{aligned} \mathbf{N} &= \mathbf{A}_{jik}^T \mathbf{C}_{ji}^{-1} \mathbf{A}_{jik} && \text{summed over all } k \text{ and all } i,j \text{ combinations} \\ \mathbf{L} &= \mathbf{A}_{jik}^T \mathbf{C}_{ji}^{-1} \mathbf{Y}_{jik} && \text{summed over all } k \text{ and all } i,j \text{ combinations} \end{aligned}$$

With only the band difference observations this system of equations will be indeterminate since the solution is insensitive to the addition of constant offsets to the \mathbf{b} terms. To stabilize the solution we add an additional observation requiring the band offset for band 8 (panchromatic) to be zero in each direction: Band 8 is constrained because it is used for scan mirror calibration and sensor alignment calibration, making it the geometric calibration reference band. This constraint is treated as another observation of the form:

$$\begin{aligned} \mathbf{A}_{00} &= \begin{matrix} 0 & 0 & 0 & 0 & 0 & 0 & 0 & 0 & 0 & 0 & 0 & 0 & 0 & 0 & 1 & 0 \\ 0 & 0 & 0 & 0 & 0 & 0 & 0 & 0 & 0 & 0 & 0 & 0 & 0 & 0 & 0 & 1 \end{matrix} \\ \mathbf{Y}_{00} &= \begin{matrix} 0 \\ 0 \end{matrix} \quad \mathbf{C}_{00} = \begin{matrix} 2 & 0 \\ 0 & 2 \end{matrix} \quad \begin{matrix} 0 \\ 0 \end{matrix} \quad 0.01 \text{ urad} \end{aligned}$$

After adding this observation to the normal equations, the minimum variance estimate for \mathbf{X} is:

$$\mathbf{X}_{\text{est}} = \mathbf{N}^{-1} \mathbf{L}$$

The measurement residuals for each input point can be calculated as:

$$\mathbf{V}_{jik} = \mathbf{A}_{jik} \mathbf{X}_{\text{est}} - \mathbf{Y}_{jik}$$

These residuals would be assessed by band pair to determine whether there were additional uncompensated biases in particular band combination measurements and to evaluate the point matching accuracy of particular band combinations.

Output: The resulting parameter vector, \mathbf{X}_{est} , contains the estimates of the 8 band offset pairs (x and y directions) in microradians. These values would be used to update the Band Offsets (expressed in microradians) in the Focal Plane Parameters parameter group in the Calibration Parameter File, as defined in Reference 24.

3.1.5.4.3 Scan Mirror Calibration

The purpose of the Scan Mirror Calibration segment of the Landsat 7 Image Assessment System is to check and, if necessary, correct the along scan and across scan mirror profiles.

As a preliminary approach to scan mirror calibration, a precision-terrain corrected Landsat panchromatic band is matched to a reference image with correlation. Currently the best candidate for the reference is the USGS digital orthophoto quadrangle (DOQ) imagery. Using the precision mapping grid, correlation windows can be selected which lie entirely within one scan thus allowing forward and reverse mirror scans to be separated.

For each successful correlation between a point in the reference image and a point in the Landsat scene, the respective image coordinates (lines, samples) in output space are mapped back through the inverse grid into input space (Resampling, section 3.1.5.3.6). After being mapped to input space, the effects of terrain are removed from the two samples to locate the (line, sample) input space coordinate associated with the measured output space (line, sample) (Terrain Correction, section 3.1.5.3.8). The remaining difference between the samples/lines is then taken to be the error in the scan mirror profile. Using the forward model, the time in scan of each sample is then calculated from the input sample (LOS Generation, section 3.1.5.3.4).

This correlation and inverse mapping procedure is used to generate a number of mirror error data points for several forward and reverse scans, each with an associated time in scan. Outlier rejection is performed by grouping the data points by scan direction and scan angle. Points are removed that deviate from the mean..

Once the data has been filtered for outliers, the data from forward and reverse are fit with fifth order Legendre polynomials as developed below. If the error in the mirror profile is beyond some predetermined value, the existing mirror coefficients can be updated in the calibration parameter file. The error polynomial coefficients are saved for trending.

Algorithm Development

The pre-launch mirror profiles are characterized as deviating from linear by a fifth order polynomial

$$b(t) = b_0 + b_1t + b_2t^2 + b_3t^3 + b_4t^4 + b_5t^5 \quad 0 < t < T_{\text{nom}} \quad (1)$$

This can also be written as an orthogonal fifth order Legendre polynomial

$$p(x) = a_0 + a_1x + a_2(3/2x^2 - 1/2) + a_3(5/2x^3 - 3/2x) + a_4(35/8x^4 - 30/8x^2 + 3/8)$$

$$+ a_5(63/8x^5 - 70/8x^3 + 15/8x) \quad -1 < x < 1 \quad (2)$$

$$\text{where } x = 2t/T_{\text{nom}} - 1$$

In order to convert back and forth between the mirror coefficients, b_i , and the Legendre coefficients, a_i , we equate the two polynomials above and gather terms of the same order. This leaves us with the transformations

$$\begin{aligned} b_0 &= a_0 - a_1 + a_2 - a_3 + a_4 - a_5 \\ b_1 &= (2a_1 - 6a_2 + 12a_3 - 20a_4 + 30a_5)/T_{\text{nom}} \\ b_2 &= (6a_2 - 30a_3 + 90a_4 - 210a_5)/T_{\text{nom}}^2 \\ b_3 &= (20a_3 - 140a_4 + 560a_5)/T_{\text{nom}}^3 \\ b_4 &= (70a_4 - 630a_5)/T_{\text{nom}}^4 \\ b_5 &= (252a_5)/T_{\text{nom}}^5 \end{aligned} \quad (3)$$

$$\begin{aligned} a_5 &= (b_5 T_{\text{nom}}^5)/252 \\ a_4 &= (b_4 T_{\text{nom}}^4)/70 + (b_5 T_{\text{nom}}^5)/28 \\ a_3 &= (b_3 T_{\text{nom}}^3)/20 + (b_4 T_{\text{nom}}^4)/10 + (b_5 T_{\text{nom}}^5)5/36 \\ a_2 &= (b_2 T_{\text{nom}}^2)/6 + (b_3 T_{\text{nom}}^3)/4 + (b_4 T_{\text{nom}}^4)2/7 + (b_5 T_{\text{nom}}^5)25/84 \\ a_1 &= (b_1 T_{\text{nom}})/2 + (b_2 T_{\text{nom}}^2)/2 + (b_3 T_{\text{nom}}^3)9/20 + (b_4 T_{\text{nom}}^4)2/5 + (b_5 T_{\text{nom}}^5)5/14 \\ a_0 &= b_0 + (b_1 T_{\text{nom}})/2 + (b_2 T_{\text{nom}}^2)/3 + (b_3 T_{\text{nom}}^3)/4 + (b_4 T_{\text{nom}}^4)/5 + (b_5 T_{\text{nom}}^5)/6 \end{aligned} \quad (4)$$

As was shown in the section on scan mirror correction (Create Model, section 3.1.5.3.3), the coefficients of the mirror scan profile are scaled by the total time of each scan which is calculated from the first half and second half scan errors

$$b_i' = b_i(T_{\text{nom}}/T_s)^i \quad (5)$$

$$b_i'(T_s)^i = b_i(T_{\text{nom}})^i \quad (6)$$

From the transformations in Eqs. 4, the relationship in Eq. 6 leads directly to

$$a_i' = a_i \quad (7)$$

where a_i' are the coefficients of a polynomial in the form of Eq. 2 but where the auxiliary variable x has been replaced by

$$x' = 2t/T_s - 1 \quad (8)$$

Therefore, using the actual scan time, T_s , instead of the nominal scan time, T_{nom} , to compute the auxiliary variable, x , takes care of the scan time scaling without changing the Legendre polynomial coefficients, a_i .

As discussed in section 3.1.5.3.3 (scan mirror correction), in addition to the fifth order deviation from a linear profile, there is also an adjustment to the quadratic terms used to fit the mid-scan error.

The linear portion of the mirror model is

$$L(t) = (a_{me}t + a_{sm}(T_s - t))/T_s \quad (9)$$

$$l(x) = (a_{me} + a_{sm})/2 + x(a_{me}-a_{sm})/2 \quad (10)$$

where a_{sm} and a_{me} are the mirror angles at start and end of scan respectively. The predicted mirror angle at the time of first half scan, t_{fh} , is

$$L(t_{fh}) = (a_{me}t_{fh} + a_{sm}t_{sh})/T_s = l() \quad (11)$$

where

$$\begin{aligned} t_{sh} &= T_s - t_{fh} \\ &= 2t_{fh}/T_s - 1 = (t_{fh}-t_{sh})/T_s \end{aligned} \quad (12)$$

Thus as shown in the section on scan mirror correction, the mid-scan correction due to deviation from linear (the difference between what the linear model predicts and what was observed, i.e. zero) is

$$A_f = -(a_{me}t_{fh} + a_{sm}t_{sh})/T_s = -l() \quad (13)$$

So the total mid-scan correction, including the mirror profile, is then

$$D_f = A_f - p() = -l() - p() \quad (14)$$

Again referring to the section on scan mirror correction, the coefficients for the quadratic adjustment to the fifth order polynomial are

$$\begin{aligned} b_0' &= 0 \\ b_1' &= (D_f T_s)/(t_{fh} t_{sh}) \\ b_2' &= -D_f/(t_{fh} t_{sh}) \end{aligned} \quad (15)$$

Using the transformations in Eqs 4, these corrections can be written in terms of Legendre coefficients as

$$\begin{aligned} a_0 &= b_0' + (b_1' T_s)/2 + (b_2' T_s^2)/3 = (D_f T_s^2)/(6t_{fh} t_{sh}) \\ a_1 &= (b_1' T_s)/2 + (b_2' T_s^2)/2 = 0 \\ a_2 &= (D_b T_s^2)/6 = -(D_f T_s^2)/(6t_{fh} t_{sh}) \end{aligned} \quad (16)$$

These can be rewritten as

$$\begin{aligned} a_0 &= (A_f - p(\))W_s = -(l(\) + p(\))W_s \\ a_1 &= 0 \\ a_2 &= -(A_f - p(\))W_s = (l(\) + p(\))W_s \end{aligned} \quad (17)$$

where $W_s = T_s^2 / (6t_{fh}t_{sh})$

Adding these to the coefficients in Eq. 2 we get

$$\begin{aligned} p'(x') &= a_0 + a_1x' + a_2(3/2x'^2 - 1/2) + a_3(5/2x'^3 - 3/2x') \\ &\quad + a_4(35/8x'^4 - 30/8x'^2 + 3/8) + a_5(63/8x'^5 - 70/8x'^3 + 15/8x') \\ &\quad + p(\)W_s(3/2x'^2 - 3/2) - A_fW_s(3/2x'^2 - 3/2) \end{aligned} \quad (18)$$

since $t_{fh} = t_{sh} = T_s/2$ and 0 looking at three special cases gives:

$$\begin{aligned} p'(\) &= p(\) + 2/3 p(\)(3/2^2 - 3/2) + 2/3 l(\)(3/2^2 - 3/2) - l(\) \\ p'(-1) &= p(-1) \\ p'(1) &= p(1) \end{aligned} \quad (19)$$

From this we see that the quadratic correction does not change the scan mirror profile at the beginning and end of scan where it is already constrained to be zero, and that any mirror profile deviation at mid-scan is suppressed by the correction quadratic. Therefore, any update to the mirror profile should obey the beginning and end of scan constraints:

$$\begin{aligned} p(-1) &= 0 \\ p(1) &= 0 \end{aligned} \quad (20)$$

Also, any update to the mirror profile at mid-scan will be suppressed by the quadratic correction which implies that any errors in the mirror profile at mid-scan can be neither measured nor corrected.

To account for these three special cases in our mirror correction model, we apply three constraints to the correction profile, $p(x')$, and treat them as additional observations:

$$\begin{aligned} p(1) &= a_0 + a_1 + a_2 + a_3 + a_4 + a_5 = 0 \\ p(-1) &= a_0 - a_1 + a_2 - a_3 + a_4 - a_5 = 0 \\ p(\) &= a_0 + a_1 + a_2(3/2^2 - 1/2) + a_3(5/2^3 - 3/2) \\ &\quad + a_4(35/8^4 - 30/8^2 + 3/8) + a_5(63/8^5 - 70/8^3 + 15/8) = 0 \end{aligned} \quad (21)$$

where the a_i 's are now the corrections to the nominal profile. These constraints have the practical effect of removing the low order terms, a_0 , a_1 , and a_2 from the correction model. The first two constraints can be reformulated and simplified

$$\begin{aligned} a_0 + a_2 + a_4 &= 0 \\ a_1 + a_3 + a_5 &= 0 \end{aligned} \quad (22)$$

Since the last constraint applies at $x=0$ which is very close to zero, it can be approximated by:

$$a_0 - 1/2a_2 + 3/8a_4 = 0 \quad (23)$$

These constraints can be rearranged to determine the low order coefficients, a_0 , a_1 and a_2 from the other three coefficients:

$$\begin{aligned} a_0 &= -7/12a_4 \\ a_1 &= -a_3 - a_5 \\ a_2 &= -5/12a_4 \end{aligned} \quad (24)$$

A fifth order polynomial which obeys these constraints can be used to model the higher order mirror non-linearity which cannot be removed by the mid-scan correction quadratic.

The measured deviations, converted to mirror angle deviations as a function of time, provide observations of the $p(x')$ mirror correction function. A weighted least squares technique is used to fit a Legendre polynomial like Eq. 2 to these observations. The constraints are then applied to the coefficients, computed by the weighted least squares procedure.

The user selects the weight for the observations based on the expected reference image and correlation accuracy.

The existing mirror polynomial coefficients are converted to Legendre space according to the transformation in Eqs. 4. If the higher order terms of the determined error polynomial are deemed by the operator to be significant and reproducible, then they are added to the existing coefficients and transformed back into mirror space according to Eqs. 3.

Inputs

As input, the mirror calibration algorithm requires a precision corrected grid, and a terrain corrected image. It also requires the same digital elevation model which was used in the terrain correction algorithm and the terrain correction table it generates. In order to calculate the time in scan for each sample, it also needs to have the forward sensor model. Finally it requires a reference image in the same framing as the terrain corrected image. The current plan is to use DOQ imagery as the reference. Also, the PCD flags which

indicate the scan mirror electronics (SME) number and scanning mode (Scan Angle Monitor or Bumper) to know which mirror profile is applicable.

Outputs

The scan mirror calibration algorithm generates a set of fifth order Legendre polynomial coefficients for corrections to the along and across scan mirror profiles for both forward and reverse scans. If the deviation from the existing profile is deemed to be significant, then the existing higher order mirror coefficients will be transformed into Legendre space, have the deviations added to them and be converted back into mirror coefficients. The lower order terms can be kept for characterization, though as shown above, they cannot be uniquely determined and therefore should not be used for calibration. In addition, all of the data generated by the correlation routines will also be stored.

Correlation Testing

One of the key components of the mirror calibration procedure is selecting an accurate reference image source. Digital orthophoto quad data is 1m resolution, panchromatic, aerial imagery which has been terrain corrected and rectified to a standard UTM projection with an accuracy specification of 6m, 1 . They are available in 7.5 arc-min quadrangles or 3.75 arc-min quarter-quads. In order to use DOQs as a reference they need to be downsampled to the same resolution as the ETM+ imagery and mosaicked to cover several scans. In the case of Landsat 7 this means downsampling to the level of the panchromatic band.

Ideally, we would like to mosaic the DOQ tiles at the highest resolution possible in order to better blend the radiometric differences which may be present. Practically speaking, however, the full resolution DOQs are too large to mosaic more than a few at a time. For example, in one of the potential test sites (Landsat 4/5 path 28, row 30) the quarter quad images are ~7700 lines by ~6900 samples and it takes ~200 of them to completely cover the first 20 scans of the Landsat scene (see Fig. 3.1.5-26). As a compromise, the DOQs will likely be mosaicked and reduced in resolution in stages.

For testing purposes, 16 quarter-quads from four full quadrangles were low-pass filtered and downsampled to 8m pixels. They were then mosaicked together and reprojected to the SOM projection in a Landsat Path-orientation at a factor of the final desired pixel size (7.5m). The mosaicked image was then low-pass filtered again and downsampled twice more to the final 30m pixel size of the test image.

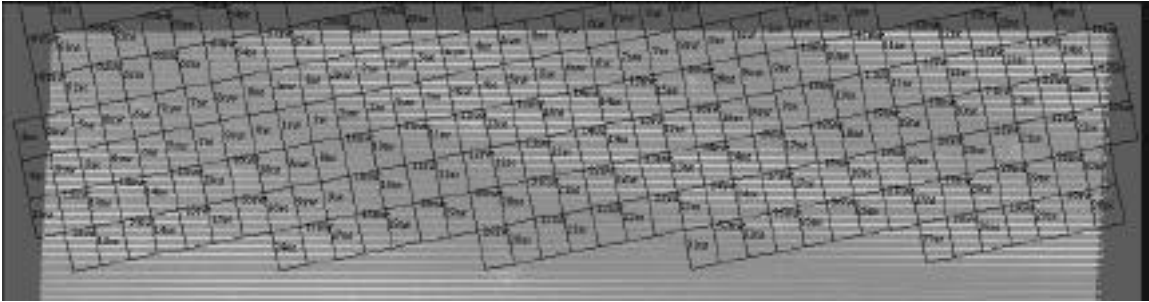


Figure 3.1.5- 26 DOQ quarter-quad images covering about 20 TM scans

Since a precision-terrain corrected image was not available, a section of a Landsat 5 systematic image was correlated with the assembled DOQ imagery using hand picked points. The TM image used for the correlation was a synthetic panchromatic image (at 30m pixel size) generated by a linear combination of bands 1, 2, 3 and 4. Using the correlation offsets, a polynomial transformation was generated to remap the TM sub-scene into the frame and projection of the DOQ. Another set of features was hand picked and the two images correlated. Without any sort of outlier rejection, the standard deviation of the correlation was ~ 0.25 pixels. Using a regular grid of correlation points, the standard deviation was ~ 0.35 pixels, again without any outlier rejection. Error analysis indicates that a correlation accuracy of 0.25 pixels should be sufficient. From these less-than-ideal tests, it appears as though this goal will be achievable particularly if the real panchromatic band of the ETM+ is to be used.

A consideration to keep in mind is that the DOQ reference images are generally taken in mid-spring. Therefore it would be best to choose test sites where seasonal variability will have the least impact.

Polynomial Fitting

In order to test the ability of the algorithm to determine corrections to the scan mirror coefficients, two systematic images were generated, one with the fifth order mirror correction polynomial applied and one without. This should result in being able to back out the original higher order coefficients. The two images were correlated using the first 96 scans. Each scan was broken down into 256 overlapping windows measuring eight lines by 128 samples in output space. The inverse grid was used to make certain that the correlation windows stayed within scans in input space.

The correlated (line, sample) pairs in the image and reference output space were run through the inverse grid to find their corresponding (line, sample) in input space. In practice, it is at this point that the terrain adjustment would be added to the input samples. Since neither image had any terrain correction applied, it was not necessary for this test. Knowing the input (line, sample) of the image and having initialized the forward model, we can get a time in scan corresponding to each correlation point. We can also get

the actual scan time, T_s , for each scan. These will allow us to determine the auxiliary variable, x' , as shown in Eq. 8. The difference between samples/lines in the two TM images (in practice, a terrain corrected ETM+ image and a reference) in input space is assumed to be an error which may be correctable by adjusting the coefficients of the scan mirror profile.

It is this difference as a function of the auxiliary variable, x' , which we attempt to fit with a Legendre polynomial. In practice we would apply the constraints in Equation 19, though this was not done for this test.

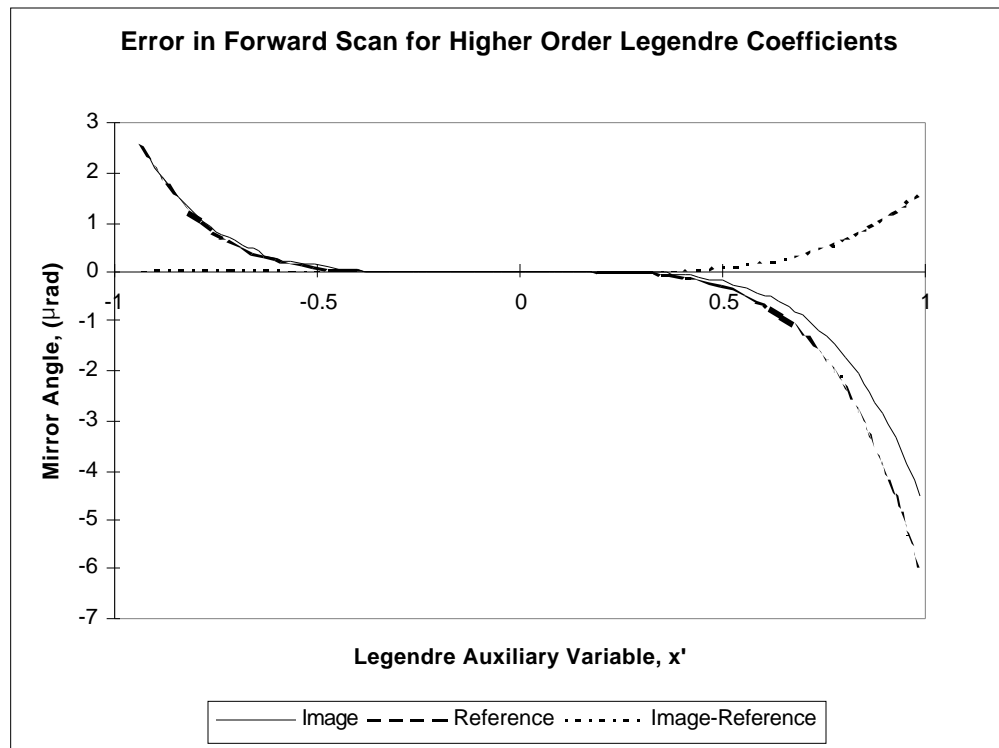


Figure 3.1.5- 27 Legendre Differences

The difference between the higher order Legendre terms (3rd, 4th, and 5th orders) of the actual and estimated forward mirror profiles.

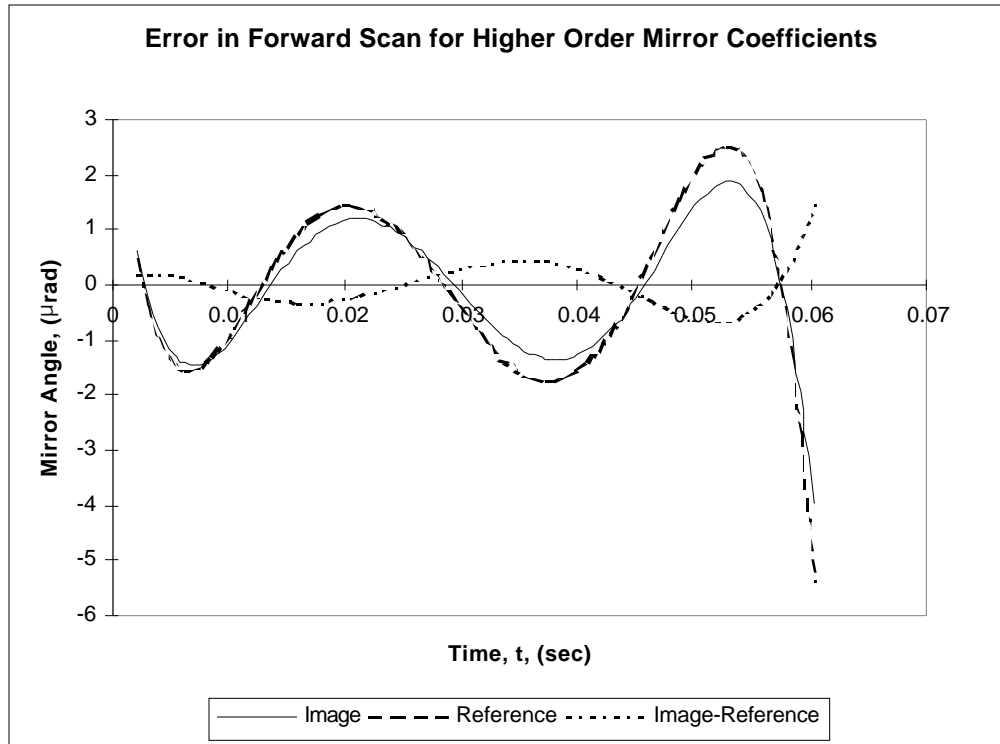


Figure 3.1.5- 28 Difference Between Actual Mirror Profiles

The difference between the higher order terms of the actual (reference) and estimated (image) forward mirror profiles.

Figures 3.1.5-27 and 3.1.5-28 show the errors in the higher order terms of the correction polynomial in Legendre terms and mirror terms respectively. In this test case, we expect higher order terms of the polynomial we find to be the same as the actual along scan mirror coefficients used in the base image. As we can see from the figures, the algorithm was able to back out the polynomial to better than 1 μrad over most of the scan and better than 2 μrad in all locations. The mirror profile repeatability specification for the Landsat 7 ETM+ is 1.75 μrad , so these measurements using 42.5 μrad IFOV TM data are of the same order as the random mirror variations.

3.1.5.5 Geometric Characterization Algorithms

3.1.5.5.1 Band to Band Registration

The Band to Band Registration Assessment segment of the Landsat 7 Image Assessment System (IAS) is used to check the registration quality between bands of the same image.

Matching Resolutions

Due to the difference in pixel sizes between bands, the higher resolution data will need to be reduced so that it matches that of the lower resolution. The band to band characterization will then be performed at the lower resolution. The higher resolution imagery will be reduced using the Gaussian Pyramid approach [Reference 25]. This approach works by low pass filtering the image data. The low pass filtering is accomplished by convolving the image with an appropriate kernel or set of weights. Applying this kernel will produce an image at a lower resolution than that of the original. The lower resolution image can then also be reduced in size. The process takes on the following form:

$$f_r(j,k) = \sum_{m=-2}^2 \sum_{n=-2}^2 w(m,n) f(2j+m, 2k+n) \quad j=1,\dots,M/2 \quad k=1,\dots,N/2$$

Where f is the original image data, f_r is the reduced sub-sampled image, and $w(m,n)$ are the low pass filter coefficients. Note that in the following case the imagery is reduced in size by one half in both the line and sample direction. The low pass filter coefficients can be represented as a set of separable one dimensional weights and are determined from the following representation [Reference 25]:

$$\begin{aligned} w(2) &= 1/4 - a/2 \\ w(1) &= 1/4 \\ w(0) &= a \\ w(-1) &= 1/4 \\ w(-2) &= 1/4 - a/2 \end{aligned}$$

where a typically takes on a value between 0.3 and 0.6. More information on this technique can be found in Reference 25.

In the case of Landsat 7 data this process will be used to reduce the 15 meter PAN band to the 30 meter multispectral bands and to the 60 meter thermal band. It will also be used to reduce the 30 meter multispectral bands to the 60 meter thermal band. In the case of Landsat 4&5 test data, the 30 meter multispectral band will be reduced to the 120 meter thermal band.

Correlation Routine

Normalized cross correlation will be used to produce a discrete correlation surface for an array of points between two bands. This correlation routine helps in removing any gray scale differences between two images. This will help to alleviate some of the problems with the different radiometric responses between the bands. The correlation routine has

the following formula when correlating between two image windowed subsets f and g , each having a length and width of M and N respectively:

$$R(x, y) = \frac{\sum_{j=-N/2}^{N/2} \sum_{i=-M/2}^{M/2} (f(j, i) - \bar{f})(g(x + j, y + i) - \bar{g})}{\left[\sum_{j=-N/2}^{N/2} \sum_{i=-M/2}^{M/2} (f(j, i) - \bar{f})^2 \right]^{1/2} \left[\sum_{j=-N/2}^{N/2} \sum_{i=-M/2}^{M/2} (g(x + j, y + i) - \bar{g})^2 \right]^{1/2}}$$

where

$$\bar{g} = \frac{1}{(M + 1)(N + 1)} \sum_{j=-N/2}^{N/2} \sum_{i=-M/2}^{M/2} g(x + j, y + i)$$

$$\bar{f} = \frac{1}{(M + 1)(N + 1)} \sum_{j=-N/2}^{N/2} \sum_{i=-M/2}^{M/2} f(j, i)$$

Once the correlation surface is generated the peak of that surface must be determined. This peak will represent the geometric shift between two windowed data sets and will be calculated to a subpixel location.

Peak Finding Method

A sub-pixel location for the peak is found by using a polynomial fit method. This method works by fitting a 2nd order polynomial around the peak of the discrete correlation surface. The polynomial will represent the surface associated with a 3x3 area around the peak. The discrete peak of the correlation surface is found first, then this peak and its corresponding eight neighbors are used for fitting the polynomial. A least squares fit can be used to calculate the polynomial coefficients once the 3x3 area and corresponding data points are found. From this polynomial the location of the peak can be solved analytically to a sub-pixel location.

The polynomial equation has the following form:

$$P(x, y) = a_0 + a_1x + a_2y + a_3xy + a_4x^2 + a_5y^2$$

The coefficients of $P(x, y)$ can be found by solving the matrix equation

$$[\mathbf{Y}] = [\mathbf{X}] [\mathbf{a}]$$

Where

$[\mathbf{Y}]$ is a 9x1 matrix corresponding to the eight correlation points found around, and including, the peak.

$[\mathbf{X}]$ is a 9x6 matrix with each row consisting of:

$$1 \quad x_i \quad y_i \quad x_i y_i \quad x_i^2 \quad y_i^2$$

where x_i and y_i are the x and y locations of the corresponding peak i in $[\mathbf{Y}]$

$[\mathbf{a}]$ are the polynomial coefficients

The solution of $[\mathbf{a}]$ is then

$$[\mathbf{a}] = ([\mathbf{X}]^T [\mathbf{X}])^{-1} [\mathbf{X}]^T [\mathbf{Y}]$$

Where T refers to the transpose of a matrix and -1 refers to the inverse of a matrix.

Once the coefficients are solved for the sub-pixel peak can be found. The maximum correlation peak can be found by taking the partial derivative of $P(x, y)$ with respect to x and y :

$$\frac{\partial}{\partial x} P(x, y) = a_1 + a_3y + 2a_4x$$

$$\frac{\partial}{\partial y} P(x, y) = a_2 + a_3x + 2a_5y$$

By setting the partial derivatives to zero and solving for x and y the sub-pixel peak location can be determined. This will lead to the following solution for the x and y offsets:

$$x_offset = \frac{2a_1a_5 - a_2a_3}{a_3^2 - 4a_4a_5}$$

$$y_offset = \frac{2a_2a_4 - a_1a_3}{a_3^2 - 4a_4a_5}$$

Outlier Detection

After computing a number of sub-pixel shifts between two bands, the data is checked for outliers. These outliers are then removed from the data set. There are two steps involved in detecting outliers. The first step involves looking at the measured offsets and comparing these with a threshold established by an error budget associated with the Landsat 7 satellite and the correlator. If any measurements are greater than this threshold it is removed as an outlier. If a large percentage of the measurements are thrown out at this point then the satellite is either behaving unexpectedly according to specifications or none of the imagery corresponding to where the measurement was taken is of good quality, a possibility for this would be a large amount of cloud cover. The second step involves comparing the measured value with the bias estimate of all the measurements left after applying the first threshold.

The first threshold is found from the following:

μrad = microradians

The known error associated with the satellite and correlator are:

Scan Mirror Repeatability 3.5 μrad

Field Angle 3.6 μrad

Jitter 1.45 μrad (spacecraft)

Jitter 0.65 μrad (ETM+)

Processing error 2.84 μrad

This leads to a total error for each band of

$$\sqrt{(3.5)^2 + (3.6)^2 + (1.6)^2 + (2.84)^2} = 6.0 \mu\text{rad}$$

The total error associated with two bands is then

$$\sqrt{(6.0)^2 + (6.0)^2} = 8.5 \mu\text{rad}$$

Converting the microradian to pixels gives approximately 0.2 pixels. (*The correlator error budget is 0.25 pixel*)

The total error budget is then

$$\sqrt{(0.2)^2 + (0.25)^2} = 0.32 \text{ pixels}$$

The maximum band alignment error 0.3 pixel

The total measurement error is then

$$\sqrt{(0.3)^2 + (0.32)^2} = 0.44 \text{ pixels}$$

The threshold is then chosen as three times the total measurement error budget
 $3 * 0.44 = 1.32$ pixels.

This value, 1.32 pixels, represents the first threshold that is to be applied to the data. All measurements above this threshold are considered to be outliers and are removed.

The second threshold is found by calculating the average or bias and standard deviation for the data set left after applying the first threshold outlier detection. The second threshold is any point that is three standard deviations above the measured bias or average. The data set left after applying the second threshold outlier detection represents the valid measurements taken.

Statistical Measure

Once the outliers have been detected and removed the resulting data is used to calculate a bias or average band offset between two bands. The standard deviation of the data set is also calculated.

$$\text{avg} = \frac{1}{N} \sum_{i=0}^N m_i$$

$$(\text{std})^2 = \frac{1}{N-1} \sum_{i=0}^N (m_i - \text{avg})^2$$

where

- avg = average
- std = standard deviation
- m_i = measured offset
- N = Number of valid measurements

Test Simulation

A test simulation was generated to determine the accuracy of the correlation and peak finding routines by using an image of path 28 row 30 and resampling it with various geometric offsets. A 16x16 truncated sinc $[\sin(x)/(x)]$ resampling function was used to produce geometric shifts. Correlation windows of 512x512 were chosen. Sixteen windows were chosen at random for measurement. The various images of geometric offsets were then correlated with the original. This gave an indication of the accuracy of the correlator itself. The results are listed below:

Offset	Average Offset	Standard Deviation
0.0	0.0	0.0
0.1	0.089817	0.003823
0.2	0.152810	0.001479
0.3	0.236563	0.002199
0.4	0.344935	0.002791
0.5	0.485531	0.006224
0.6	0.632771	0.008459
0.7	0.745469	0.008163
0.8	0.831895	0.006718
0.9	0.903604	0.004832

This indicates that the correlator works to within one-tenth of a pixel. This represents an ideal situation in that the image is being correlated to itself. Through work with different band combinations an accuracy of 0.25 pixels can be expected across bands from the correlator. A more thorough explanation of errors associated with correlation can be found in Reference 21. The Image to Image characterization algorithm also performed a similar test simulation; this can also be used as a reference on the accuracy of the correlator.

Measured Landsat 4 & 5 Data

Correlation will be done in such a manner that all bands can be either directly or indirectly referenced to each other. The test site that is chosen to perform band to band registration should have features that are present throughout all bands. It was found that desert scenes with little vegetation presented the best scenario. A scene corresponding to path 41 row 36 was chosen as a test site. Correlation windows were chosen at uniform increments throughout the image. When correlating the multispectral bands an offset of 1000 lines was chosen from the top and bottom and 1000 samples from the right and left sides of the image. Windows were then chosen at 500 lines and 500 sample increments throughout the image. The window size chosen was 256x256. When correlating two bands with one being the thermal band offsets of 250 lines, 250 samples, increments of 125 lines, 125 samples, and window sizes of 128x128 were chosen. The following values were then calculated:

X Offsets

(Offsets are in terms of multispectral pixels)

Reference	Search	average	standard deviation
1	2	0.003244	0.010120
1	3	0.001516	0.021785
1	4	-0.025383	0.113919
1	5	-0.261743	0.061539
1	7	-0.252938	0.053082
2	3	-0.000870	0.012164

IAS Geometric ATBD Version 3

2	4	-0.014538	0.134436
2	5	-0.266884	0.055054
2	7	-0.249701	0.047483
3	4	-0.035892	0.079654
3	5	-0.267662	0.050735
3	7	-0.250002	0.048614
4	5	-0.227007	0.083736
4	7	-0.194449	0.145899
5	7	0.012561	0.020213

(Offsets in terms of thermal pixels)

Reference	Search	average	standard deviation
1	6	-0.786044	0.177695
2	6	-0.788873	0.164740
3	6	-0.808790	0.159983
4	6	-0.758903	0.194022
5	6	-0.757974	0.108728
6	7	0.754215	0.165351

Y OFFSETS

(Offsets in terms of multispectral pixels)

Reference	Search	average	standard deviation
1	2	0.003527	0.009219
1	3	0.014177	0.019110
1	4	0.024184	0.060681
1	5	0.366080	0.062386
1	7	0.382187	0.051700
2	3	0.010344	0.011238
2	4	0.014033	0.075062
2	5	0.362300	0.047765
2	7	0.374961	0.044400
3	4	0.006703	0.067899
3	5	0.350089	0.034363
3	7	0.365271	0.036863
4	5	0.319364	0.073798
4	7	0.328139	0.097649
5	7	0.007921	0.014011

(Offset in terms of thermal pixels)

Reference	Search	average	standard deviation
1	6	0.737981	0.177695
2	6	0.726864	0.197395
3	6	0.718318	0.169007
4	6	0.747355	0.191474
5	6	0.633007	0.095764

6	7	-0.611179	0.153688
---	---	-----------	----------

It should be noted that the measured between band alignment does not meet the specifications for the Landsat 7 system. This data will be used by the Focal Plane Band to Band Calibration algorithm to relate these parameters back to the focal plane to adjust the focal plane alignment, if deemed necessary.

3.1.5.5.2 Image to Image Registration

The Image to Image Assessment segment of the Landsat 7 Image Assessment System (IAS) is used to check the registration quality between two images. The two images are assumed to be from the same band and same (path, row) taken at different times, processed to the same level-- either precision or terrain corrected products.

Accuracy Requirements

According to the Landsat 7 IAS Requirements Document, “The IAS shall provide the capability to perform image to image registration to an accuracy of 0.4 multispectral sensor GSD, 0.9p, in the along-track and cross-track directions providing all inputs are within specification.” The understanding is that this requirement refers to two temporally spaced images processed to the same level using the same ground control. Furthermore, since the accuracy requirements for systematically processed images are on the order of ~250m (400m, 0.9p), this requirement is assumed applicable only to precision and/or terrain corrected images.

As for requirements placed on the image to image correlation technique, “The IAS shall be capable of digitally correlating common features in the...same bands of separate images to an accuracy of 0.1pixel, 0.9p.” This is equivalent to requiring that the correlation technique be capable of backing out a known offset to within 0.1 pixel, 0.9p (~0.06 pixels at one sigma).

Procedure

The IAS Image to Image Assessment segment provides two options for selecting image-to-image points. Correlation points can be generated either by creating a regular grid of hundreds of points, or by manually selecting fifty to a hundred well distributed, “human-recognizable” ground control features. Given that images only need to be processed to the full precision and terrain corrected levels for a small number of test sites, the latter is the more likely operational implementation. Using the grid of points, however, may be useful in geometric analysis.

The normalized cross correlation technique is defined as

$$R(x, y) = \frac{\sum_{j=-N/2}^{N/2} \sum_{i=-M/2}^{M/2} f(j, i) - \bar{f} \quad g(x + j, y + i) - \bar{g}}{\left[\sum_{j=-N/2}^{N/2} \sum_{i=-M/2}^{M/2} \left[f(j, i) - \bar{f} \right]^2 \right]^{1/2} \left[\sum_{j=-N/2}^{N/2} \sum_{i=-M/2}^{M/2} \left[g(x + j, y + i) - \bar{g} \right]^2 \right]^{1/2}}$$

where

$$\bar{f} = \frac{1}{(M + 1)(N + 1)} \sum_{j=-N/2}^{N/2} \sum_{i=-M/2}^{M/2} f(j, i)$$

$$\bar{g} = \frac{1}{(M + 1)(N + 1)} \sum_{j=-N/2}^{N/2} \sum_{i=-M/2}^{M/2} g(x + j, y + i)$$

The resulting correlation surface is searched for a peak. In order to determine the sub-pixel location of the true correlation maximum, a surface is fit to the peak and its neighbors. The sub-pixel location of the peak value for the best-fit function is determined analytically and stored. The correlation functions included options for fitting parabolic and Gaussian surfaces using a 5 x 5 neighborhood of pixels around the peak. The correlation function was modified to use a 3 x 3 neighborhood as testing showed these results to be more accurate and reliable. This is discussed in greater detail below.

The verification routine uses the points and offsets determined by the correlation function to calculate statistics. For each correlation point, it reports the line, sample and total errors in the search image relative to the reference. It also calculates the mean, standard deviation, median, range, and RMSE for those errors and determines the number (and percentage) of points not meeting user specified accuracy requirements. All of these values will be stored for trending.

In order to assist geometric assessment, the statistics compiled by verification routine can be plotted. Useful plots include, but are not limited to: surface plots of line or sample error versus line and sample, vector plots showing line and sample error distributed on the image plane, or color coded residuals overlaid on an image.

Some outlier detection and rejection is performed within the correlation function. The routine flags and rejects correlation points if they are: too near the edge of the data window, similar in magnitude to subsidiary peaks, or below a user-specified strength threshold. There is also a flag which rejects points if the diagonal distance between the reference and search sub-images is greater than a user-specified value.

Whether further outlier rejection will be used on the final residuals is yet to be determined since initially, analysis will primarily be concerned with determining whether outliers indicate a problem in the data or a problem in the system. An exception flag should be raised if the line and sample error mean and standard deviations are in excess of the requirement value specified above.

Inputs

Image to image assessment requires a reference image which has been processed to the precision or terrain corrected level and a search image processed to the same level with the same ground control, (and the same DEM in the case of terrain corrected images). It also requires a set of pre-selected image features or grid of whose locations are refined by the correlation function.

Outputs

The correlation function generates a file containing the points and offsets which is used by the verify routine to compile statistics. The verify routine generates a report file containing information about all the points used for correlation including line, sample and total errors. It also lists overall statistics including mean, standard deviation, median and RMSE for line, sample and total errors and the number of points not meeting user specified error thresholds. The information in the report is used for trending .

Algorithm Testing

To test the accuracy and precision of the correlation routine, a base image using band 1 of a Landsat 5 test scene (path 28, row 30) of northwestern Iowa was generated. Artificial shifts in the sample direction were then incorporated into the image in 0.1 pixel increments using cubic convolution resampling accurate to 1/32 of a pixel. Image to image correlation was then performed with artificial offsets ranging from 0.0 to 1.0 pixels using a set of 51 manually picked points. The resulting plots of the mean and standard deviation

values are shown in Figures 3.1.5-29 and 3.1.5-30. At an offset of 0.5 pixels, the correlation routine using a 5 x 5 neighborhood about the correlation peak became unreliable giving a bimodal error distribution surrounding the true offset. A possible explanation for this peculiar behavior is that the objects used in the correlation are typically linear features approximately one pixel wide (e.g., roads) surrounded by relatively uniform backgrounds (e.g., fields). In these cases we would not expect a parabola to be a good fit beyond one pixel to either side of the peak.

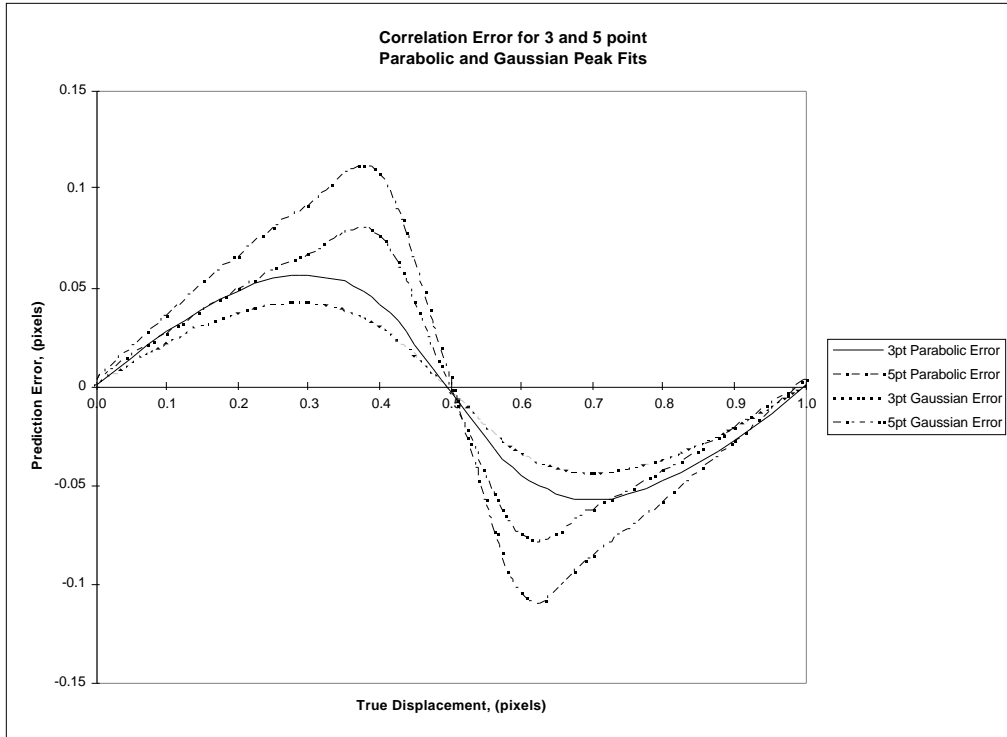


Figure 3.1.5-29 Correlation Errors

Correlation errors using 3x3 and 5x5 pixel neighborhoods, and parabolic and Gaussian peak surface fits for an artificially induced sample offset.

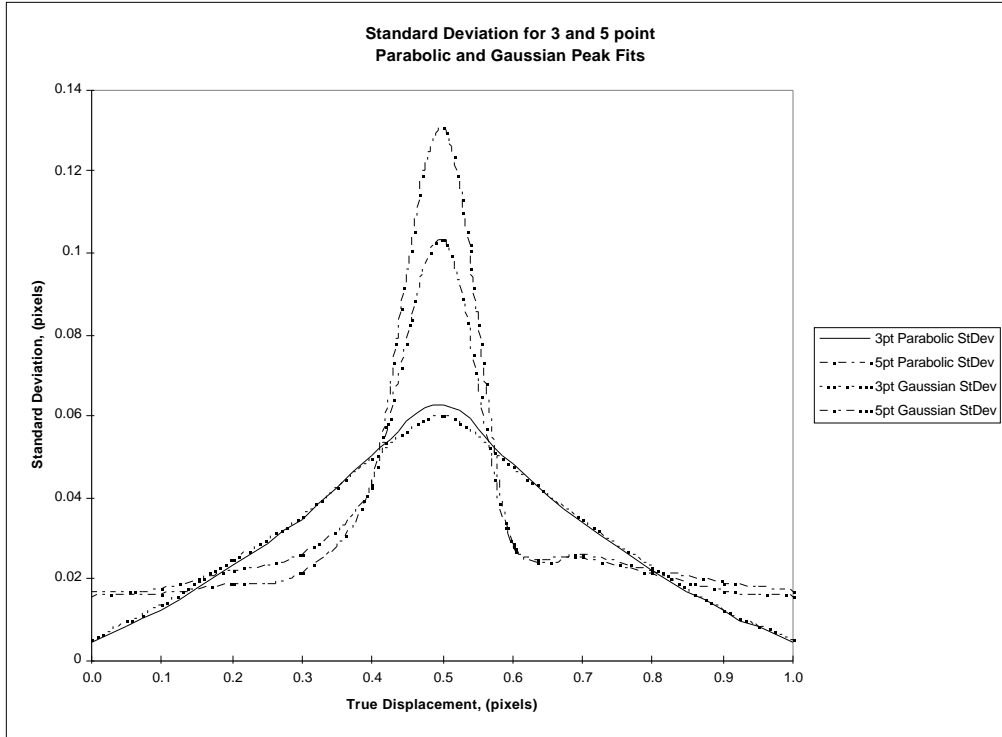


Figure 3.1.5- 30 Correlation Standard Deviations

Standard deviation of the errors 3x3 and 5x5 pixel neighborhoods, and parabolic and Gaussian peak surface fits for an artificially induced sample offset.

As an example, consider the case of a bright, one-pixel-wide road cutting through a uniformly dark field. If this road were displaced to the right by 0.5 pixels, the resultant image would have the road represented by two pixels of medium brightness surrounded again by the dark field. This situation is shown schematically in Figure 3.1.5-31 as a one dimensional cross section. Figure 3.1.5-32 shows the cross correlation (non-normalized) of these two data sets and the resulting parabolas which occur when trying to fit the data with five points using both the left and right maxima as the center point. The resulting peaks of the parabolas in Fig. 3.1.5-32 occur at 7.27 and 7.73 rather than at 7.5 where the true peak should occur. So while the average value is correct, the standard deviation for this case is unacceptable as are shown in Figs. 3.1.5-29 and 3.1.5-30.

By inspection of Fig. 3.1.5-31, it is evident that fitting a parabola using three points rather than five, the peak will occur at 7.5 regardless of which maxima is taken as the center point. Figure 3.1.5-29 shows the three point method to be more accurate than the five point method. For these reasons, the correlation routine was modified to use a 3 x 3 neighborhood around the peak rather than a 5 x 5 neighborhood.

By looking at the shape of the cross correlation data in Fig. 3.1.5-32, one would expect that a Gaussian curve might be a better fit than a parabola, thus giving reduced errors.

The results of doing so are also shown in Fig. 3.1.5-29 and indeed they lead to a ~20% reduction in error at the peak locations. The sinusoidal shape of the error curve shown in Fig. 3.1.5-29 is consistent with the theoretical errors determined by Dvornychenko (Reference 21).

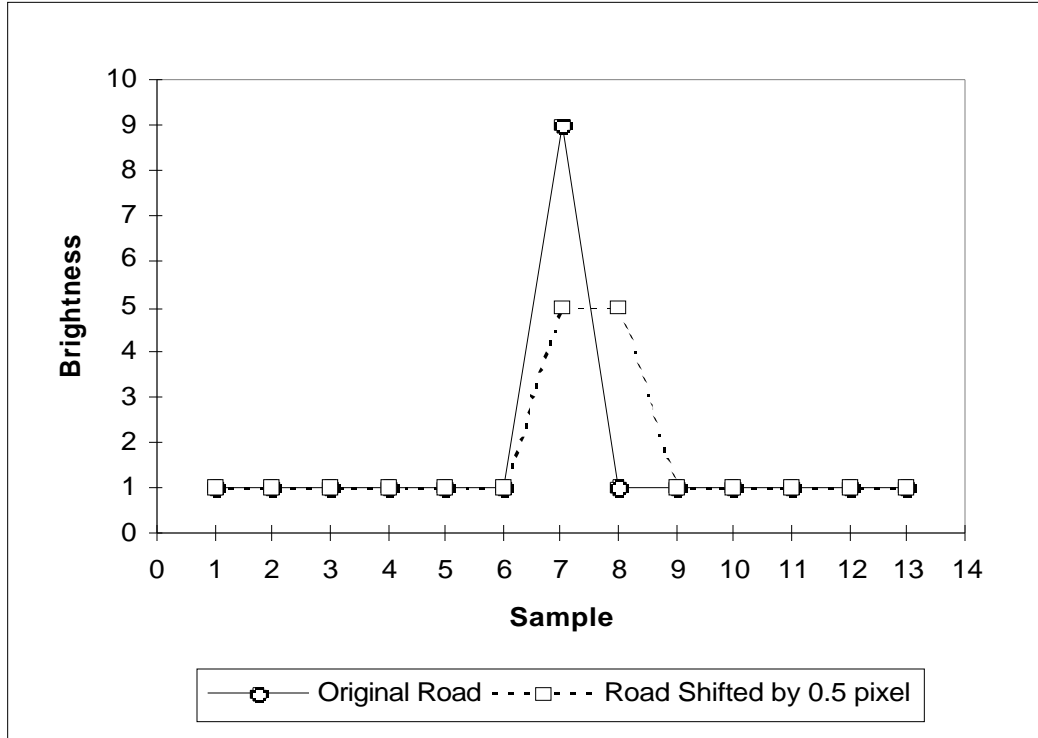


Figure 3.1.5- 31 Road Cross Section Example

Schematic cross-section of a bright road running through a dark field and how it would appear when shifted 0.5 pixel to the right

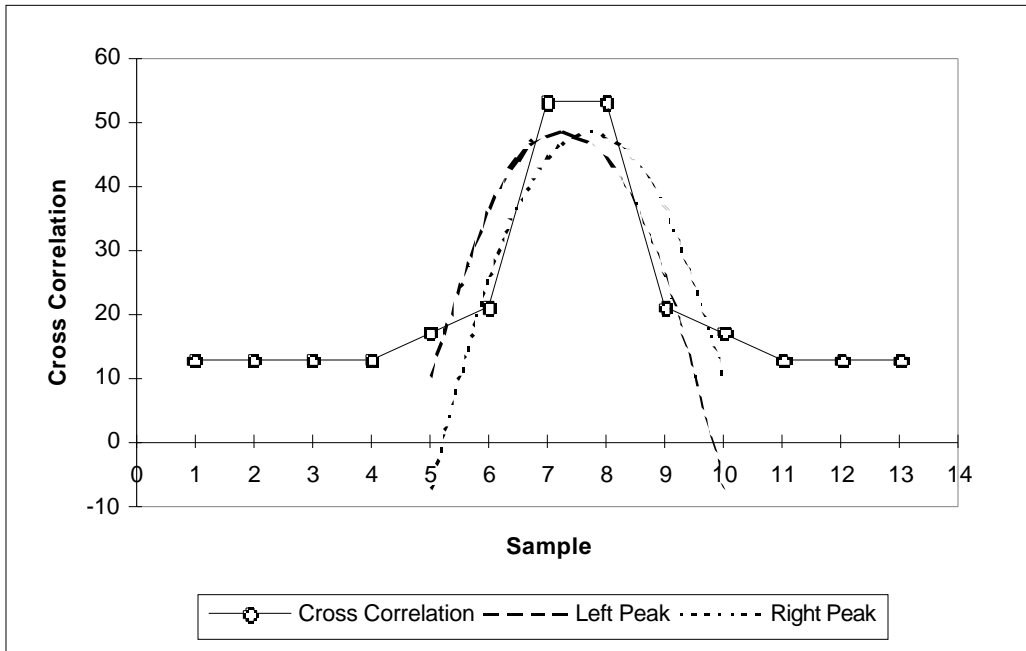


Figure 3.1.5- 32 Correlation Errors

Cross correlation of original and shifted data and fitting parabolas to the data using five point centered on either the left or right maxima.

Further Investigations

While it appears as though the accuracy of the modified correlation routine is sufficient to meet the requirements, it must be noted that these tests were run under ideal conditions, i.e., the same image data (although shifted and aliased by using a cubic convolution resampler accurate to 1/32 pixel). Under real circumstances where there may be significant changes in the scenes from image to image, the standard deviations can be expected to increase.

Normalized cross-correlation is designed to take some image differences into account and has been used successfully in projects involving Landsat MSS and TM imagery. However, it has not been used to measure the registration accuracy under such stringent requirements as in the IAS.

Further investigations may include widening the reference chips to greater than 64x64. This should help by having more data available and thus smoothing out the correlation surface. Also, other techniques such as edge or phase correlation may be useful when correlating images with differing spectral data (e.g., data from different seasons).

3.1.5.5.3 Geodetic Accuracy

This section describes the algorithm, input data, output data, and proposed usage of the output data applied in the Geodetic Characterization Module for the Landsat 7 Image Assessment System.

The Algorithm

In the system data flow chart, this algorithm immediately follows the precision correction solution module. Thus, this description should be read in the context related to the description of precision correction solution module. The GCP data quality requirement applies to the input data of precision correction solution module, and is based on the assumption that GCP marking and correlation are done to 0.1 pixel accuracy.

Purpose:

The purpose of this algorithm is to verify the absolute accuracy of the systematic and precision products by analyzing the Ground Control Point measurement residuals before and after the precision correction solution.

Process:

This algorithm applies standard statistical error analysis on the residual file of the precision correction solution. The residual file contains residuals for GCPs before and after precision correction. The algorithm takes one input file (the residual file), and generates two output files (the record file and the outlier data file). The following steps are performed:

1. Calculate and write to the record file the following 3 values:
 - the total number of GCPs in the residual;
 - the mean latitude of all GCPs;
 - the mean longitude of all GCPs;

2. Calculate and write to the record file the following 5 values for the pre-fit residuals:
 - Mean value of the cross-track residuals;
 - Mean value of the along-track residuals;
 - RMSE about the mean value for cross-track residuals;
 - RMSE about the mean value for along-track residuals;
 - Correlation coefficient between along- and cross-track residuals;

3. Calculate and write to the record file the following 5 values for the post-fit residuals:
 - Mean value of the cross-track residuals;
 - Mean value of the along-track residuals;
 - Standard deviation for cross-track residuals;

- Standard deviation for along-track residuals;
 - Correlation coefficient between along- and cross-track residuals;
4. Compare the post-fit residuals with their Standard Deviations, mark those GCPs with > 2 sigma residual as outliers;
 5. Write to the outlier data file the information for each outlier GCP;

The Input Data

This module requires only one input data file, which is the output residual file by the Precision Correction Module. This file contains the residual information from Iteration 0, which is the pre-fit residual, through the Final Iteration, which is the post-fit residual.

GCP Data Accuracy Requirement

Following properties of the GCP measurements are required to produce a meaningful precision correction solution and geodetic characterization result:

- GCP coordinate should be in a system consistent with the that of satellite ephemeris. WGS84 is preferred, NAD83 in North America is acceptable.
- The accuracy of the GCP coordinate should be on the level of 3 meters in horizontal and 20 meters in elevation to guarantee 0.1 pixel accuracy;
- Number of GCPs: A minimum number of 15 valid GCPs is required for reliable characterization ($6/\text{number of precision correction parameters} + 9/\text{reasonable number degree of freedom}$). To allow certain portion of outlier editing, 25 to 50 input GCPs are suggested.

Usage of the Output Data

- The outlier information file will be used to remove the GCP from both the GCP data file and the EPH data file for precision correction solution (see algorithm description for precision correction solution module). A new round of precision correction solution and geodetic characterization will be performed after the editing;
- The record file will be used as a measure of the absolute accuracy of the systematic product (pre-fit residual statistics) and precision product (post-fit residual statistics).
- Trending analysis can be done on the parameters provided in the record file.
- Error characterization for check point data (GCPs not used for the precision correction solution) will be done in a different round after the systematic model is updated with the precision correction parameters.

3.1.5.5.4 Geometric Accuracy

For the purposes of determining geometric accuracy, three tests are to be performed:

1. Visual inspection. The output image will be inspected visually for any geometric distortions. These distortions could include scan misalignment, artifacts produced by the resampling process such as ringing, or detector (line to line) discontinuity.
2. Plot of the residuals of the ground control points and their corresponding locations in the terrain corrected image. This can be either a vector plot indicating the lines/sample offsets or an image with the residuals color coded according to their magnitude superimposed on a paper product of the image.
3. A polynomial fit involving the ground control points and their corresponding locations in the terrain corrected output product.

Polynomial Fit

A polynomial fit will be used to estimate the amount of scaling in x and y, rotation, offset in x and y, and non-orthogonality angle associated with a terrain corrected image. The polynomial will take the form:

$$\begin{aligned}x_o &= a + b x_i + c y_i \\y_o &= d + e x_i + f y_i\end{aligned}$$

Where

x_o = output projection x coordinate (measured)
 y_o = output projection y coordinate (measured)
 x_i = input projection x coordinate (truth)
 y_i = input projection y coordinate (truth)
a,b,c,d,e,f transformation coefficients

The polynomial coefficients will be determined from a least squares fit of the x and y coordinates of features located in the terrain corrected product and their corresponding x and y coordinates for the same feature in the ground control source. The transformations that “corrects” x_o, y_o to x_i, y_i is given by:

$$x_i = S_x(x - x_o) \cos(\theta) - S_y(y - y_o) \sin(\theta)$$

$$y_i = S_x(x - x_o) \sin(\theta) + S_y(y - y_o) \cos(\theta)$$

The error or distortions can then be determined from the polynomial transformation coefficients by the following:

$$S_x = \frac{\sqrt{e^2 + f^2}}{bf - ce}$$

$$S_y = \frac{\sqrt{b^2 + c^2}}{bf - ce}$$

$$\text{theta} = \tan^{-1}\left(\frac{-e}{f}\right)$$

$$\text{alpha} = \tan^{-1}\left(\frac{-be - cf}{bf - ce}\right)$$

S_x = scale error in x direction

S_y = scale error in y direction

alpha = non-orthogonality angle

theta = rotation angle

a = offset in x direction

d = offset in y direction

a,b,c,d,e,f transformation coefficients

The scale error can be converted to pixels by the following:

$$(S_x - 1) * (\text{image pixel size in } x)$$

$$(S_y - 1) * (\text{image pixel size in } y)$$

Theta can be converted to pixels by the following:

$$\text{theta} * (\text{size of image diagonal})$$

$$\text{size of image diagonal} = \text{SQRT}((\text{image pixel size } x)^2 + (\text{image pixel size } y)^2)$$

Alpha can be converted to pixels by the following:

$$\text{alpha} * (\text{maximum pixel size})$$

$$\text{maximum pixel size} = \text{MAX}(\text{image pixel size in } x, \text{image pixel size in } y)$$

All of these values should be very close to zero except S_x and S_y which should be close to one. If any of these are not zero, or S_x and S_y are not close to one, then they represent the amount of geometric distortions not corrected for by the system.

The residuals left after applying the polynomial coefficients to the terrain corrected x and y coordinates will represent any higher order distortions. These values should also be very small.

Note: This algorithm requires a terrain corrected image produced from the IAS system along with at least fifty well distributed ground control points. The PAN band would give the highest precision when calculating errors, however any band can be used in the process. All points, from both the image and the control source, need to be in the same projection with the same datum and pixel size. The control points and the points taken from the IAS terrain corrected product should be to a sub-pixel accuracy. The absolute accuracy of the points picked will depend on the method chosen for point matching.

3.1.6 Variance or Uncertainty Estimates

The following sections contain error budget analyses for the key Landsat 7 ETM+ geometric accuracy requirements. These analyses were used to predict the Level 1Gs geodetic accuracy performance and to develop algorithm and support data accuracy requirements for the geometric calibration and characterization activities.

3.1.6.1 Level 1 Processing Accuracy

The fundamental Level 1 Processing accuracy requirement is to be able to produce systematically corrected (1Gs) products which are accurate to within 250 meters per coordinate (one sigma) at nadir. This is stated in the IAS Element Specification as requirement number 3.2.3.4. An error budget for 1Gs geodetic accuracy performance can be built up using the expected accuracy of the data components which are part of the Landsat 7 ETM+ geometric model. These components include spacecraft ephemeris and attitude knowledge, spacecraft clock errors, knowledge and stability of the alignment of the ETM+ instrument to the Landsat 7 spacecraft, and knowledge and stability of the internal geometry of the ETM+ instrument. Accuracy bounds for most of these data elements are specified in the Landsat 7 System Specification. Allocations for ground processing and test point mensuration are included in the total geodetic accuracy error budget.

Errors in each of the geometric model data components were assumed to be independent zero mean random variables in the geodetic accuracy analysis. The relevant accuracy values were extracted from the Landsat 7 System Specification, converted to 1 sigma values if necessary, and then mapped to position errors in meters on the ground. For along track and across track angular error values this mapping was done by multiplying the angular error (in radians) by the nominal Landsat 7 height above ground of 705 kilometers. The spacecraft clock error was converted to ground meters by multiplying the time error by a conservative estimate of the nominal Landsat 7 orbital velocity of 7.5 kilometers per second.

Two cases are considered in the geodetic accuracy error budget: 1) the expected accuracy at-launch based on the pre-launch knowledge of the alignment between the Landsat 7 navigation base reference coordinate system and the ETM+ optical axis, and 2) the expected accuracy in routine operations after the IAS has calibrated the instrument to spacecraft alignment. The 250 meter accuracy specification applies to both the along track and across track directions, but the presence of the spacecraft clock error makes the along track direction the critical case. The at-launch along track accuracy analysis is presented in Table 3.1.6.1-1. The columns in the table contain the following information:

- Column 1: identifies the data element error source,
- Column 2: shows the error contribution mapped to ground meters at nadir (1 sigma),
- Column 3: shows the error contribution in the units in which it is specified (1 sigma),
- Column 4: identifies the specification units,
- Column 5: shows the original source of the specified value since some are root-sum-square (RSS) combinations of lower level components,
- Column 6: shows where the error source was allocated at the system level (e.g., to the spacecraft, instrument, or ground system).

IAS Geometric ATBD Version 3

Source	Meters 1	Spec 1	Units	Comments	Segment
Vehicle Attitude	154	45.0	arcsec	45.0 arcsec (1) (R,P,Y)	Satellite
Scan Mirror Repeatability	3	0.72	arcsec	1.75 microradians * 2 (1)	ETM+
Field Angle	3	0.78	arcsec	RSS of:	
				0.18 arcsec (1) calibration	IAS
				0.76 arcsec (1) stability (0.2 pan)	ETM+
Alignment Knowledge (R,P,Y) - stability	58	17.0	arcsec	RSS of:	
				8.0 arcsec (1) ETM+ to NBR	Satellite
				15.0 arcsec (1) LOS to ETM+	ETM+
Alignment Uncertainty (R,P,Y) - calibration	846	247.4	arcsec	RSS of:	
				720.0 arcsec (3) pre-launch	Satellite
				60.0 arcsec (1) pre-launch	ETM+
Ephemeris (I,C,R)	133	133.33	meter	400 meter (3) from sum of:	
				375 m (3) predict	FDI
				20 m (3) interpolation	Satellite
Jitter (R,P,Y)	2	0.44	arcsec	RSS of:	
				0.30 arcsec (1) low frequency	Satellite
				0.30 arcsec (1) high frequency	Satellite
				0.134 arcsec (1) high frequency	ETM+
Timing (along track)	38	5	msec	15 msec (3) random error	Satellite
Mensuration	15	15	meter	0.5 pixels (1)	User
Processing Error	2	2	meter	Model budget	IAS
RSS Estimate	873				
RSS Margin	-				
Specification	250				

Table 3.6.1.1- 1 At-Launch 1Gs Geodetic Error Budget

As Table 3.6.1.1-1 demonstrates the 250 meter geodetic accuracy requirement is not expected to be met based on the at-launch knowledge of the ETM+ instrument to Landsat 7 spacecraft alignment.

The Landsat 7 System Specification requires the IAS to estimate the on-orbit alignment to an accuracy of 24 arc seconds (as compared to the pre-launch accuracy of about 248 arc seconds). This improvement in alignment knowledge accuracy allows the geodetic accuracy budget to meet the 250 meter specification with significant margin. Table

3.6.1.1-2 updates the along track accuracy analysis with the post-calibration alignment knowledge accuracy. The table column definitions are the same as for Table 3.6.1.1-1.

Source	Meters 1	Spec 1	Units	Comments	Segment
Vehicle Attitude	154	45.0	arcsec	45.0 arcsec (1) (R,P,Y)	Satellite
Scan Mirror Repeatability	3	0.72	arcsec	1.75 microradians * 2 (1)	ETM+
Field Angle	3	0.78	arcsec	RSS of:	
				0.18 arcsec (1) calibration	IAS
				0.76 arcsec (1) stability (0.2 pan)	ETM+
Alignment Knowledge (R,P,Y) - stability	58	17.0	arcsec	RSS of:	
				8.0 arcsec (1) ETM+ to NBR	Satellite
				15.0 arcsec (1) LOS to ETM+	ETM+
Alignment Uncertainty (R,P,Y) - calibration	82	24.0	arcsec	24.0 arcsec (1) (R,P,Y)	IAS
Ephemeris (I,C,R)	133	133.33	meter	400 meter (3) from sum of:	
				375 m (3) predict	FDF
				20 m (3) interpolation	Satellite
Jitter (R,P,Y)	2	0.44	arcsec	RSS of:	
				0.30 arcsec (1) low frequency	Satellite
				0.30 arcsec (1) high frequency	Satellite
				0.134 arcsec (1) high frequency	ETM+
Timing (along track)	38	5	msec	15 msec (3) random error	Satellite
Mensuration	15	15	meter	0.5 pixels (1)	User
Processing Error	2	2	meter	Model budget	IAS
RSS Estimate	231				
RSS Margin	97				
Specification	250				

Table 3.6.1.1- 2 1Gs Geodetic Error Budget After Alignment Calibration

3.1.6.2 Geometric Calibration Accuracy

The development of the three IAS geometric calibration algorithms included estimation error analyses to ensure that the relevant geometric parameters could be estimated with sufficient accuracy to justify updating the pre-launch knowledge in post-launch releases of the Calibration Parameter File. The results of these analyses are presented in the following sections.

3.1.6.2.1 Sensor Alignment Calibration Accuracy

As noted above, the IAS is required to calibrate the ETM+ instrument to Landsat 7 spacecraft alignment knowledge to an accuracy of 24 arc seconds in order to achieve a 1Gs product geodetic accuracy of 250 meters. This is stated in the IAS Element Specification as requirement number 3.2.3.12. The IAS sensor alignment algorithm uses the results of a series of precision correction solutions to extract the systematic alignment bias from the random scene-to-scene attitude error, as described above. The goal of the sensor alignment error analysis was to determine the number of calibration scenes required to achieve the 24 arc second alignment knowledge accuracy as a function of the accuracy of the supporting definitive ephemeris and ground control data.

The precision correction solution model was used to perform an error propagation analysis to predict the accuracy of the pointing error (alignment plus attitude) estimates produced by a single precision correction solution. This analysis was based on the assumption that all inputs were accurate to their pre-launch specification values, and that 14 well distributed ground control points were successfully measured with an accuracy of 15 meters (ground position error plus image mensuration error) for each point. The input accuracy assumptions and the resulting pointing error accuracy estimates are summarized in Table 3.1.6.2.1-1.

Input	1 error	Rationale
Along Track Position	63 meters	RSS of 50 meter estimate of FDF definitive ephemeris accuracy and 38 meter spacecraft clock error
Across Track Position	50 meters	Estimate of FDF definitive ephemeris accuracy
Radial Position	50 meters	Estimate of FDF definitive ephemeris accuracy
Roll	252 arcsec	RSS of 247 arcsec pre-launch alignment knowledge error, 17 arcsec alignment stability error, and 45 arcsec attitude knowledge error
Pitch	252 arcsec	RSS of 247 arcsec pre-launch alignment knowledge error, 17 arcsec alignment stability error, and 45 arcsec attitude knowledge error
Yaw	252 arcsec	RSS of 247 arcsec pre-launch alignment knowledge error, 17 arcsec alignment stability error, and 45 arcsec attitude knowledge error
Ground Control	15 meters	RSS of 12 meter position error (1:50,000-scale map source) and 7.5 meter (0.5 panchromatic pixel) image mensuration error
Roll Estimate	13.1 arcsec	<i>A posteriori</i> error estimate
Pitch Estimate	16.6 arcsec	<i>A posteriori</i> error estimate
Yaw Estimate	16.7 arcsec	<i>A posteriori</i> error estimate

Table 3.1.6.2.1- 1 Pointing Error Estimate Accuracy Analysis - Inputs and Results

The roll estimate accuracy is somewhat better than the pitch and yaw estimates primarily because the across track roll must be separated from the across track position error while the pitch and yaw both must be separated from the along track position error which is less accurate due to the spacecraft clock error.

The roll, pitch, and yaw pointing error estimates generated by the precision correction process represent the combined effect of static alignment error, attitude error, and dynamic alignment error. This can be expressed as:

$$\text{pointing error observation} = \text{attitude} + \text{static alignment} + \text{dynamic alignment}$$

It is the static alignment error which we seek to calibrate. Rearranging the previous equation yields:

$$\text{static alignment} = \text{pointing error observation} - \text{attitude} - \text{dynamic alignment}$$

The attitude and dynamic alignment errors are assumed to be zero mean, so the best estimate of the static alignment error is just the observed pointing error estimated by the precision correction solution. The variance of the static alignment estimate is the sum of the variance of the three terms on the right hand side:

$$\sigma_{\text{alignment}}^2 = \sigma_{\text{observation}}^2 + (45)^2 + (17)^2$$

where: 45 arc seconds = expected attitude standard deviation

17 arc seconds = expected dynamic alignment standard deviation

Table 3.1.6.2.1-2 summarizes the resulting standard deviations for the three alignment error components.

Component	Standard Deviation (Single Estimate)
Roll	49.9 arc seconds
Pitch	50.9 arc seconds
Yaw	50.9 arc seconds

Table 3.1.6.2.1- 2 Alignment Estimate Accuracy

As multiple test scene results become available the observed pointing errors will be combined using a Kalman filter as described above. To a first approximation, the effect on the resulting alignment estimate will be to improve the accuracy as the square root of the number of test scenes processed. The resulting improvement in alignment knowledge accuracy as a function of the number of calibration scenes processed is shown in Figure 3.1.6.2.1-1.

The figure suggests that the 24 arc second alignment accuracy requirement can be met after five calibration scenes have been processed. The accuracy estimates based on this relatively simple model of the alignment estimation process have been confirmed by processing simulated data (with known alignment biases introduced) through the precision correction and sensor alignment prototype software and analyzing the results. These tests have shown that the alignment knowledge can be expected to reach the 24 arc second accuracy threshold after five or six calibration test scenes have been processed.

3.1.6.2.2 Scan Mirror Calibration Accuracy

Although there is no formally specified accuracy requirement for the scan mirror calibration process, an accuracy threshold of 1.75 microradians (in mirror space) was selected as the goal for mirror profile estimation accuracy. This value corresponds to the scan mirror repeatability specification called out in the Landsat 7 System Specification in section 3.7.8.1.17.4. Determining the scan mirror profile to this accuracy will keep the systematic mirror profile knowledge within the random variation of the scan mirror motion.

Error propagation analysis (based on a set of relatively conservative assumptions regarding the accuracy of the input data) was used to determine the number of ETM+ scans and the number of test points per scan which must be correlated with a DOQ reference image to achieve a 1.75 microradian estimation accuracy. The input data and image-to-image correlation accuracy assumptions used are presented in Table 3.1.6.2.2-1.

Source	1 error	Rationale
DOQ Reference Image	8.5 urad	Corresponds to 6 meter DOQ accuracy spec.
ETM+ 1Gt Image	21.25 urad	Corresponds to 1 panchromatic pixel
Correlation Error	10.625 urad	Corresponds to 0.5 panchromatic pixel
Net Observation Error	25.23 urad	RSS of DOQ, 1Gt, and Correlation Errors
Obs Error - Mirror Space	12.62 urad	One half the object space value above
<i>A priori</i> Coefficient Error	42.5 urad	Corresponds to 1 reflective band pixel
Number of Points per Scan	60	Corresponds to 1 per geometric grid cell

Table 3.1.6.2.2- 1 Scan Mirror Calibration Accuracy Analysis Input Assumptions

The error propagation analysis assumed a set of test points which were well distributed as a function of scan angle to form the normal equations which would be used to estimate the mirror profile Legendre polynomial coefficients. The normal equations were then inverted to form the predicted *a posteriori* error covariance matrix from which variance estimates for the Legendre coefficients were extracted. These coefficient variances were then summed to compute the net mirror profile uncertainty. The number of test points used to construct the normal equation matrix was then varied until the net mirror profile uncertainty was less than 1.75 microradians. Two separate cases were investigated: 1) estimation accuracy for an unconstrained fifth order polynomial with six unknown coefficients; and 2) estimation accuracy for a fifth order polynomial constrained to meet the beginning of scan, end of scan, and mid-scan constraints imposed by the ETM+ mid-scan correction process as described in the scan mirror calibration algorithm section.

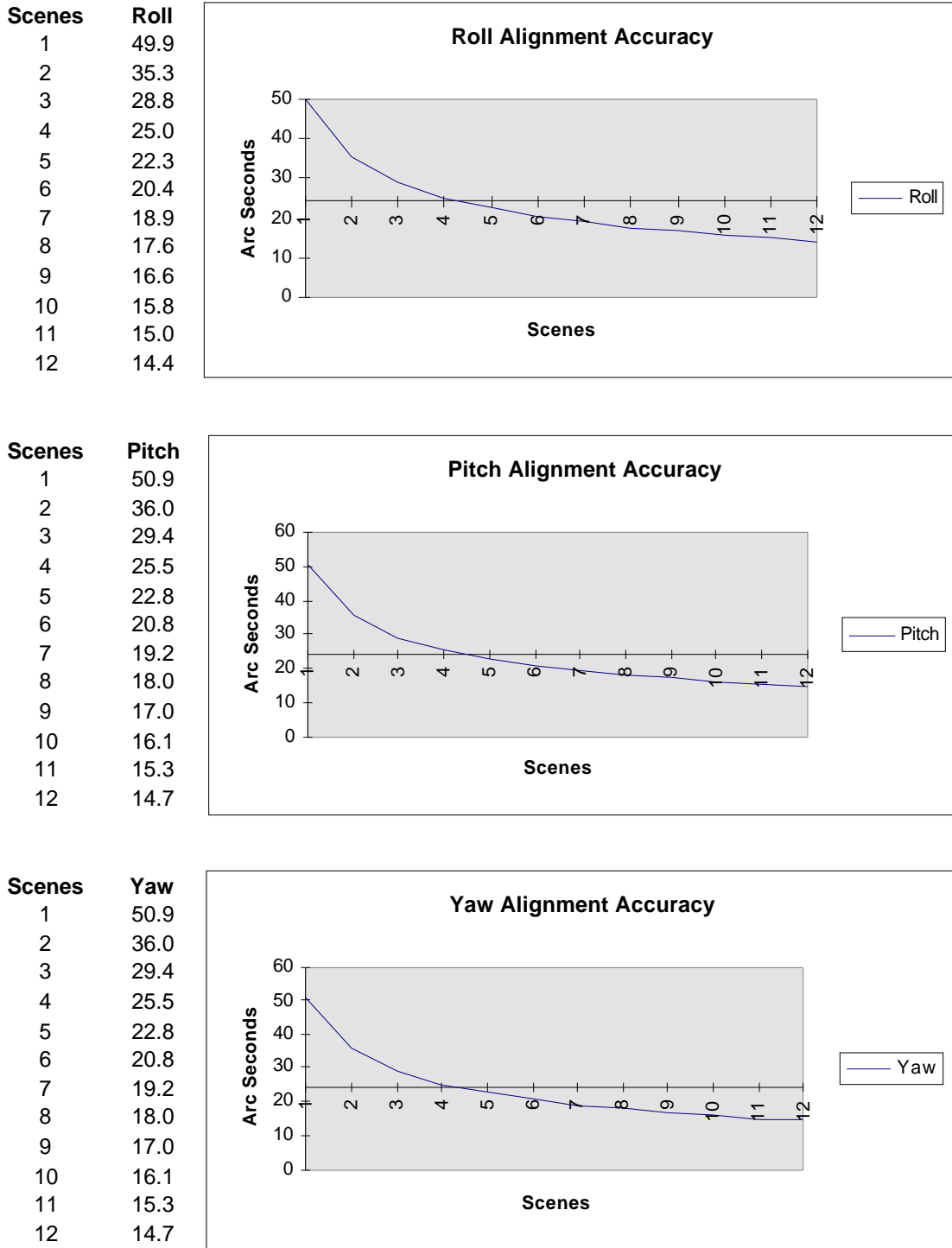


Figure 3.1.6.2.1- 1 Alignment Estimation Accuracy vs. Number of Scenes

In the unconstrained case it is necessary to process 40 scans (forward or reverse) to achieve the 1.75 microradian accuracy target. This implies that the DOQ reference images

must be a full scan wide (cross track) and at least 80 scans long (along track). Allowing for some loss of data due to cloud cover and poor correlation targets leads to a requirement for 90-100 scans, or about one-quarter of a WRS scene. Applying the scan constraints simplifies the estimation problem by reducing the number of degrees of freedom in the solution and, consequently, reduces the data requirements to 15 forward or reverse scans. This can be satisfied by a DOQ reference image which is a full scan wide and 30 scans long, or about one-eighth of a WRS scene.

Based on this analysis, we conclude that a single scan mirror calibration test site covering at least one-quarter of a WRS scene would be sufficient to provide usable results. The goal is to provide at least two test sites each covering a full WRS scene, if possible. As noted above, the input data accuracy assumptions are conservative, so using a full scene reference image, a more accurate 1Gt product, and better image-to-image correlation, the performance of the algorithm with real Landsat 7 data is expected to exceed the 1.75 microradian design threshold.

3.1.6.2.3 Band Placement Calibration Accuracy

The IAS is required to determine band center field angles to an accuracy of 0.18 arc seconds (1 per coordinate) per IAS Element Specification requirement number 3.2.3.10. The band-to-band registration assessment algorithm uses test points which appear in all 8 ETM+ bands and performs cross-band image correlation to measure any residual sub-pixel band to band offsets. These measurements are then used in the band placement calibration algorithm to estimate band center offsets in the ETM+ focal planes, relative to band 8 (panchromatic) which is treated as the reference band. These algorithms are described above.

In the course of developing the band-to-band registration assessment algorithm it was determined that, given a suitable test scene, it is possible to perform cross-band image correlation to an accuracy of approximately 0.1 pixels using pre-selected test points, and to an accuracy of approximately 0.25 pixels using randomly generated test points. When correlating bands of differing resolution (i.e., bands 6 or 8 to any of the others), the measurements are performed at the coarser band resolution. Thus, the 0.1 or 0.25 pixel measurement accuracy corresponds to a larger angular uncertainty for band offset measurements for band pairs which include band 6. This makes band 6 the critical case which drives the number of band-to-band test points required to meet the 0.18 arc second accuracy specification.

An error propagation analysis was used to determine the number of test points required to achieve a band center location accuracy of 0.18 arc seconds as a function of the expected accuracy of the test point measurements. This analysis assumed that all test points were measured in all band pairs and that the mapping between image pixel

measurements and focal plane offsets could be approximately modeled as a constant scale factor. The availability of measurements from seven band pair combinations makes the band center location solution over determined so a least squares procedure was set up to form the normal equation matrix which would be used to estimate band center offsets from test point measurements. These normal equations were then inverted to compute the predicted *a posteriori* covariance matrix for the band center estimates. The square roots of the diagonal terms of this matrix were taken to be estimates of the band center location standard deviations. The number and accuracy of the input test point measurements were then varied to examine the sensitivity of the band center estimate standard deviations to the input data volume and accuracy. As expected, the predicted standard deviation for band 6 location was highest. Figure 3.1.6.2.3-1 shows a plot of the number of test points needed to achieve a predicted standard deviation of 0.18 arc seconds versus the accuracy of the input test point measurements.

As the figure shows, the accuracy requirement can be met with 20-25 high quality hand picked test points or with 125-150 automatically generated test points. The accuracy of hand picked points should be more reliable since the analyst selecting the test points can ensure their quality and consistency. Based on the relatively small number of test points needed (if they are sufficiently accurate), it was decided to use approximately 25 analyst selected test points to perform the band-to-band registration assessment and subsequent band placement calibration. The error propagation analysis predicts a band center location accuracy of 0.09 arc seconds for bands 1-5,7 and 0.15 arc seconds for band 6. Band 8 is the reference and is assumed to be known exactly. This meets the requirement for all bands if the test point measurements are accurate to 0.12 pixels and for all but the thermal band if the measurements are accurate to 0.19 pixels.

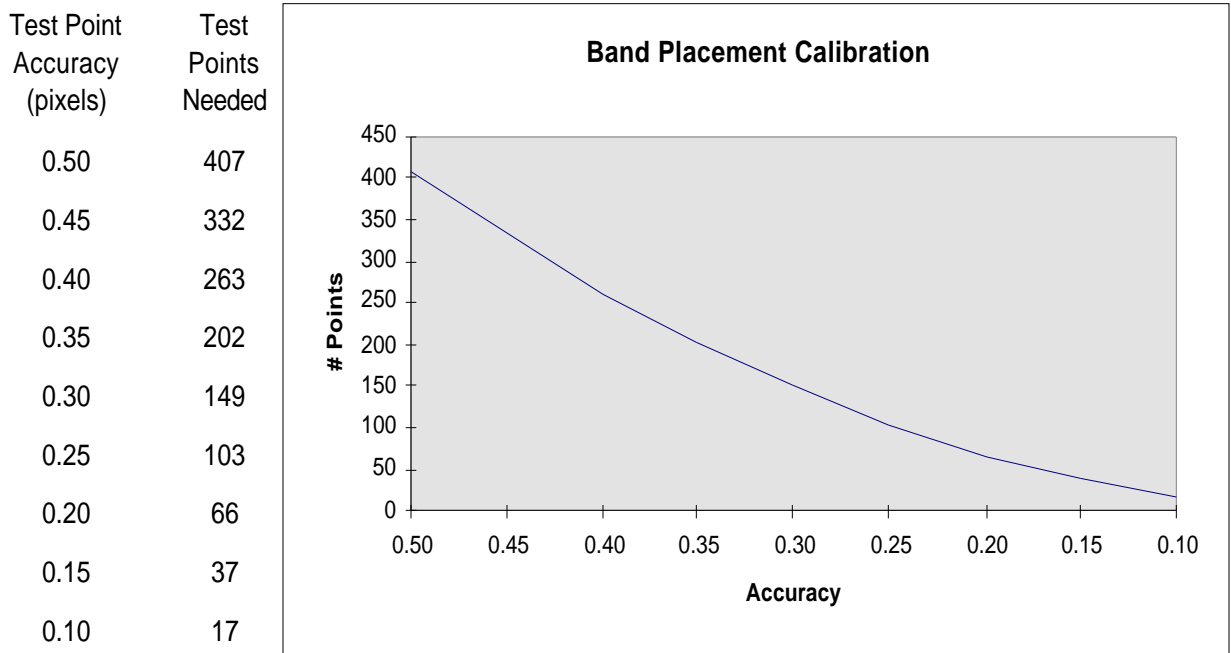


Figure 3.1.6.2.3- 1 Band-to-Band Test Point Number vs. Accuracy

3.1.6.3 Geometric Characterization Accuracy

Only two of the four geometric characterization algorithms implemented in the Landsat 7 IAS have quantifiable accuracy requirements. The geometric accuracy assessment is primarily a qualitative evaluation of the internal distortions present in ETM+ images. Geodetic accuracy assessment provides a verification of the Level 1Gs product geodetic accuracy requirement analyzed above. Test point mensuration error was included in the error budget for Level 1 processing geodetic accuracy to account for the contribution of the assessment process. The band-to-band and image-to-image registration accuracy assessments have specific performance requirements (called out in the IAS Element Specification) which are analyzed in the following sections.

3.1.6.3.1 Band-To-Band Registration Accuracy

The IAS is required to be capable of performing band-to-band registration to an accuracy of 0.28 pixels (at the ground sample distance of the coarser of the two bands) per coordinate at the 90% confidence level. This requirement is stated in the IAS Element Specification as requirement number 3.2.3.6. The error budget for band-to-band registration includes the high frequency jitter displacements which can occur in the time interval over which the eight ETM+ bands sample the same ground location. Since the

maximum time between band samples is approximately 2 milliseconds, which corresponds to the jitter sensor sampling period, the band-to-band jitter error is essentially the error in the difference between two jitter measurements. Other components of the band-to-band registration error include band field angle errors, processing model error, and test point mensuration error.

Table 3.1.6.3.1-1 shows the error components combined into an error budget for the band-to-band registration assessment process. The table columns contain the following information:

- Column 1: identifies the data element error source;
- Column 2: contains the total effect of the error source in units of 30 meter pixels at the 90% confidence level (this is equal to the square root of two times the error for one band for the errors which are independent for all bands);
- Column 3: contains the contribution of the error source to a single band in units of 30 meter pixels at the 90% confidence interval;
- Column 4: contains the original specified or estimated error source one sigma accuracy;
- Column 5: contains the units of the original error specification;
- Column 6: provides a brief text explanation of the error estimate source;
- Column 7: shows where the error source was allocated.

The field angle stability and test point mensuration contributions are relative errors which are only counted once. High frequency jitter, field angle knowledge, and processing errors apply independently to all bands and are therefore counted twice in the band-to-band error budget.

Based on the analysis shown in Table 3.1.6.3.1-1 the 0.28 pixel (90%) requirement can be met but there is little error budget margin. Manually selected test points must be used to ensure the highest correlation accuracy since relaxing the correlation accuracy to 0.11 pixels exceeds the registration budget.

Source	Both Bands	30m pixels (90%)	Spec 1	Units	Comments	Segment
High Frequency Jitter	0.079	0.056	0.3	arcsec	0.30 arcsec (1)	Satellite
ETM+ Jitter (high frequency)	0.035	0.025	0.134	arcsec	0.134 arcsec (1) high freq	ETM+
Field Angle Knowledge	0.048	0.034	0.18	arcsec	0.18 arcsec (1) calibration	IAS
Field Angle Stability	0.143	0.143	0.76	arcsec	0.76 arcsec (1) stability (0.2 pan)	ETM+
Processing Error	0.140	0.099	1.8	meter	Model budget	IAS
Mensuration	0.164	0.164	0.1	pixel	Correlation accuracy	IAS
RSS Estimate	0.277	(90%)				
RSS Margin	0.041	(90%)				
Specification	0.280	(90%)				

Table 3.1.6.3.1- 1 Band-to-Band Registration Error Budget

3.1.6.3.2 Image-To-Image Registration Accuracy

The IAS has a requirement to perform image-to-image registration to an accuracy of 0.4 pixels (at the multi-spectral band pixel ground sample distance of 30 meters) per coordinate at the 90% confidence level. This requirement is stated in the IAS Element Specification as requirement number 3.2.3.8. The error budget for image-to-image registration includes the high frequency components of the overall Landsat 7 ETM+ geometric error budget which model the internal geometric variability unique to each image, the expected accuracy of the precision correction process which uses image-to-image tie points to perform the image registration, and the expected mensuration accuracy for the registration assessment test points.

The high frequency internal errors are a subset of the geodetic error budget components presented in Table 3.6.1.1-2 and include the jitter, scan mirror variability, and modeling/processing errors. The image-to-image registration correction model accuracy is required to be 3.6 meters (1) according to the IAS Element Specification requirement number 3.2.3.9. The same estimation error covariance propagation model used to analyze the sensor alignment estimation accuracy was used to verify this requirement. In this case, the expected accuracy of the PCD ephemeris and attitude data was combined with 20 ground control points assumed to be accurate to 10 meters (corresponding to control from a 1:24,000-scale map and 0.5 pan pixel identification/mensuration error) to yield

predicted post-fit ephemeris and attitude accuracy estimates. These estimates were then propagated to ground coordinate accuracy for a range of scan angles and then root-sum-squared to establish an accuracy estimate for the precision correction in ground space. This procedure resulted in an accuracy estimate of 3.5 meters (1 σ) for the precision correction process. The specification value of 3.6 meters was used for the image-to-image error budget.

The final component of the error budget is the image-to-image test point correlation accuracy. Testing with Landsat 5 data has shown that correlation accuracy of 0.1 pixel is achievable for selected targets. Pre-selected test points will be used to evaluate the image-to-image registration accuracy.

Table 3.1.6.3.2-1 shows these components combined into an error budget for the image-to-image registration assessment process. The table columns contain the following information:

- Column 1: identifies the data element error source;
- Column 2: contains the total effect of the error source in units of 30 meter pixels at the 90% confidence level (this is equal to the square root of two times the error for one image for those errors which are contained in both the reference and object images);
- Column 3: contains the contribution of the error source to a single image in units of 30 meter pixels at the 90% confidence interval;
- Column 4: contains the original specified or estimated error source one sigma accuracy;
- Column 5: contains the units of the original error specification;
- Column 6: provides a brief text explanation of the error estimate source;
- Column 7: shows where the error source was allocated.

Note that the high frequency errors are independent for the two images and therefore contribute twice whereas the precision correction and mensuration errors apply to the process of relating the two images to each other and are therefore only counted once.

Source	Both Images	30m pixels (90%)	Spec 1	Units	Comments	Segment
High Frequency Jitter	0.079	0.056	0.3	arcsec	0.30 arcsec (1)	Satellite
Low Frequency Jitter	0.079	0.056	0.3	arcsec	0.30 arcsec (1)	Satellite
ETM+ Jitter (high frequency)	0.035	0.025	0.134	arcsec	0.134 arcsec (1) high freq	ETM+
Scan Mirror Repeatability	0.191	0.135	0.72	arcsec	1.75 microradians * 2 (1)	ETM+
Processing Error	0.140	0.099	1.8	meter	Model budget	IAS
Correction Model Error	0.198	0.198	3.6	meter	Estimation error	IAS
Mensuration	0.164	0.164	0.1	pixel	Correlation accuracy	IAS
RSS Estimate	0.318	(90%)				
RSS Margin	0.243	(90%)				
Specification	0.400	(90%)				

Table 3.1.6.3.2- 1 Image-to-Image Registration Error Budget

Based on the analysis shown in Table 3.1.6.3.2-1 the 0.4 pixel (90%) requirement can be met but there is little error budget margin. Pre-selected test points must be used to ensure the highest correlation accuracy since relaxing the correlation accuracy to 0.14 pixels exceeds the registration budget. Similarly, it is necessary to use the precision correction process to fit the object image directly to the reference image rather than fitting both to a separate control source, leading to independent correction model errors which, when combined, would exceed the 3.6 meter image-to-image correction model budget.

4. Constraints, Limitations, Assumptions

Atmospheric Refraction Correction

The atmosphere causes a ray of light to bend towards the satellite as it propagates through the atmosphere. The amount of bending depends on the angle of propagation and the density of the atmosphere at a given instant. For Landsat 7, the magnitude of this affect is less than one meter at end of scan. Currently, this affect is not accounted for.

Resampling

Resampling Weight Tables (i.e. for cubic convolution, MTF, or other resampling kernels) are calculated at 1/32 pixel increments. These weights assume evenly spaced pixels and are used in the sample direction.

Spline weights (used for resampling over the scan-gap where the pixels are not necessarily evenly spaced) are also calculated at 1/32 pixel increments. These weights are applied in the line direction in the area between two scans. The weights are set up for a shift of 0.0 to the maximum gap possible from the system. A value of 3.0 covers the maximum gap possible in the LANDSAT 5 satellite. A value of 6.0 will be needed for the LANDSAT 7 satellite, to cover the panchromatic band. *When the panchromatic band is used for LANDSAT 7 this could cause some anomalies in cases of large varying grey values between pixels that are located in an area with a large scan gap.*

Speed of Light Correction

Due to the non-infinite velocity of light, the velocity of a point on the surface of the Earth and the velocity of the satellite, cause pixel location errors if not accounted for. The speed of light correction due to the Earth's rotation is sub-meter and is currently not accounted for.